Technical University of Crete

School of Mineral Resource Engineering

Master Thesis

Postgraduate Program in Petroleum Engineering

Properties and phase behavior of CO2-rich fluids

Author:

Milan Nedeljkovic

Supervisor:

Professor Nikolaos Pasadakis

This thesis is submitted in fulfillment of the requirements for the Master degree of Petroleum Engineering in the School of Mineral Resources Engineering at Technical University of Crete

Chania, October 2021.

The MSc Program in Petroleum Engineering of the Technical University of Crete, was attended and completed by Mr. Milan Nedeljkovic, due to the EKO Serbia A. D. Member of Hellenic Petroleum Group Scholarship award

Contents

List of tables

List of Figures

Acknowledgements

This master thesis is submitted in fulfillment of the requirements for the Master degree of Petroleum Engineering in the School of Mineral Resources Engineering, Technical University of Crete. This project has been done in the collaboration with Heriot Watt University and HydraFact Ltd. company.

First and foremost, I would like to express my special thanks of gratitude to Professor Dr Bahman Tohidi for giving me this golden opportunity to take a part in this wonderful project. Specially, I am extremely grateful to co-supervisor of my work, Dr Ramin Mousavi for his invaluable guidance, useful advices, scientific comments and patience during the process of creating this thesis.

I would also like to express my gratitude to other members of my committee – Professor Dr Nikolaos Pasadakis and Professor Dr Dimitris Marinakis for all valuable knowledge provided during studies at Technical University of Crete.

My gratitude extends to the company EKO Serbia A. D. Member of Hellenic Petroleum Group, for the funding opportunity to undertake my master studies at the Technical University of Crete. Without you, nothing of this would be possible.

Finally, I cannot describe by words my gratitude to my family for supporting me during my studies. I am very grateful to all my colleagues with whom I spent a wonderful and unforgettable year at island of Crete.

Thank you all,

Milan Nedeljkovic

Abstract

The main goal of this master thesis project is to compare two PVT simulation software packages. The simulator software programs under study are the KBC's (now acquired by Yokogawa Company) Multiflash and HydraFLASH from HydraFact Ltd. Both simulators are supposed to make same predictions and compared to existing experimental data. However, it is shown that performance of them might exhibit significant differences, even though same equations of state were applied for calculations in both software.

Introduction chapter provides brief description of Carbon Capture and Storage process, as well as overview of properties of carbon dioxide. In Chapter 2, popular equations of states employed for calculations will be presented, as well as short description of software packages used for this project. In chapter 3 density will be discussed, which is one of the most important thermophysical property for CCS processes. Both multi-component and binary mixtures will be examined. In chapter 4, speed of sound property will be discussed. Chapter 5 presents solubility of CO_2 in water and salt aqueous phase, and lastly Chapter 6, provides information about hydrate dissociation data between two software and experimental data. In the conclusions part our thoughts regarding both software packages will be finalized and therefore final judgement will be made.

By finalizing this study, a more solid judgement on performance of these two software programs on the different simulations has been built.

1. Introduction

Over the last few years, the amount of CO_2 in the atmosphere continuously grows. This is believed to be hugely due to the burning of fossil fuel. CO_2 is a greenhouse gas, which means it contributes to the greenhouse effect by absorbing infrared radiation. "An increase in the atmospheric concentrations of greenhouse gases produces a positive climate forcing, or warming effect. From 1990 to 2019, the total warming effect from greenhouse gases added by humans to the Earth's atmosphere increased by 45 percent. The warming effect associated with carbon dioxide alone increased by 36 percent", according to EPA[1] (EPA, 2021). Therefore, technologies which can restrict the emission of CO_2 to the atmosphere are demanded. One of those technologies includes Carbon Capture and Storage process, commonly known as CCS process (Bjørner & Kontogeorgis, 2016).

Knowledge of relevant thermodynamic behavior of fluid phase systems is crucial in order to design and operate that process in an efficient manner. This is the case with many processes, including CSS processes. In order to design and operate CCS systems of concern, correct predictions of the fluid's behavior are necessary. For pure carbon dioxide (CO_2), thermodynamic and transport properties are well-known and accurately reported by already established models. However, impurities in most CO_2-rich systems, change properties of fluid. Even though they can exist in very small amounts, changes in phase behavior and density is evident, regardless small amounts. That is the reason why an accurate model is needed in order to predict CO_2 and impurities properties.

Phase behavior is of great importance in designing transportation system such as pipeline and shipping. CO_2-rich fluids transportation pipelines are very important due to enlarged focus on carbon capture and storage technologies and enhanced oil recovery by CO_2 flooding. In the transportation pipelines, there is a lower pressure limit so two-phase flow can be avoided, and care must be taken when compression process is designed. Critical point of pure CO_2 is 31 °C and 74 bara, while triple point is at

[1] United States Environmental Protection Agency

temperature –56.4 °C and pressure 5.2 bara. However, as aforementioned small amount of impurities could change the phase behavior of the system significantly. For corrosion inhibition purposes, it is key to predict the condition in which water rich phase is formed. Water solubility is known to be lower in presence of impurities like methane (CH_4), sulfur-dioxide (SO_2) etc. Also, methane and carbon-dioxide form hydrates which can lead to pipeline blockage during oil and gas transportation and production. Planned or unexpected depressurization can lead to strong cooling which causes gas hydrates formation. That is the reason why correct prediction of hydrate formation conditions is crucial for the petroleum industry.

1.1. Properties of CO_2

Pure carbon-dioxide is an inert, incombustible gas without color and odor. It is formed during respiration, combustion, and organic decomposition. Its molecular weight at standard conditions is 44.010 g/mol. Density of carbon dioxide at atmospheric conditions is 50% greater than density of air. It is present in the Earth's atmosphere at a low concentration and acts as a greenhouse gas. Besides gaseous state, it can be in liquid form too, especially at specific reservoir conditions. Also, it can appear in solid state, at low temperatures and higher pressures. In Figure 1, phase diagram of pure CO_2 is shown.

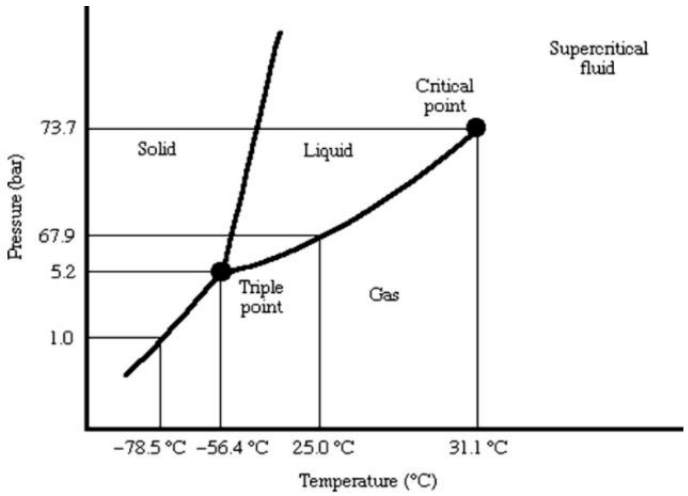

Figure 1 Phase diagram of CO_2. Source: (Cheng.com, Online 2021.)

By increasing pressure and temperature, liquid phase appears and it coexists with solid and vapour phase at triple point of CO_2 which is at temperature of -56.4 °C and pressure 5.2 bara (Figure 1). Liquid and vapor phase coexist from triple point to critical point. Under critical temperature, at huge range of pressures, CO_2 can be found in liquid or in a gaseous phase. Above critical temperature, CO_2 can only exist as a gas, regardless the pressure values. Transporting CO_2 in the liquid-dense and supercritical state is far more favorable in the industry because of relatively high density with relatively low viscosity of CO_2 streams above the critical pressure. As to avoid two-phase flow during the transportation, captured CO_2 in gaseous state is compressed to pressures up to 80 bara (above critical pressure). That guarantees that phase change will not appear with variation of temperature across the pipeline.

However, the presence of impurities will influence critical pressure, and it could lead to existence of liquid and vapour phases. The most important impurity expected in co-captured CO_2 is a sulphure, which can be either in form of sulfur dioxide (SO_2) or hydrogen sulfide (H_2S). Other significant impurities are: NO_x, H_2, CO, and least expected nitrogen, oxygen and carbon. How presence of impurities affect critical pressure is illustrated in Figure 2, where phase envelopes of CO_2-CH_4 and CO_2-H_2 mixtures were compared with phase envelope of pure CO_2. Clearly, figure shows that different impurities in CO_2-mixture give different properties to mixture. Mixture of CO_2 with 5% of CH_4 has narrower phase envelope than mixture of CO_2 and N_2.

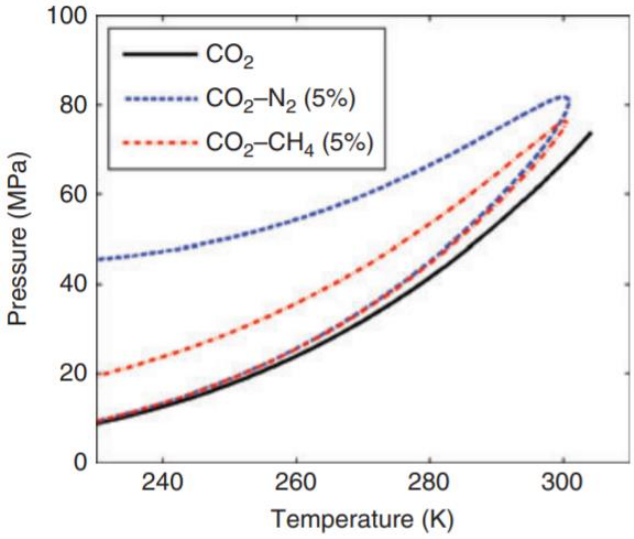

Figure 2 Impact of impurities on CO_2 phase envelope. Source: (Li, Wilhelmsen, & Yan, 2015)

The existence of impurities such as oxygen, hydrogen- sulfide, methane and hydrogen, remarkably affects total thermodynamic properties of CO_2 mixtures. With impurities in CO_2, critical points move to higher pressures. Moreover, phase changes do not happen at constant temperature or pressure, but ranges in temperature and pressure. This improves the possibility to get two phases during the CCS processes.

1.2. Carbon Capture and Storage

As already mentioned, carbon capture and storage (CCS) was created as a favorable technologies for lowering CO_2 emissions from industry into the atmosphere and to decrease global warming problem. In the report on energy technology perspectives, in the blue map presented by IEA (International Energy Agency), it is shown that CCS accounts for 20% of the total reduction of CO_2 emissions (IEA, 2011). Carbon capture and storage (CCS) technology could theoretically capture between 85-95% of all CO_2 produced (Metz, Davidson, De Coninck, Loos, & Meyer, 2005). Figure 3 shows briefly the CCS process.

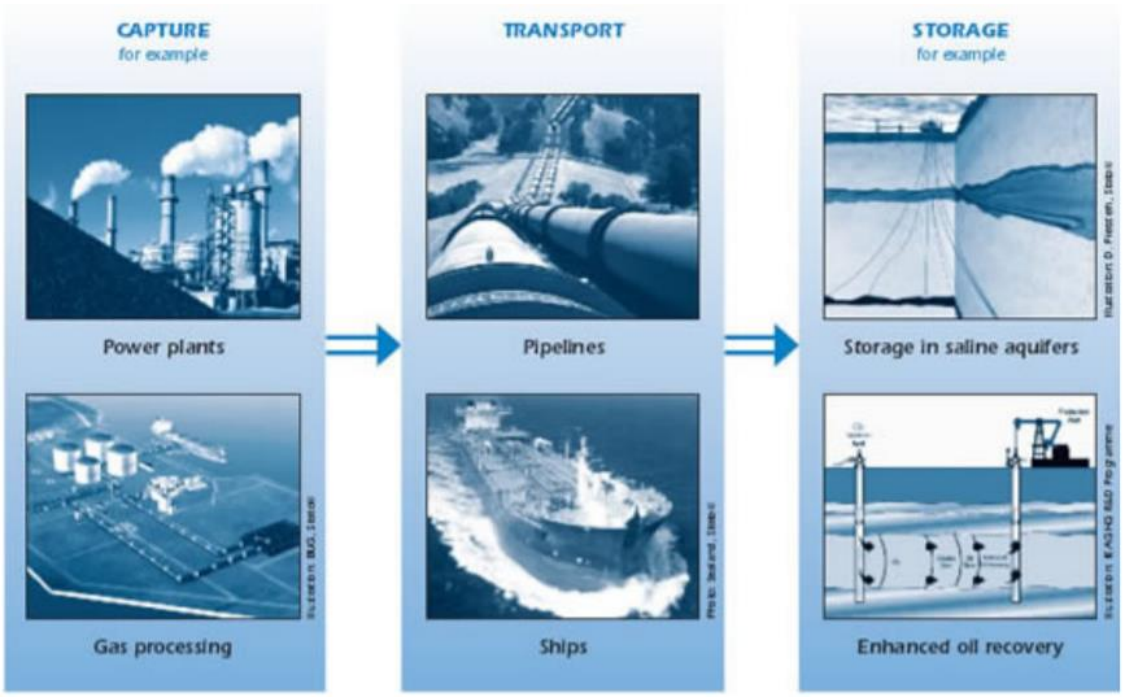

Figure 3 The CCS process. Source: (IEA, 2011)

According to IPCC Special report, “CCS involves the use of technology, first to collect and concentrate the CO2 produced in industrial and energyrelated sources, transport it to a suitable storage location, and then store it away from the atmosphere for a long period of time. CCS would thus allow fossil fuels to be used with low emissions of greenhouse gases” (IPCC, 2005). The three main components of the CCS process are capture, transport and storage. This is illustrated in Figure 4.

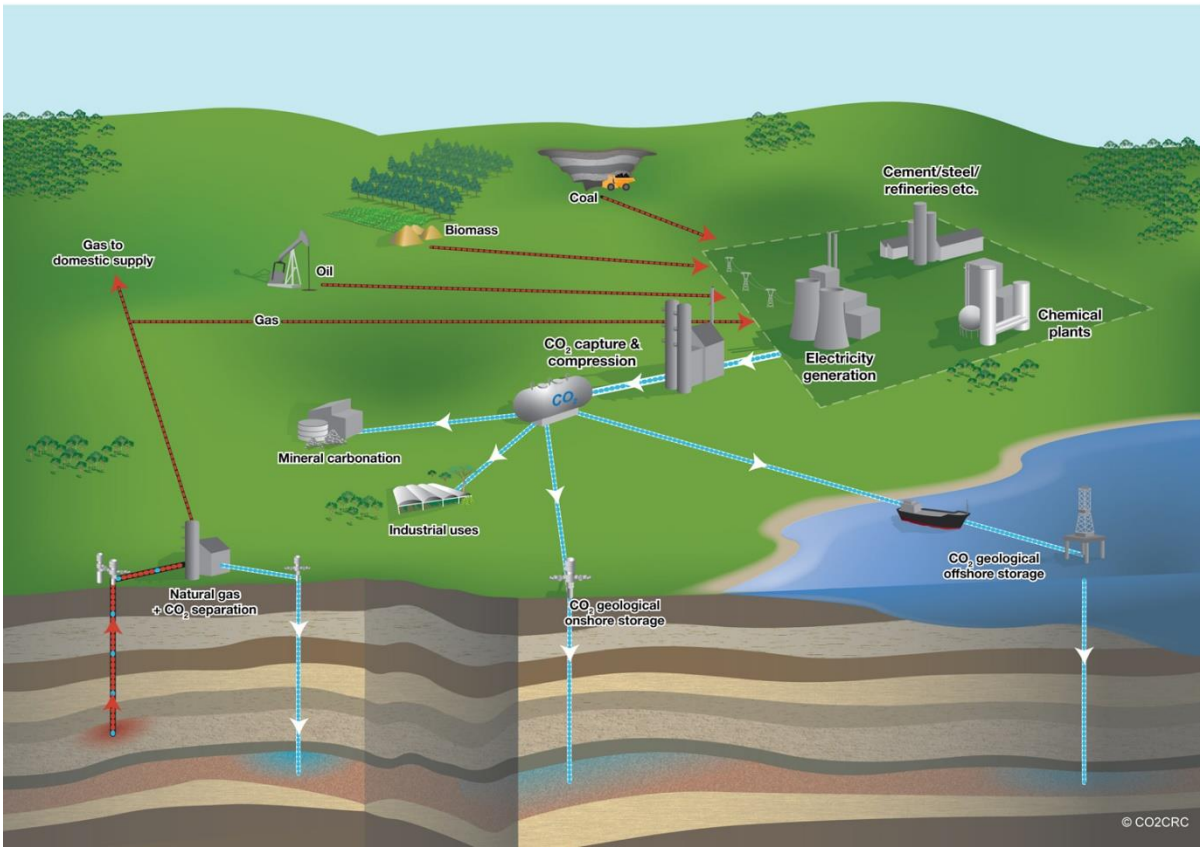

Figure 4 CCS systems. Source: (Courtesy CO_2CRC)

1.2.1. Capture

The very first step in carbon capture and storage (CCS) process is to capture carbon-dioxide. Energy from fossil fuels such as coal, oil and natural gas is released during combustion and conversion process, which results in the emission of by-product such as CO_2. In Figure 5, three main options for capturing CO_2 are shown, and those are: pre-combustion, post-combustion and oxy-fuel combustion. Each capture technology has

advantages and disadvantages depending on which plant type that should be integrated as well as to other factors.

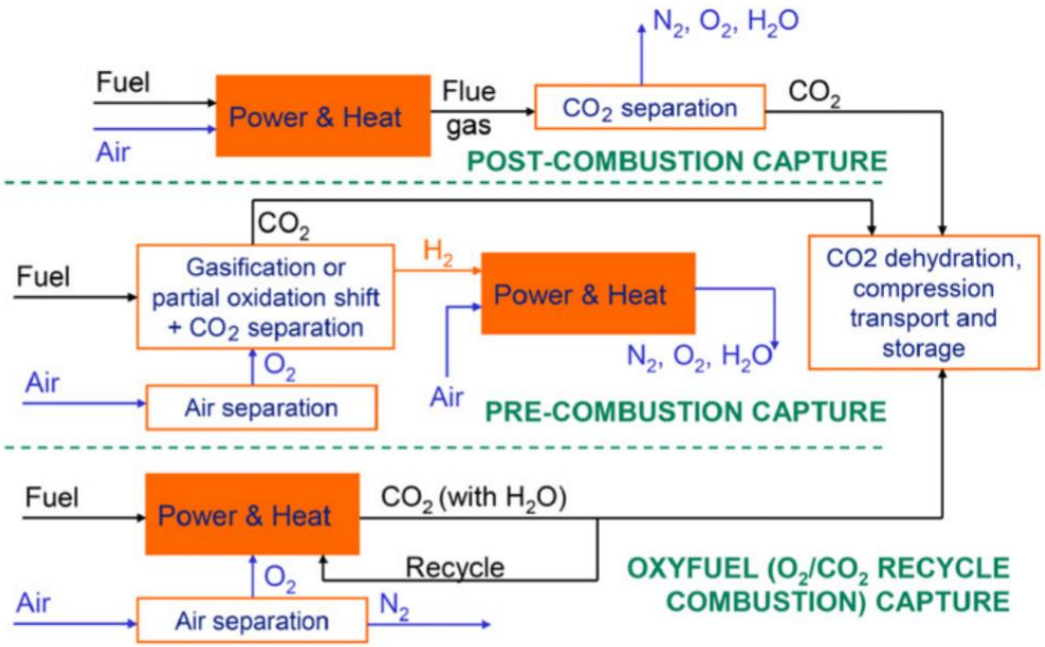

Figure 5 Methods for capturing CO_2. Source: (Gibbins & Chalmers, 2008)

Pre-combustion capture process works by extracting carbon from the fuel before it is burnt. Firstly, the fuel is gasified by heating in small amounts of oxygen, which then produces synthesis gas which is primarily a mixture of carbon monoxide and hydrogen. Carbon monoxide is then converted to CO_2, by adding steam. The hydrogen is isolated and can be burnt without production of any CO_2. After that, CO_2 is captured and ready for transport and storage, while the hydrogen-rich gas is combusted in turbine to produce electricity. The fuel conversion steps needed for pre-combustion have more complexity than the processes involved in post-combustion, which makes this technology much hard to apply to existing power plants. Pre-combustion capture is used for processing of natural gas, while its application in power generation will be via new build projects.

Post-combustion process removes CO_2 after the fuel has been burnt, just before the combustion products are released to the atmosphere (IEA, 2008). CO_2 can be captured using a liquid solvent or other separation methods. In an absorption-based approach, once absorbed by the solvent, CO_2 is released by heating to form a high purity CO_2

stream. This technology is widely used to capture CO_2 for use in the food and beverage industry.

Oxyfuel combustion processes use oxygen rather than air for combustion of fuel. This produces exhaust gas that is mainly water vapor and CO_2 that can be easily separated to produce a high purity CO_2 stream. In oxyfuel combustion capture systems, the CO_2 capture efficiency is very close to 100%. The challenge is that air separation technology is needed for producing oxygen.

1.2.2. Transport

Transporting CO_2 is the second stage in the value chain of CCS. Pipelines and ships are two major options in transporting CO_2 produced from the power plants to the storage sites. Both options have their own advantages and disadvantages with respect to the risk of leakage and investment cost. Transporting CO_2 through the pipelines is an established technology as pipelines have been used widely for transporting natural gas. To avoid two-phase flow during CO_2 transport, CO_2 is dried and compressed to pressures higher than 8 MPa (supercritical region). In that way, density of CO_2 will also increase, which in return will make CO_2 easier and less costly for transport. Pipelines can be both onshore and offshore.

CO_2 can be transported by ship as a pressurized cryogenic liquid using conventional technology, as used for liquefied petroleum gas (LPG). The leakage of CO_2 during shipping may occur due to collision, foundering, stranding, and fire. This risk can be minimized through a careful planning of routes and high standards of ship configuration, training, and management (IPCC, 2005).

Lastly, road and rail tankers are also possible options for CO_2 transportation. These systems transport CO_2 at -20 °C and at 2 MPa pressure. However, compared to pipelines and ships, they are least economical, except on a small scale, and they are unlikely to be used for big-scale CCS.

An important aspect of the choice of the type of transportation is its cost. Figure 6 shows comparison of costs of ship and pipeline transport of CO_2. In every case, the costs depend strongly on the distance and the transported quantity. It is clear that for shorter distances (up to 500 km), ship transportation is relatively expensive. Main reasons for that are fixed costs of liquefaction, buffer storage and ship loading and unloading. However, for greater distances (above 700 km) ship transportation would be more affordable choice for transporting CO_2 than offshore pipeline, as well as for distances greater than 1500 km, when compared to onshore pipelines.

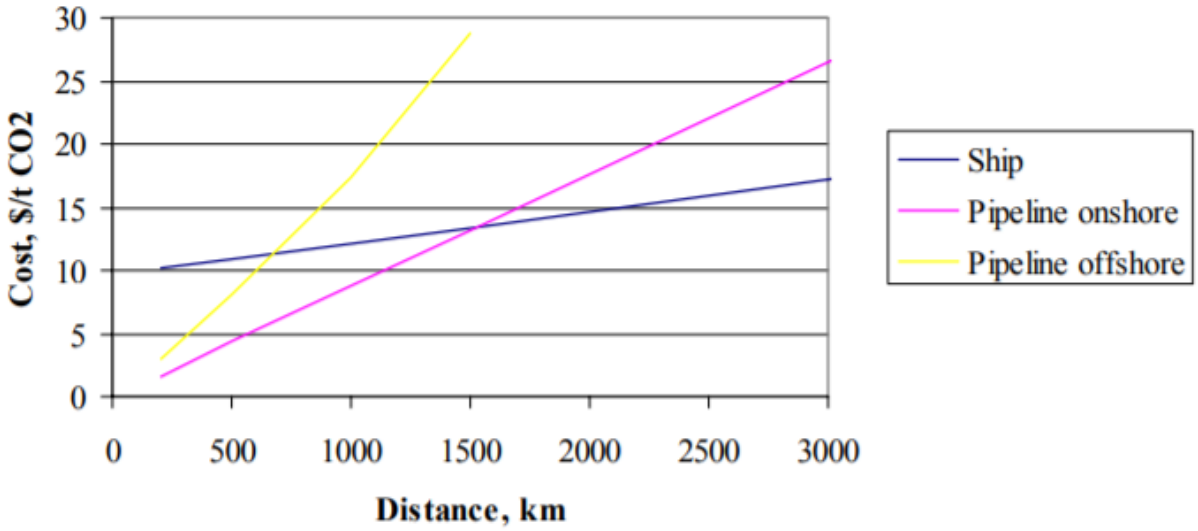

Figure 6 Comparison cost of ship and pipelines for transporting CO2. Source: IEA greenhouse gas R&D programme report

Besides costs, one of the most crucial parameters which affect the choice of the transportation system is the type of storage, which can be geological or ocean.

1.2.3. Storage

The last stage of CCS value chain process is storing CO_2 into suitable sites, after it has been captured and transported. Geological storage of carbon dioxide represents an injection of the concentrated stream of CO_2 into a rock formation below the earth's surface. CO_2 can be stored into geological formations such as oil and gas reservoirs, deep saline formations and coal beds, or it can be stored into ocean. Before storage, CO_2 is compressed to a dense 'supercritical' fluid phase and then injected into the rock formation at depth below 800 m. Well-drilling technology, injection technology and

computer simulation of storage reservoir performance are developing more and more in order to utilize the design and operation of geological storage. Injection of CO_2 into the oil reservoirs can be an effective tertiary EOR[2] method for increasing total recovery factor. Successful implementations of CCS projects require good evaluation and assessment of storage sites. The major factors that strongly affects geological storage of CO_2 include the formation depth, state of CO_2 in underground conditions, existence of fractures or faults in the formation which can generate paths for migration and wellbore integrity.

Ocean storage is conducted by injection of CO_2 into the water column (below 1 km) through the anchored pipeline or a moving ship, or by deposition of CO_2 through the pipeline or offshore platform onto the sea floor at depths below 3000 m where CO_2 has higher density than water and there it can create a 'lake' delaying dissolution of CO_2 into the neighboring environment. The dissolved and dispersed CO_2 would eventually become part of the global carbon cycle and eventually equilibrate with the CO_2 in the atmosphere.

Mineral carbonation includes transferring CO_2 to solid inorganic carbonates using alkaline and alkaline-earth oxides, like magnesium oxide (MgO) and calcium oxide (CaO), which exist in naturally occurring silicate rocks. This technology is in the research phase.

[2] Enhanced oil recovery

2. Modeling

In first part of this chapter, most commonly used equation of states for modelling and measuring experimental data will be briefly described and presented. In the second part of this chapter, two commercial simulators which are used in this study for comparison, will be presented.

For petroleum engineers, most important equations of state are the cubic EoS, such as SRK and PR which have excellent performance for simple gases and hydrocarbon mixtures. However, for more complex fluids (which includes polar solvents, asphaltenes, polymers, water, inhibitors, alcohols etc.), these equations of state fail to produce sufficient results. For this type of fluids, Cubic-Plus-Association (CPA) EoS shows better performance.

The Soave-Relich-Kwong (SRK) equation of state (EoS) was firstly developed in 1972, and it was a modification of the existing Van der Waals (VdW) EoS (E-Education Institute, PennState, 2021). Until now, all modifications regarding the VdW EoS looked at how the parameter "*a*" was dependent on temperature. Soave further expanded this by proposing that parameter "*a*" had actually two variable dependencies, where:

$$a = a(T, \omega) \tag{2.1.}$$

That means parameter "*a*" does not only depend on temperature, but also on the Pitzer acentric factor ω**,** which is a measure of the sphericity and configuration of the molecule. The SRK EoS is used for predictions which include polar system (Steel, Liu, Mackay, & Maroto-Valer, 2016). It is expressed as

$$\left(P + \frac{a}{v(v+b)}\right)(v-b) = RT \tag{2.2.}$$

Where p is a pressure, R is the ideal gas constant and T is the temperature. Additionaly, v is the molar volume, a is the attractive parameter and b is the repulsive parameter.

Peng-Robinson (PR) EoS poses high similarity with SRK EoS which is already described. Currently, the PR EoS is the most accepted EoS in the petroleum industry, for its usage in natural gas systems (E-Education Institute, PennState, 2021). In terms of performance, both PR and SRK equation of states are quite similar in their performance, with the Peng-Robinson working slightly better at the critical point. This makes PR EoS more efficient in regards to vapor-liquid equilibrium, while the SRK EoS produce better results with polar systems. As the interest of the oil and gas industry is much more in gas/condensate systems than polar systems, the Peng-Robinson EoS is considered to be a better EoS than SRK (E-Education Institute, PennState, 2021). The PR EoS is expressed as:

$$\left(P + \frac{a}{v^2 + 2bv + b^2}\right)(v - b) = RT \qquad (2.3.)$$

where p is a pressure, R is the ideal gas constant and T is the temperature. Additionaly, v is the molar volume, a is the attractive parameter and b is the repulsive parameter.

It can be seen from the EoS that it retains the depndency of the attractive term on both the temperature and acentric factor, which was expressed by Soave. The only difference is that both models present different fitting parameters that are used to describe that dependency.

Initially, Patel and Teja proposed a three-parameter cubic EoS which provided good representation of vapor-liquid equilibrium (VLE) for several mixtures. However, Patel-Teja (PT) EoS has some limitations, which were noticed by Valderrama – „Patel and Teja were able to collerate the two empirical parameters in terms of the accentric

factor. However, the correlations are valid only for non polar fluids. Another problem with PT EoS is the introduction of additional mathematical complexity which is not present in other common EoS, such as SRK or PR“ (Valderrama, 1990). Therefore, Valderrama proposed a new generalized correlations for parameters in the PT EoS, which solve aforementioned problems by transforming PT EoS into a generalized EoS, today known as Valderrama–Patel–Teja (VPT) Equation of State (Valderrama, 1990).

The VPT EoS is used alongside non-density dependent mixing rules. The combination of the Valderrama–Patel–Teja EoS and the non-density dependent mixing rules results in an effective tool for modelling systems which contains polar and non-polar compounds such as water and CO_2 systems. Valderrama–Patel–Teja (VPT) Equation of State is expressed as:

$$P = \frac{RT}{v - b} - \frac{a}{v(v + b) + c(v'b)} \tag{2.4.}$$

where p is a pressure, R is the ideal gas constant and T is the temperature. Additionaly, v is the molar volume, a is the attractive parameter, b is the repulsive parameter and c is parameter of the VPT EoS.

Perturbed Chain form of the Statistical Associating Fluid Theory (PC-SAFT) EoS is an extension of the higher-order Statistical Associating Fluid Theory (SAFT) EoS that was developed by Gross and Sadowski (Gross & Sadowski, 2001). The SAFT models are based on first-order perturbation theory which is proposed by Wertheim, which states that the potential energy which is related to relative complex molecular fluids could be described as the sum of both potential energy of reference fluid and correction or perturbation term (Diamantonis & Economou, 2011). The SAFT and PC-SAFT EoS are expressed as the sum of the residual Helmholtz free energy terms that are a by-product of the different kinds of molecular interactions that happen within the system (Diamantonis, Boulougouris, Mansoor, Tsangaris, & Economou, 2013):

$$a^{res} = a^{hs} + a^{disp} + a^{chain} + a^{assoc} \quad (2.5.)$$

where:

a^{hs} is hard sphere term. It stands for the Helmholtz free energy for a hard sphere in a hard sphere fluid at the same packing fraction as in the chain fluid.

a^{disp} is dispersion term, and it stands for the dispersion contribution to the Helmholtz free energy.

a^{chain} is chain term, which is for chain contribution to the Helmholtz free energy

a^{assoc} is association term. The association Helmholtz energy due to hydrogen bonding was also estimated from Wertheim's association theory.

The residual Helmholtz free energy is the difference between the Helmholtz free energy and the Helmholtz free energy of the ideal gas (at the corresponding density and temperature). The only difference between these two equations of state is that they use different reference fluids. For example, a hard sphere reference fluid is used for SAFT, while it is a hard chain reference fluid that is used for PC-SAFT. This results in a difference in the functional forms of both models. Both EoSs can be precisely used for modelling complex CO2 mixtures, for instance, those containing ionic liquids and amines.

In the past years, the Cubic-Plus-Association (CPA) EoS has been applied for thermodynamic modeling in a broad range of industrially important chemicals, primarily in relation with the petroleum industry. One of the main advantages of the CPA equation of state is that it reduces to the SRK cubic EoS in the absence of associating compounds and is therefore compatible with existing tools for oil characterization. While in Multiflash software, CPA EoS is presented as CPA-Infochem model, in HydraFLASH software, it only exists as a sCPA. This equation of state has been successfully applied in modeling different data in this master thesis project. sCPA stands for Simplified Cubic Plus Association (sCPA) EoS, which is like SAFT EoS, also based on the perturbation theory (Kontogeorgis, Yakoumis, & Vlamos, Application

of the sCPA equation of state for polymer solutions, 2000). sCPA EoS will be the most used EoS for setting up models in this thesis project. The sCPA EoS includes two terms. The first term is the SRK EoS (used to describe physical interactions) and the second term is a chemical expression by Wertheim (used to model hydrogen bonding compounds) (Kontogeorgis, Yakoumis, & Vlamos, 2000). The fact that this model has both a cubic and association term is what gives the sCPA EoS its name. The sCPA EoS is the most effective when used on non-polar and only slightly polar systems (Kontogeorgis G. , Yakoumis, Meijer, Hendriks, & Moorwood, 1999). Also, it is very effective for a few hydrogen bonding systems. Additionally, the sCPA EoS can achieve excellent correlation for binary mixtures such as water and alkanes, water and methanol, methanol and alkanes and methanol (or water) and gases. This results in the sCPA EoS being extremely flexible and it is used in many gas processing, reservoir fluids and flow assurance studies (Kontogeorgis G. , Yakoumis, Meijer, Hendriks, & Moorwood, 1999). CPA EoS showed a much higher accuracy, when it comes to capability of the thermodynamic model to make the correct predictions, compared to the usual choices of cubic EoS such as PR (Peng & Robinson, 1976) or SRK (Redlich & Kwong, 1949) (Speranza & al., 2017). sCPA has following expression:

$$P = \frac{RT}{v-b} - \frac{a(T)}{v(v+b)} \quad - \quad \frac{1}{2}\frac{RT}{v}\left(1+\rho\frac{\partial \ln g}{\partial \rho}\right)\sum_i x_i \sum_{A_i}(1-X_{A_i}) \qquad (2.6.)$$

Where v is the molar volume, x_i is the mole fraction of component i, T is the temperature, P is the pressure, R is the universal gas constant and b is the covolume. X_{A_i} is the mole fraction of sites type A in molecule i not bonded to other active sites.

2.1. HydraFLASH

HydraFLASH is a commercial PVT software which is commercialized by Hydrafact Ltd. in collaboration with Heriot-Watt University in Edinburgh, Scotland. It is a gas hydrate and thermodynamic prediction software which is designed for the calculation of the phase equilibrium and physical properties of petroleum reservoir fluids, such as oil, gas, water, salt, alcohols, glycols, hydrates & ice, over a big range of pressure and temperature conditions (HYDRAFACT, 2021). In this project, the HydraFLASH software version 3.7 was used, with approved license. HydraFLASH was originally created in 1986 and therefore has a long history of predicting hydrate formation equilibrium points accurately (i.e., temperature and pressure).

HydraFLASH software allows modelling of multicomponent systems, multiphase aqueous and hydrocarbon systems in the existence of hydrates and inhibitors. Its main function is modeling hydrocarbons for the petroleum industry, but it can also be used for calculating CO_2 solubility in brine, hydrate dissociation data, asphaltene etc. In Figure 7, there is a list of available equation of states for calculation settings.

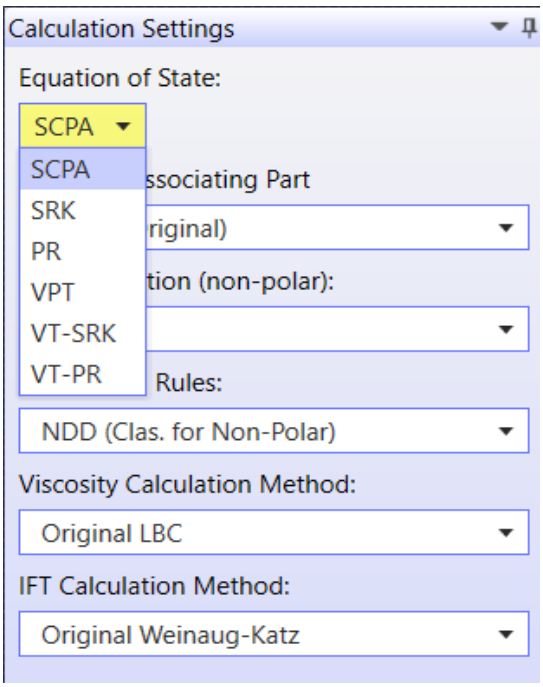

Figure 7 HydraFLASH software calculation settings window

Big advantage of this software is that it allows user to change and pick equation of state. This is very important as some EoS are more applicable for some kind of calculations than others. Equation of states which are available in HydraFLASH software are Simplified Cubic Plus Association (sCPA), Soave-Relich-Kwong (SRK), Peng-Robinson (PR), Valderrama–Patel–Teja (VPT), Volume Translated SRK (VT-SRK) and Volume Translated PR (VT-PR) equation of state. In this thesis project, Simplified Cubic Plus Association (sCPA) equation of state will be primarily used as a model for calculating different data in HydraFLASH, as of its consistently good performance. Besides option for picking and changing EoS, this software also allows setting up desired options within chosen EoS, such as CPA non associating part, alpha function, SRK mixing rules, viscosity calculation method and IFT calculation method.

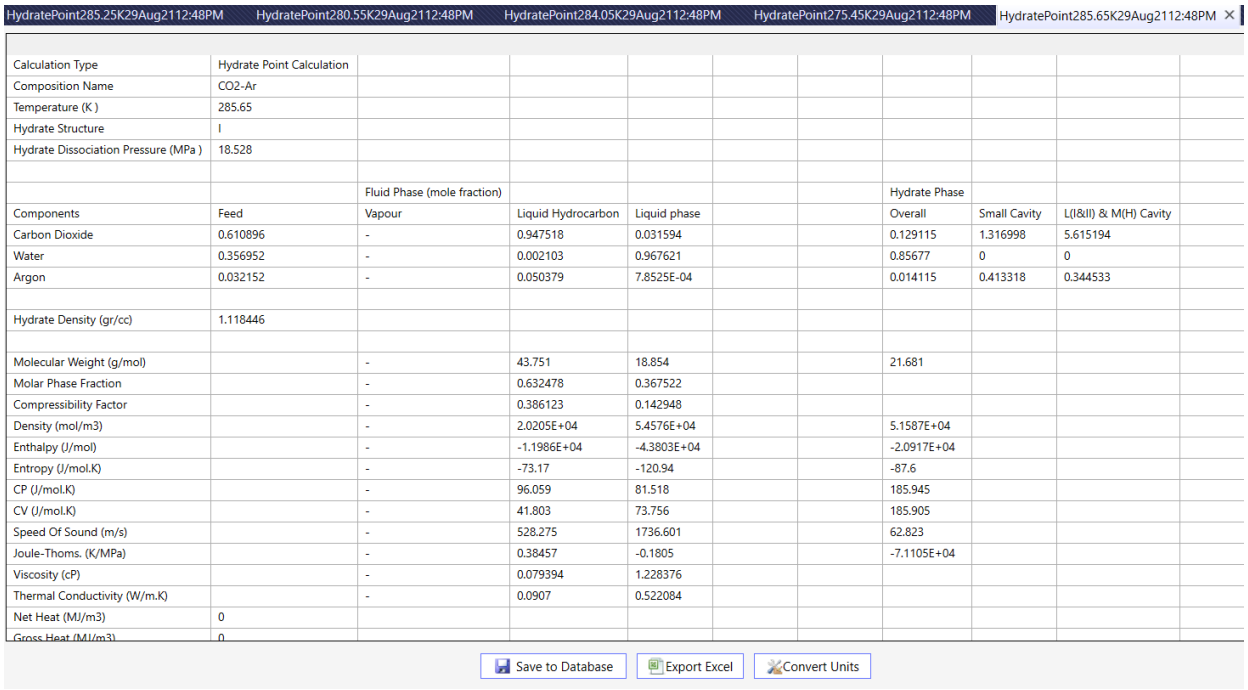

HydratePoint285.25K29Aug2112:48PM | HydratePoint280.55K29Aug2112:48PM | HydratePoint284.05K29Aug2112:48PM | HydratePoint275.45K29Aug2112:48PM | HydratePoint285.65K29Aug2112:48PM

Calculation Type	Hydrate Point Calculation									
Composition Name	CO2-Ar									
Temperature (K)	285.65									
Hydrate Structure	I									
Hydrate Dissociation Pressure (MPa)	18.528									
		Fluid Phase (mole fraction)					Hydrate Phase			
Components	Feed	Vapour	Liquid Hydrocarbon	Liquid phase			Overall	Small Cavity	L(I&II) & M(H) Cavity	
Carbon Dioxide	0.610896	-	0.947518	0.031594			0.129115	1.316998	5.615194	
Water	0.356952	-	0.002103	0.967621			0.85677	0	0	
Argon	0.032152	-	0.050379	7.8525E-04			0.014115	0.413318	0.344533	
Hydrate Density (gr/cc)	1.118446									
Molecular Weight (g/mol)		-	43.751	18.854			21.681			
Molar Phase Fraction		-	0.632478	0.367522						
Compressibility Factor		-	0.386123	0.142948						
Density (mol/m3)		-	2.0205E+04	5.4576E+04			5.1587E+04			
Enthalpy (J/mol)		-	-1.1986E+04	-4.3803E+04			-2.0917E+04			
Entropy (J/mol.K)		-	-73.17	-120.94			-87.6			
CP (J/mol.K)		-	96.059	81.518			185.945			
CV (J/mol.K)		-	41.803	73.756			185.905			
Speed Of Sound (m/s)		-	528.275	1736.601			62.823			
Joule-Thoms. (K/MPa)		-	0.38457	-0.1805			-7.1105E+04			
Viscosity (cP)		-	0.079394	1.228376						
Thermal Conductivity (W/m.K)		-	0.0907	0.522084						
Net Heat (MJ/m3)	0									
Gross Heat (MJ/m3)	0									

Save to Database | Export Excel | Convert Units

Figure 8 Numerical result window for hydrate dissociation of CO_2-Ar mixture in presence of water.

Another big advantage of this software program, is that it allows user to input series of different pressure and temperature conditions when calculating different data. Finally, HydraFLASH results can be showed numerically (Figure 8), graphically or can be exported to an Excel sheet.

2.2. Multiflash

Multiflash is an advanced PVT simulator software which was initally developed by Infochem, while today is owned by KBC, which is acquired by Yokogawa Company. It is used for modeling and solving the phase behavior of complex mixtures and pure components, upstream flow assurance, as well as production and process simulations in the petroleum industry (KBC, 2021). Multiflash special set of tools, models and equations of state allow user to perform many different calculations such as PT flash calculations, PVT analysis, hydrate formation data, wax appearance, asphaltene precipitation etc. Multiflash has a huge set of equations of state (cubic, non-cubic, high accuracy EoS), which user is allowed to pick and change. However, the most common used cubic EoS are shown in models quick load part in software's window (Figure 9), and those are RKSA (Redlich–Kwong-Soave "Advanced"), RKSA Infochem, PRA (Peng-Robinson "Advanced"), PR78A and CPA Infochem (Cubic-Plus-Association). In this project, CPA Infochem will be mostly applied model for our calculations.

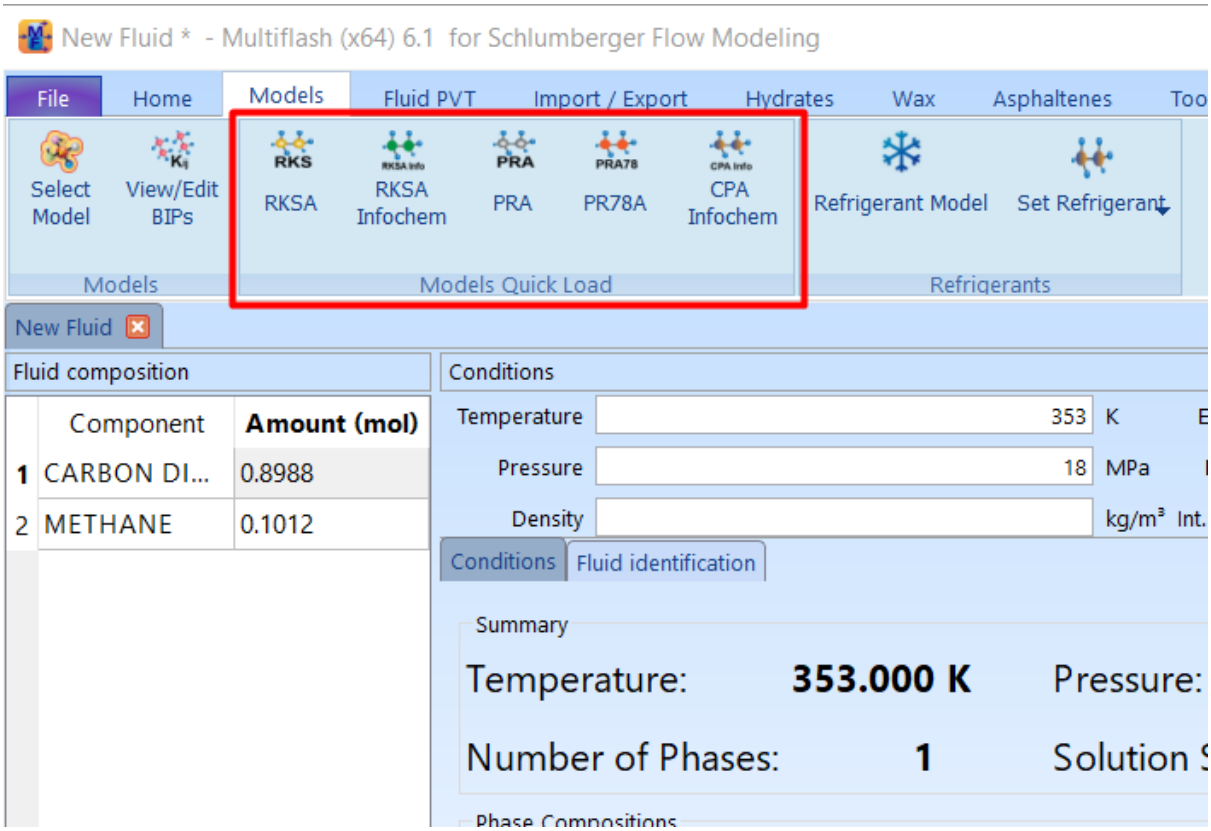

Figure 9 Multiflash software calculation settings window

For simulation of hydrate dissociation data, which calculations will be also conducted in this work, Multiflash proposes three models, and those are: CPA (not applicable for salt components), CPA with electrolytes (applicable for salt components) and RKSA. Multiflash results can also be presented both numerically and graphically, but option for exporting results to Excel is not available in this software.

3. Density

Density is a thermodynamic property which has high importance for CSS processes, as it influences the dimensions of all equipment and storage capacity. It is also very important with respect to energy use in process equipment, and is also needed to high degree of accuracy for most mass flow measurement principles.

As was already mentioned, the CCS process includes three primary elements: capture, transport and storage. For capture, there are three principal technologies: post-combustion capture, pre-combustion capture and oxyfuel combustion. The goal of each of these capture technologies is to produce a stream of concentrated carbon dioxide for compression, transport and storage. However, as none of these capture processes are 100% efficient, gas stream will include a different variation of impurities. The type and concentration of the impurities depends on the type of fuel, capture technology and plant design. The major impurities which are included in the CO_2 stream are nitrogen, oxygen, hydrogen, methane, sulfur dioxide, carbon monoxide, argon and water. These impurities can notably affect the physical properties of the fluid mixtures in comparison to pure CO_2, and therefore they will have a huge influence on the design, safety and cost implications for the compression and transportation of CO_2 for geological storage. Hence, the accurate design of CCS processes needs correct models for calculation properties of CO_2 streams, such as density, enthalpy and entropy. Correct density data of CO_2-rich mixtures are crucial for developing such models (equations of state) and for optimization of existing models.

In this chapter we will perform two density calculations. In the first one, we will examine multi-component mixtures, while in second part, binary mixtures will be discussed. Both experimental data of densities will be compared with predictions obtained using two commercial software, HydraFLASH and Multiflash.

3.1. Density of multi-component mixture

3.1.1. Experimental data

For this type of experiment data, three multi-component mixtures with high content of CO_2 were considered. Mixtures were taken from Nazeri experiment (Nazeri, Chapoy, Burgass, & Tohidi, 2017). Besides CO_2 as a main component, mixtures include other components such as hydrocarbons, nitrogen, hydrogen, oxygen, argon and carbon monoxide, which we define as impurities. First mixture - Mixture 1, consists of 0.9564 mol% of CO_2 and 0.0436 mol% of impurities, and it is a mixture with the highest percent of CO_2. Mixture 2 consists of slightly less CO_2 content of 0.8983 mol % and 0.1017 mol% of impurity. Lastly, Mixture 3 consists of 0.6999 mol% of CO_2 and 0.3001 % of light hydrocarbons. Compositions of these mixtures are showed in Table 1.

Table 1 Compositions of multi-component mixtures (mole%)

Components	Mixture 1	Mixture 2	Mixture 3
Carbon Dioxide	95.64	89.83	69.99
Methane	0.62	0.00	20.02
Ethane	0.00	0.00	6.61
Propane	0.00	0.00	2.58
n-Butane	0.00	0.00	0.39
i-Butane	0.00	0.00	0.39
Nitrogen	1.41	5.05	0.00
Hydrogen	0.82	0.00	0.00
Oxygen	0.08	3.07	0.00
Argon	1.21	2.05	0.00
Carbon Monoxide	0.21	0.00	0.00

During the experiment, oscillating U-tube technique was used. This technique for measuring density is based on an electronic measurement of the frequency of oscillation, from which density value is measured. This principle is based on the Mass-Spring model. Oscillating U-tube densitometer consists of a measuring cell and an evaluation unit which measures the oscillation period. Measuring cell includes a U-shaped tube which function is to electronically vibrate at characteristic frequency. Oven controls the temperature of the densitometer in range between −70 °C to 200 °C (203 -

473 K). Densities of mixtures were measured in the gas, liquid and supercritical phases at pressures up to 126 MPa and at temperatures T/K = 273, 283, 298, 323, 373 and 423 (Nazeri, Chapoy, Burgass, & Tohidi, 2017).

3.1.2. Results

In this work, CPA equation of state was used for thermodynamic modelling. Therefore, in both software CPA model was set up. In Multiflash, CPA-Infochem was set up, while in HydraFLASH sCPA model was applied. After mixtures were introduced to the software, they were then flashed with series of constant pressure and temperature, commonly known as PT Flash. HydraFLASH software has an important advantage here, since it allows PT Flash calculations of many different temperatures and pressures at once, unlike Multiflash, which is limited to a single input of pressure and temperature. Once results were obtained from both software packages, density results were collected and added to Excel spreadsheets. In order to better statistically describe and present results of both software packages, columns with Absolute Error and Relative Error were added to show how much data from numerical model differs from experimental data. The absolute error is calculated by the subtraction of the actual experimental value and the value calculated by software. The ratio of absolute error of the calculation and the experimental value is defined as relative error. By calculating the relative error, we can have an idea of how good the calculation is compared to the actual experimental data. Also, relative average deviation (%RAD) were calculated for both software. Numbers in bold represent better matching with experimental data.

In Figures 10 and 11, the predicted phase envelopes of first mixture using both packages are shown, with added points of experimental data of pressures for three isotherms (273 K, 283 K and 298 K). For the first isotherm – 273 K, at pressure of 6.71 MPa, the fluid is in liquid state (Nazeri, Chapoy, Burgass, & Tohidi, 2017). However, at that point in HydraFLASH software, fluid is in two phase region, while in Multiflash is in single liquid phase, which means that Multiflash will provide more accurate results. Similarly, at isotherm 283 K and pressure point of 6.36 MPa, fluid is in liquid phase in

experiment, but in two software packages at that point, fluid is inside two phase region, which will results in higher deviations, both numerically and graphically.

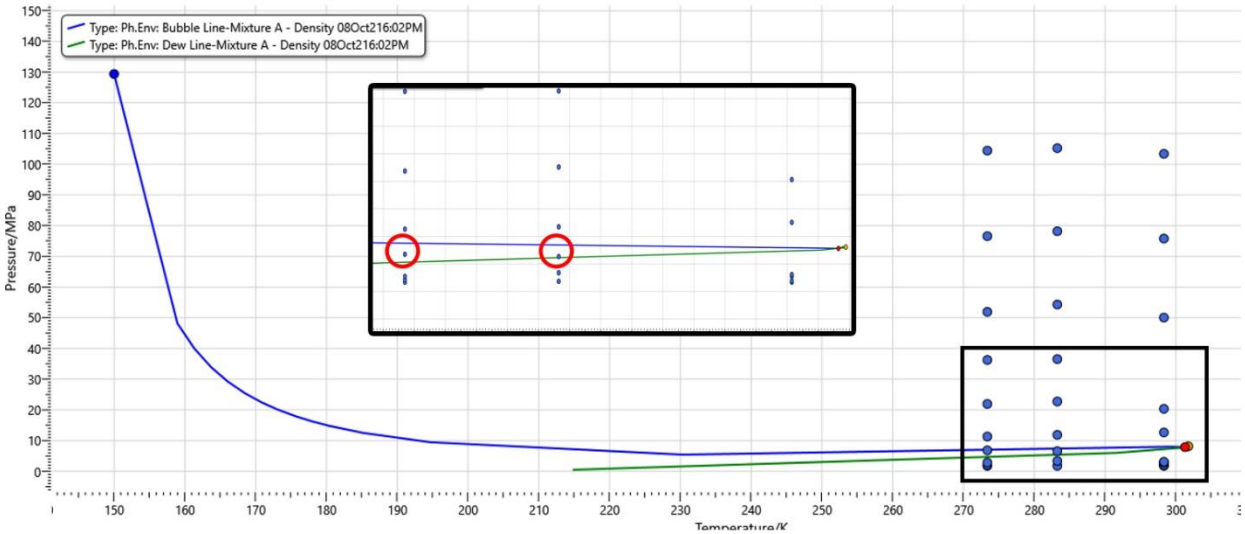

Figure 10 Phase behavior of Mixture 1 in HydraFLASH software with zoomed-in area

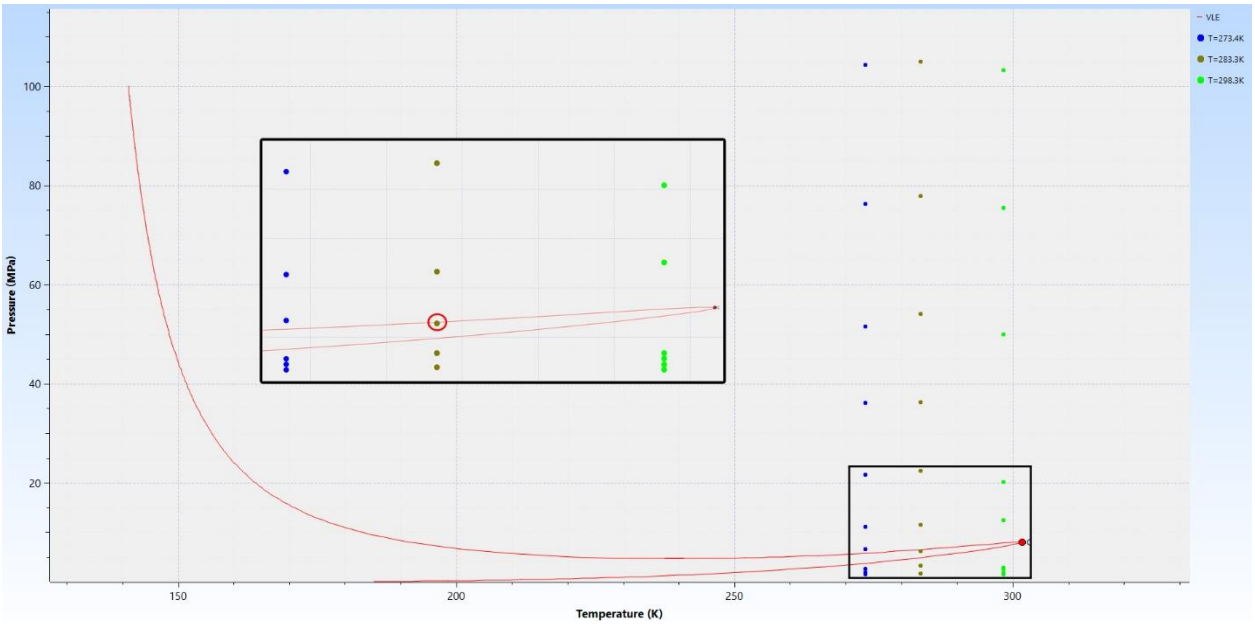

Figure 11 Phase behavior of Mixture 1 in Multiflash software with zoomed-in area

Experimental data and predictions from HydraFLASH and Multiflash software are numerically presented in Tables 2–4 and graphically showed in Figures 12–29. Quantitatively, Multiflash gives better performance in density predictions than HydraFLASH. But, there are a quite a few exceptions in which HydraFLASH shows better results. For all of three mixtures at pressures lower than 5 MPa, both software

programs did an exceptional job in matching experimental data. That is mainly because under 5 MPa, in both software, fluid was mostly in a single gas phase. However, because of the different phase envelope produced for the same fluid, results between two software programs will deviate a bit. At lowest isotherm – 273 K, in HydraFLASH fluid will enter two phase region between pressures 5.53 MPa and 12.2 MPa, while in Multiflash software, pressure area of two phase region is much shorter – between 3.73 MPa and 5.78 MPa. Therefore, for pressures higher than 5 MPa, Multiflash will undoubtedly produce better results in density predictions, since fluid will be in single liquid phase as in the experiment, while in HydraFLASH at those pressures fluid will be inside two phase region and therefore its results will deviate a bit. HydraFLASH results don't deviate too much at slightly higher pressures, up to 50 MPa. But, at pressures higher than 100 MPa, HydraFLASH software showed far poorer performance than Multiflash. At those pressures, difference in results between two software was the highest. Interesting fact is that for all mixtures, HydraFLASH offered better results at isotherms 298.4 K and 323.5 K and pressures up to 50 MPa. HydraFLASH calculations were furthest from experimental data at isotherm 323.5 K and pressures above 100 MPa, which can be clearly seen on Figures 9, 15 and 21. But, since those pressures are not of much interest in CCS processes, Multiflash advantage here is negligible. Relative average deviation (%RAD) for Multiflash was 3.7%, 4.2% and 4.0%, while for HydraFLASH it was 8.7%, 8.9% and 6.5%, respectively.

Regarding the mixtures itself, HydraFLASH provides better results as more CO_2 is presented. Therefore, the best results were performed for Mixture 1. For Mixtures 2 and 3, slightly poorer performance was spotted. At isotherm 323.40 K for both mixtures, much lower agreement with experimental data is showed. For isotherms 273.40 K and 283.30 K, as well as higher temperatures (above 373.50 K) identical behavior with the Mixture 1 graphs is noticed.

In the conclusion, density data obtained from Multiflash software was statistically closer to original experimental data than HydraFLASH data, especially on very high pressures and temperatures. However, for pressures up to 5 MPa, regardless

mixture compositions, HydraFLASH is a safer and more accurate option for modelling density data.

Table 2 Mixture 1 Density results

Conditions		Density (kg/m^3)			Absolute Error ρexp -ρmod (kg/m^3)		Relative Error (ρexp-ρmod)/ρexp (%)	
T (K)	P (MPa)	ρexp	ρmodhydra	ρmodmulti	HydraFLASH	Multiflash	HydraFLASH	Multiflash
273.40	1.71	38.40	36.96	36.78	1.44	1.62	**3.76**	4.22
273.40	2.07	47.40	46.24	45.96	1.16	1.44	**2.45**	3.04
273.40	2.73	66.40	65.32	64.80	1.08	1.60	**1.62**	2.41
273.40	6.71	888.00	942.16	844.02	54.16	43.98	6.10	**4.95**
273.40	11.31	927.80	1005.59	902.04	77.79	25.76	8.38	**2.78**
273.40	21.80	983.90	1089.43	986.22	105.53	2.32	10.73	**0.24**
273.40	36.27	1034.20	1155.09	1060.28	120.89	26.08	11.69	**2.52**
273.40	51.73	1073.60	1199.65	1115.93	126.05	42.33	11.74	**3.94**
273.40	76.40	1121.70	1246.15	1179.90	124.45	58.20	11.09	**5.19**
273.40	104.38	1164.40	1280.73	1232.33	116.33	67.93	9.99	**5.83**
273.40	126.02	1192.10	1300.20	1264.10	108.10	72.00	9.07	**6.04**
283.30	1.81	37.60	37.17	37.27	0.43	0.33	1.14	**0.88**
283.30	3.37	80.40	79.10	79.57	1.30	0.83	1.61	**1.03**
283.30	6.36	810.80	714.73	740.41	96.07	70.39	11.85	**8.68**
283.30	11.68	888.90	805.74	837.01	83.16	51.89	9.36	**5.84**
283.30	22.57	956.30	861.60	943.13	94.70	13.17	9.90	**1.38**
283.30	36.41	1004.60	1211.22	1023.53	206.62	18.93	20.57	**1.88**
283.30	54.13	1052.10	1239.11	1092.91	187.01	40.81	17.77	**3.88**
283.30	78.00	1099.30	1270.28	1158.45	170.98	59.15	15.55	**5.38**
283.30	105.09	1141.30	1296.01	1212.39	154.71	71.09	13.56	**6.23**
283.30	124.85	1167.10	1310.47	1243.44	143.37	76.34	12.28	**6.54**
298.30	1.68	32.10	31.86	31.94	0.24	0.16	0.75	**0.50**
298.30	1.96	38.60	37.77	37.89	0.83	0.71	2.15	**1.84**
298.30	2.76	57.00	55.89	56.15	1.11	0.85	1.95	**1.49**
298.30	3.08	64.80	63.73	64.08	1.07	0.72	1.65	**1.11**
298.30	12.55	778.40	692.37	727.99	86.04	50.41	11.05	**6.48**
298.40	20.26	865.20	801.55	840.56	63.65	24.64	7.36	**2.85**
298.40	50.12	999.60	1019.62	1029.40	20.02	29.80	**2.00**	2.98
298.40	75.62	1061.80	1410.07	1113.24	348.27	51.44	32.80	**4.84**
298.40	103.39	1111.80	1357.06	1176.34	245.26	64.54	22.06	**5.81**
298.40	126.33	1145.60	1351.92	1216.15	206.32	70.55	18.01	**6.16**
323.40	1.45	24.00	24.57	24.63	0.57	0.63	**2.39**	2.63
323.40	2.19	37.40	38.24	38.38	0.84	0.98	**2.25**	2.62
323.40	3.60	66.00	66.93	67.36	0.93	1.36	**1.41**	2.06
323.40	5.22	104.60	105.53	106.62	0.93	2.02	**0.89**	1.93
323.40	8.27	209.50	206.39	211.16	3.11	1.66	1.48	**0.79**
323.40	15.88	642.40	566.39	593.94	76.01	48.46	11.83	**7.54**
323.40	22.59	758.50	692.62	725.32	65.88	33.18	8.69	**4.37**
323.40	29.52	822.10	771.37	806.07	50.73	16.03	6.17	**1.95**
323.40	54.07	941.50	937.50	966.26	4.00	24.76	**0.42**	2.63
323.40	77.97	1008.70	1063.83	1055.86	55.13	47.16	5.47	**4.68**
323.40	106.00	1065.50	1469.18	1128.17	403.68	62.67	37.89	**5.88**

323.40	126.46	1099.10	1537.78	1168.49	438.68	69.39	39.91	**6.31**
373.50	2.12	29.10	30.88	30.91	1.78	1.81	**6.11**	6.22
373.50	2.75	40.20	40.63	40.70	0.43	0.50	**1.08**	1.24
373.50	3.52	50.30	52.95	53.06	2.65	2.76	**5.26**	5.49
373.50	5.24	79.90	82.10	82.37	2.20	2.47	**2.76**	3.09
373.50	10.61	191.40	189.72	191.06	1.68	0.34	0.88	**0.18**
373.50	26.16	568.50	530.47	534.15	38.03	34.35	6.69	**6.04**
373.50	53.57	805.30	820.50	807.24	15.20	1.94	1.89	**0.24**
373.50	77.94	900.80	968.07	929.18	67.27	28.38	7.47	**3.15**
373.60	104.58	970.60	1097.93	1018.15	127.33	47.55	13.12	**4.90**
373.60	123.18	1008.70	1186.44	1065.44	177.74	56.74	17.62	**5.63**
423.40	0.95	11.40	11.80	11.79	0.40	0.39	3.51	**3.42**
423.40	2.09	25.30	26.36	26.35	1.06	1.05	4.18	**4.14**
423.40	3.59	44.50	46.18	46.15	1.68	1.65	3.77	**3.71**
423.40	5.28	66.80	69.43	69.37	2.63	2.57	3.94	**3.85**
423.40	7.74	101.70	104.98	104.82	3.28	3.12	3.22	**3.07**
423.40	34.18	521.30	508.66	496.51	12.64	24.79	**2.42**	4.76
423.40	53.52	682.40	707.61	674.37	25.21	8.03	3.69	**1.18**
423.40	76.14	791.70	869.33	807.33	77.63	15.63	9.81	**1.97**
423.40	104.16	880.10	1017.42	918.49	137.32	38.39	15.60	**4.36**
423.40	121.85	922.50	1093.53	971.56	171.03	49.06	18.54	**5.32**

Table 3 Mixture 2 Density results

Conditions		Density (kg/m^3)			Absolute Error ρexp -ρmod (kg/m^3)		Relative Error (ρexp-ρmod)/ρexp (%)	
T (K)	P (MPa)	ρexp	ρmod$_{hydra}$	ρmod$_{multi}$	HydraFLASH	Multiflash	HydraFLASH	Multiflash
273.20	1.79	38.40	38.16	38.00	0.24	0.40	**0.63**	1.04
273.20	2.24	49.80	49.59	49.35	0.21	0.45	**0.42**	0.91
273.30	8.80	841.60	883.43	811.31	41.83	30.29	4.97	**3.60**
273.30	10.92	867.70	920.62	843.50	52.92	24.20	6.10	**2.79**
273.30	21.00	941.00	1027.58	943.06	86.58	2.06	9.20	**0.22**
273.30	52.04	1048.90	1165.58	1093.12	116.68	44.22	11.12	**4.22**
273.30	104.16	1145.60	1258.09	1215.31	112.49	69.71	9.82	**6.09**
273.30	125.71	1174.90	1280.41	1248.52	105.51	73.62	8.98	**6.27**
283.30	1.74	37.00	34.87	34.99	2.13	2.01	5.75	**5.43**
283.30	2.28	46.50	47.38	47.60	0.88	1.10	**1.89**	2.37
283.30	10.67	803.70	722.43	755.77	81.27	47.93	10.11	**5.96**
283.30	20.84	895.00	875.09	888.56	19.91	6.44	2.22	**0.72**
283.30	52.46	1012.60	1193.62	1062.71	181.02	50.11	17.88	**4.95**
283.30	104.12	1114.40	1269.38	1193.56	154.98	79.16	13.91	**7.10**
283.30	125.26	1145.30	1288.44	1228.43	143.14	83.13	12.50	**7.26**
298.40	2.08	39.20	39.56	39.71	0.36	0.51	**0.92**	1.30
298.40	3.53	75.30	73.06	73.60	2.24	1.70	2.98	**2.26**
298.40	12.58	702.10	617.40	652.09	84.70	50.01	12.06	**7.12**
298.40	20.81	827.00	762.83	800.00	64.17	27.00	7.76	**3.26**
298.40	51.34	979.90	1000.44	1008.23	20.54	28.33	**2.10**	2.89
298.40	104.10	1097.00	1321.32	1160.03	224.32	63.03	20.45	**5.75**
298.40	125.88	1130.30	1323.11	1199.44	192.81	69.14	17.06	**6.12**
323.50	2.57	45.30	44.71	44.92	0.59	0.38	1.30	**0.84**

323.50	3.70	67.50	67.35	67.84	0.16	0.34	**0.23**	0.50
323.50	12.27	409.10	361.31	379.71	47.79	29.39	11.68	**7.18**
323.50	20.91	687.50	618.38	649.33	69.12	38.17	10.05	**5.55**
323.50	51.56	909.30	897.75	927.22	11.55	17.92	**1.27**	1.97
323.50	105.06	1047.70	1398.31	1107.95	350.61	60.25	33.46	**5.75**
323.50	125.48	1082.40	1486.12	1150.23	403.72	67.83	37.30	**6.27**
373.60	1.53	20.70	21.70	21.72	1.00	1.02	**4.83**	4.95
373.60	2.57	34.50	37.22	37.29	2.72	2.79	**7.87**	8.09
373.60	17.22	353.90	324.85	329.96	29.05	23.94	8.21	**6.76**
373.60	21.00	439.70	404.02	410.44	35.68	29.26	8.12	**6.65**
373.60	52.56	777.70	783.65	775.79	5.95	1.91	0.77	**0.25**
373.60	103.94	951.80	1067.68	998.37	115.88	46.57	12.17	**4.89**
373.60	125.15	996.10	1166.48	1053.54	170.38	57.44	17.10	**5.77**
423.40	2.40	30.40	29.98	29.99	0.42	0.41	1.39	**1.36**
423.40	3.41	43.60	43.09	43.11	0.51	0.49	1.17	**1.12**
423.40	18.47	283.70	265.16	264.78	18.54	18.92	**6.54**	6.67
423.40	21.75	335.50	315.24	314.17	20.26	21.33	**6.04**	6.36
423.40	52.79	660.60	674.34	649.20	13.74	11.40	2.08	**1.73**
423.40	102.77	862.50	982.18	897.26	119.68	34.76	13.88	**4.03**
423.40	124.65	915.90	1075.08	963.70	159.18	47.80	17.38	**5.22**

Table 4 Mixture 3 Density results

Conditions		Density (kg/m^3)			Absolute Error ρexp -ρmod (kg/m^3)		Relative Error (ρexp-ρmod)/ρexp (%)	
T (K)	P (MPa)	ρexp	ρmodhydra	ρmodmulti	HydraFLASH	Multiflash	HydraFLASH	Multiflash
273.30	1.07	20.00	18.99	18.95	1.01	1.05	**5.07**	5.25
273.30	2.13	41.60	41.01	40.87	0.59	0.73	**1.42**	1.75
273.30	12.71	685.50	680.48	646.91	5.02	38.59	**0.73**	5.63
273.30	20.89	740.20	761.82	723.62	21.62	16.58	2.92	**2.24**
273.30	52.28	838.10	895.46	862.20	57.36	24.10	6.84	**2.87**
273.30	103.76	920.20	982.97	965.88	62.77	45.68	6.82	**4.96**
273.30	124.50	944.30	1003.91	992.84	59.61	48.54	6.31	**5.14**
283.30	1.12	18.70	19.02	19.05	0.32	0.35	**1.71**	1.86
283.30	2.09	36.80	37.73	37.85	0.93	1.05	**2.54**	2.85
283.30	4.87	110.80	113.11	114.47	2.31	3.67	**2.08**	3.31
283.30	9.52	564.70	494.64	515.12	70.06	49.58	12.41	**8.78**
283.30	20.63	701.40	674.84	680.45	26.56	20.95	3.79	**2.99**
283.30	51.89	814.30	901.44	837.35	87.14	23.05	10.70	**2.83**
283.30	103.37	902.80	984.59	949.48	81.79	46.68	9.06	**5.17**
283.30	125.37	929.60	1005.76	979.80	76.16	50.20	8.19	**5.40**
298.40	1.10	18.60	17.53	17.56	1.07	1.04	5.75	**5.59**
298.40	2.09	36.00	35.02	35.13	0.98	0.87	2.73	**2.42**
298.40	5.18	108.20	106.32	107.52	1.88	0.68	1.73	**0.63**
298.40	10.96	462.00	405.00	423.17	57.01	38.83	12.34	**8.40**
298.30	20.83	642.90	593.99	617.04	48.91	25.86	7.61	**4.02**
298.30	51.73	779.90	792.02	800.54	12.12	20.64	**1.55**	2.65
298.30	102.11	873.80	1004.78	923.33	130.98	49.53	14.99	**5.67**
298.30	124.97	903.90	1018.24	957.95	114.34	54.05	12.65	**5.98**
323.50	1.22	19.30	17.78	17.81	1.52	1.49	7.86	**7.71**

323.50	2.11	32.70	31.77	31.87	0.93	0.83	2.85	**2.54**
323.50	5.23	90.60	89.64	90.47	0.96	0.13	1.06	**0.14**
323.50	11.81	316.80	280.74	290.09	36.06	26.71	11.38	**8.43**
323.50	20.23	531.80	480.32	498.79	51.48	33.01	9.68	**6.21**
323.50	49.82	718.00	710.90	732.32	7.10	14.32	**0.99**	1.99
323.50	103.43	837.20	1019.60	885.97	182.40	48.77	21.79	**5.83**
323.50	124.84	868.20	1090.52	922.51	222.32	54.31	25.61	**6.26**
373.60	2.10	24.50	26.52	26.55	2.02	2.05	**8.24**	8.37
373.60	5.24	68.90	70.57	70.83	1.67	1.93	**2.43**	2.80
373.60	10.43	156.30	155.45	156.62	0.85	0.32	0.54	**0.20**
373.60	20.73	364.20	336.28	340.21	27.92	23.99	7.67	**6.59**
373.60	46.52	601.30	596.25	596.79	5.05	4.51	0.84	**0.75**
373.60	63.16	668.40	688.53	682.40	20.13	14.00	3.01	**2.09**
373.60	63.34	667.70	689.39	683.17	21.69	15.46	3.25	**2.32**
373.60	103.40	767.80	841.35	808.64	73.55	40.84	9.58	**5.32**
373.60	122.28	800.70	901.18	848.59	100.48	47.89	12.55	**5.98**
373.60	125.29	804.90	910.51	854.25	105.61	49.35	13.12	**6.13**
423.40	2.12	23.20	23.23	23.23	0.03	0.03	**0.13**	0.13
423.40	5.22	58.20	59.24	59.26	1.04	1.06	**1.79**	1.82
423.40	10.36	120.50	123.59	123.59	3.09	3.09	**2.56**	2.56
423.40	20.94	258.30	261.47	260.70	3.17	2.40	1.23	**0.93**
423.50	29.08	371.60	356.24	353.53	15.36	18.07	**4.13**	4.86
423.50	49.87	527.20	533.71	521.76	6.51	5.44	1.24	**1.03**
423.50	103.36	704.50	781.98	737.82	77.48	33.32	11.00	**4.73**
423.50	124.80	746.20	846.39	789.18	100.19	42.98	13.43	**5.76**

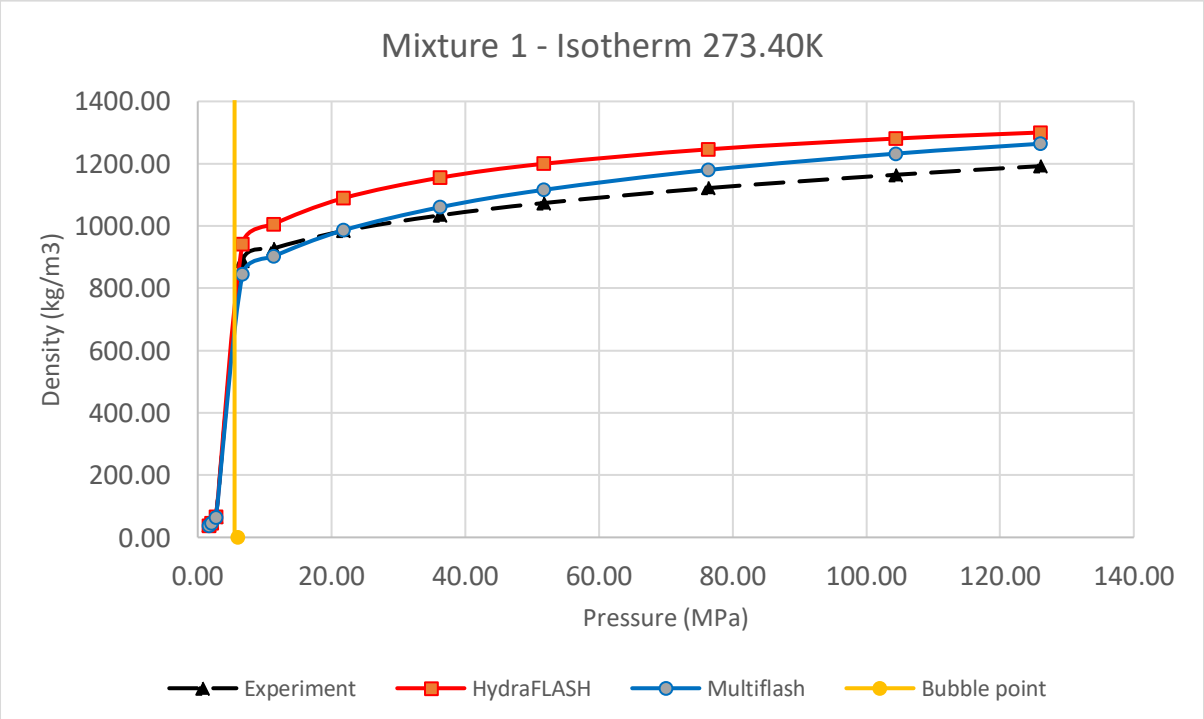

Figure 12 Density results for Mixture 1, Isotherm 273.40 K with saturation pressure at 5.99 MPa

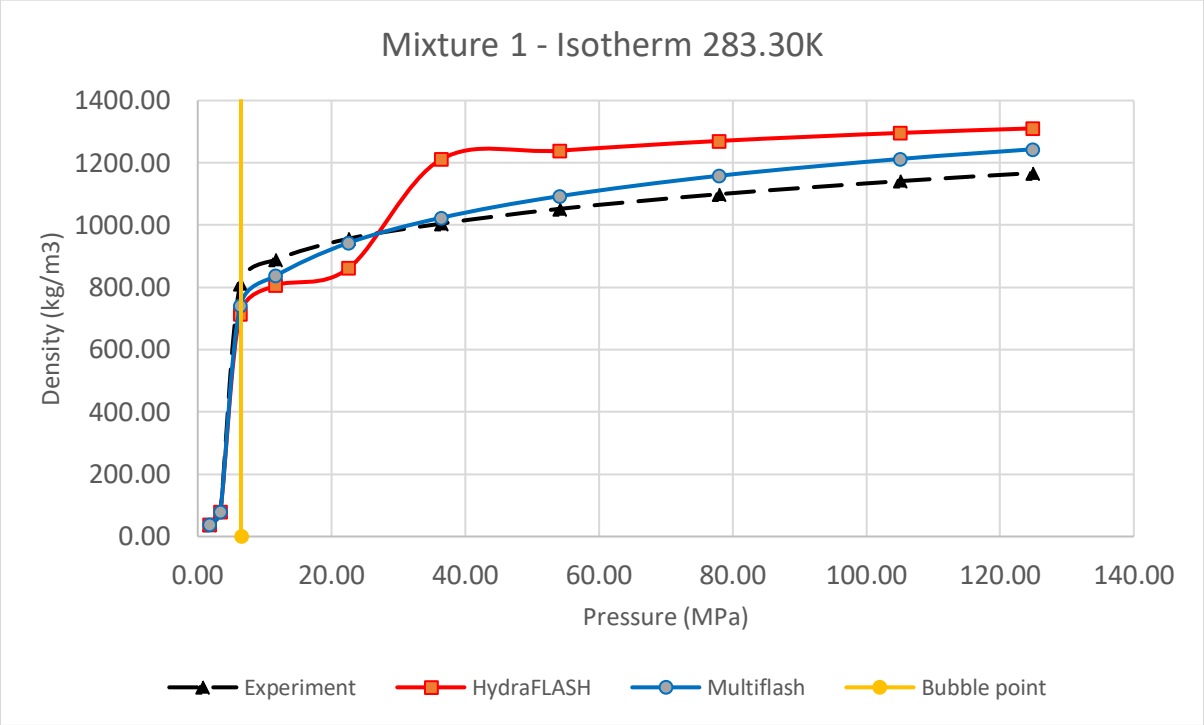

Figure 13 Density results for Mixture 1, Isotherm 283.30 K with saturation pressure at 6.61 MPa

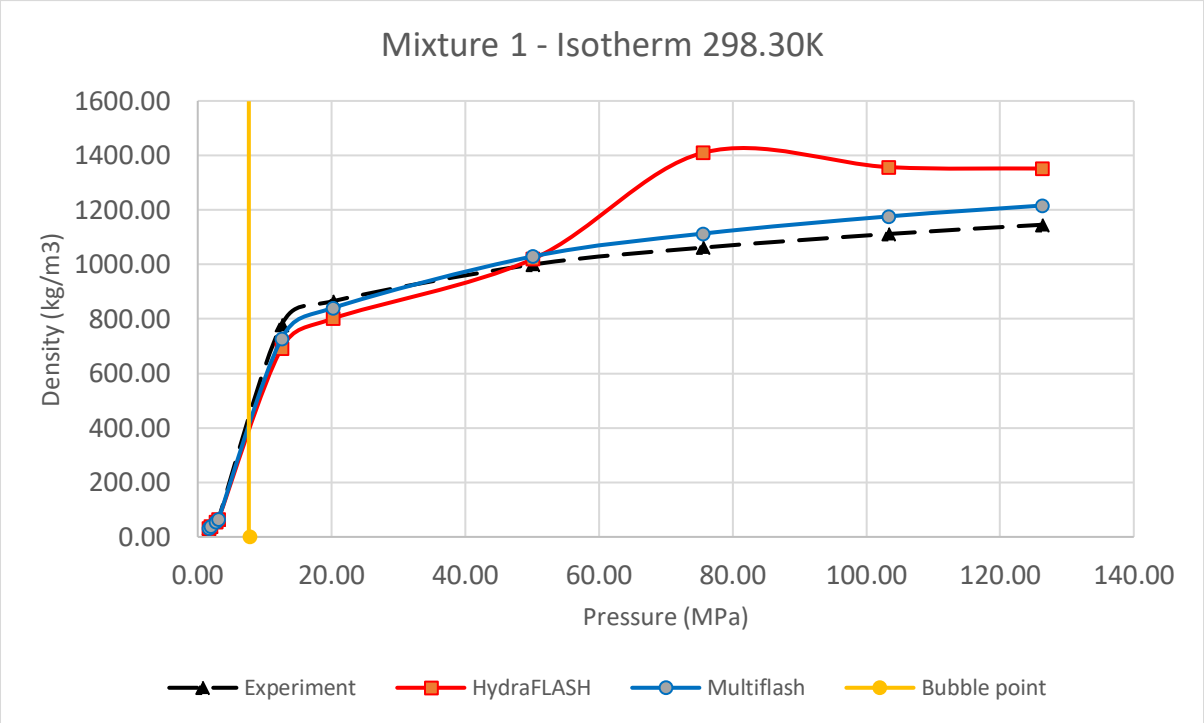

Figure 14 Density results for Mixture 1, Isotherm 298.30 K with saturation pressure at 7.8 MPa

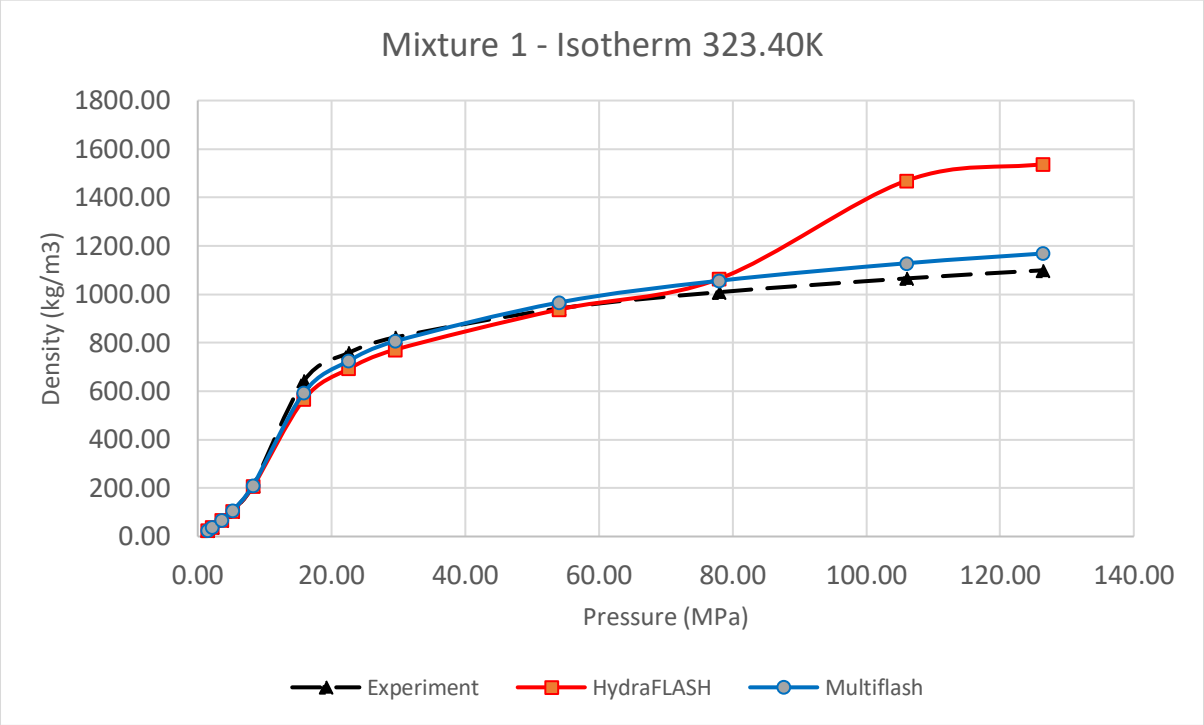

Figure 15 Density results for Mixture 1, Isotherm 323.40 K

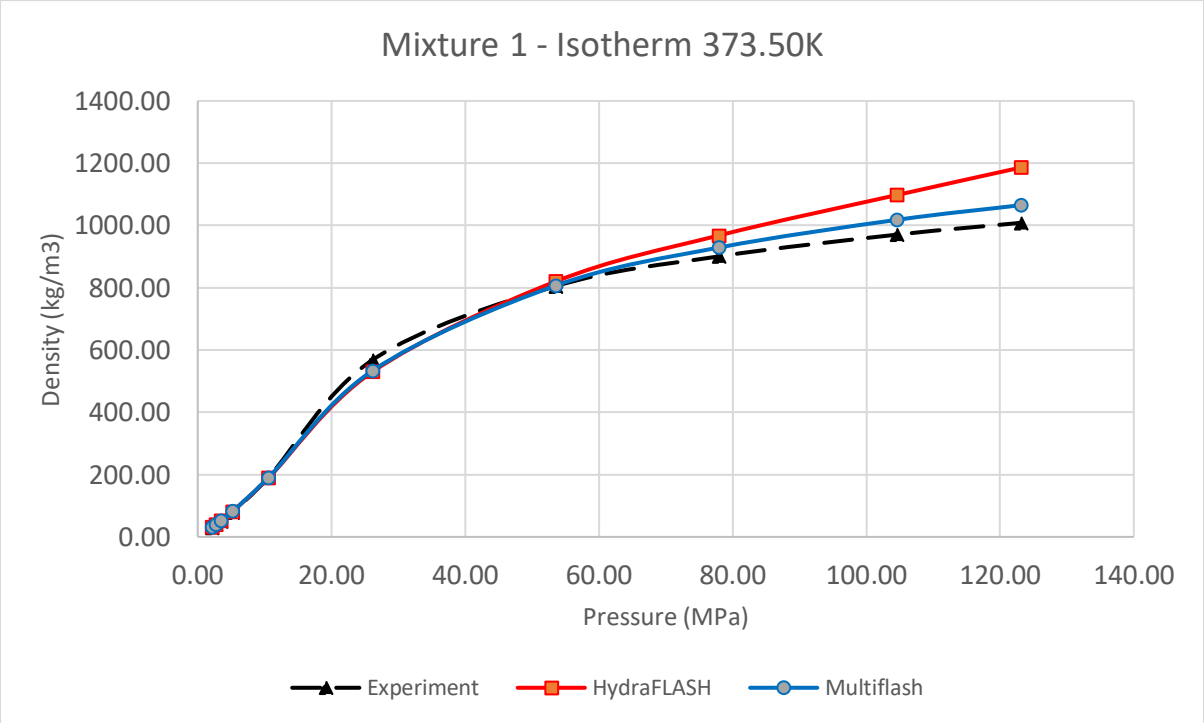

Figure 16 Density results for Mixture 1, Isotherm 373.50 K

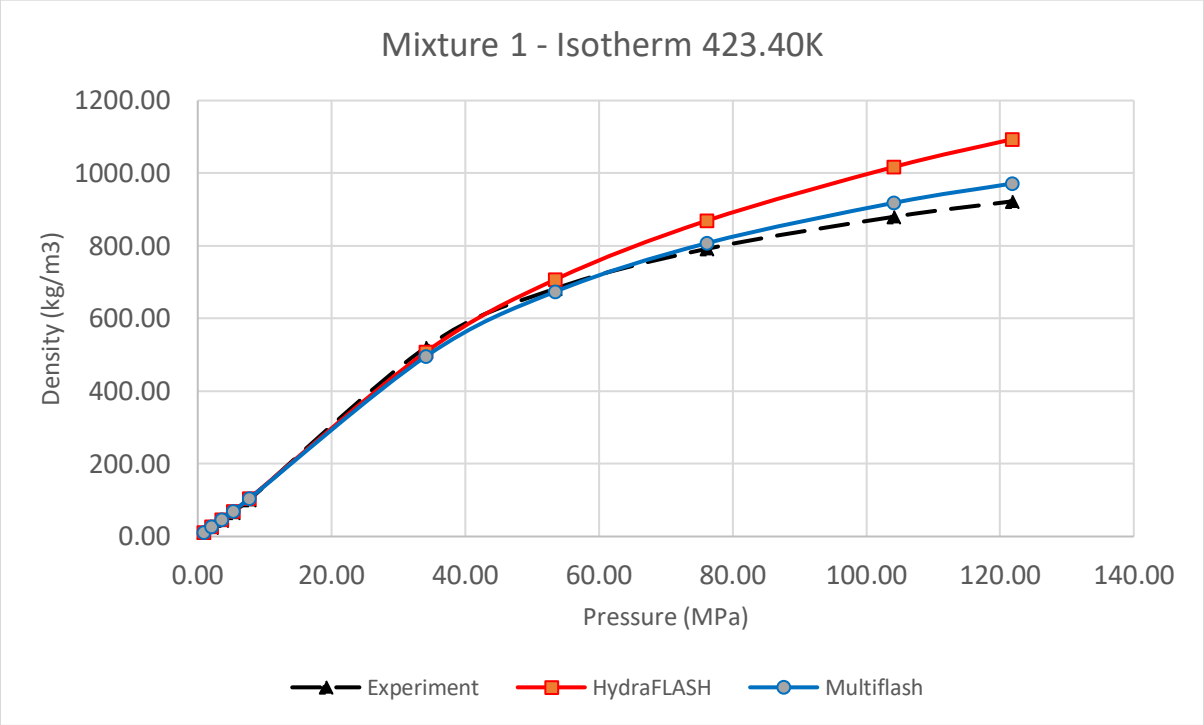

Figure 17 Density results for Mixture 1, Isotherm 423.40 K

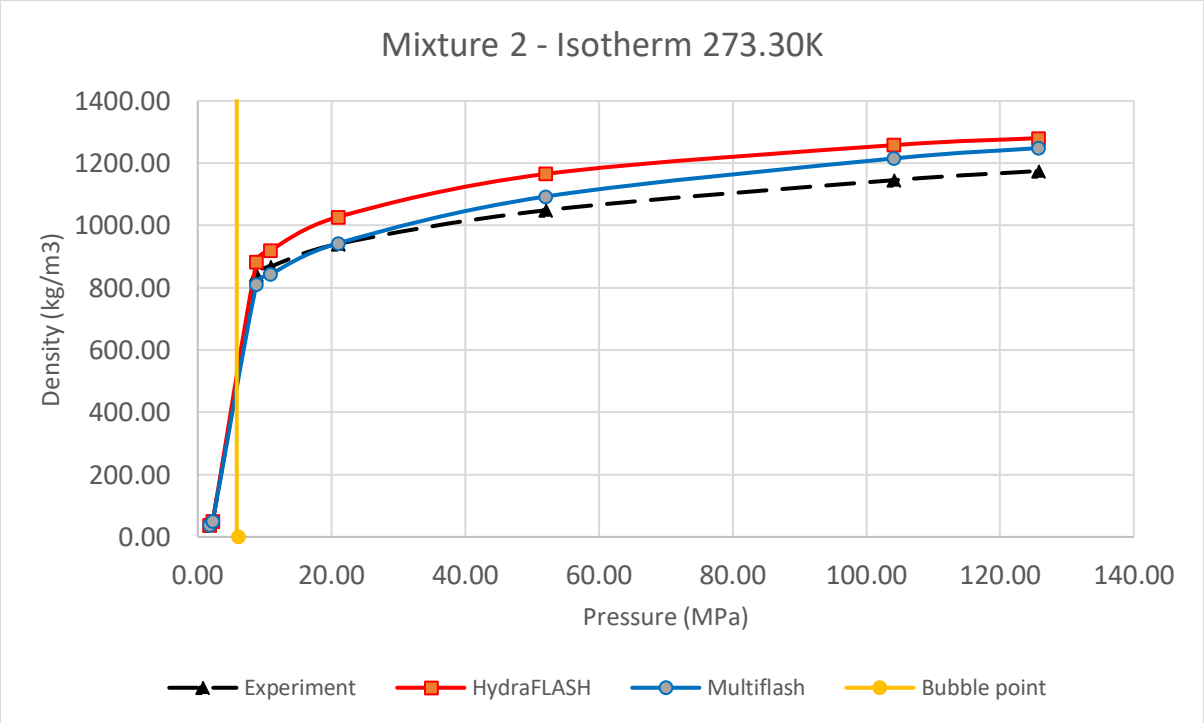

Figure 18 Density results for Mixture 2, Isotherm 273.30 K with saturation pressure at 6.06 MPa

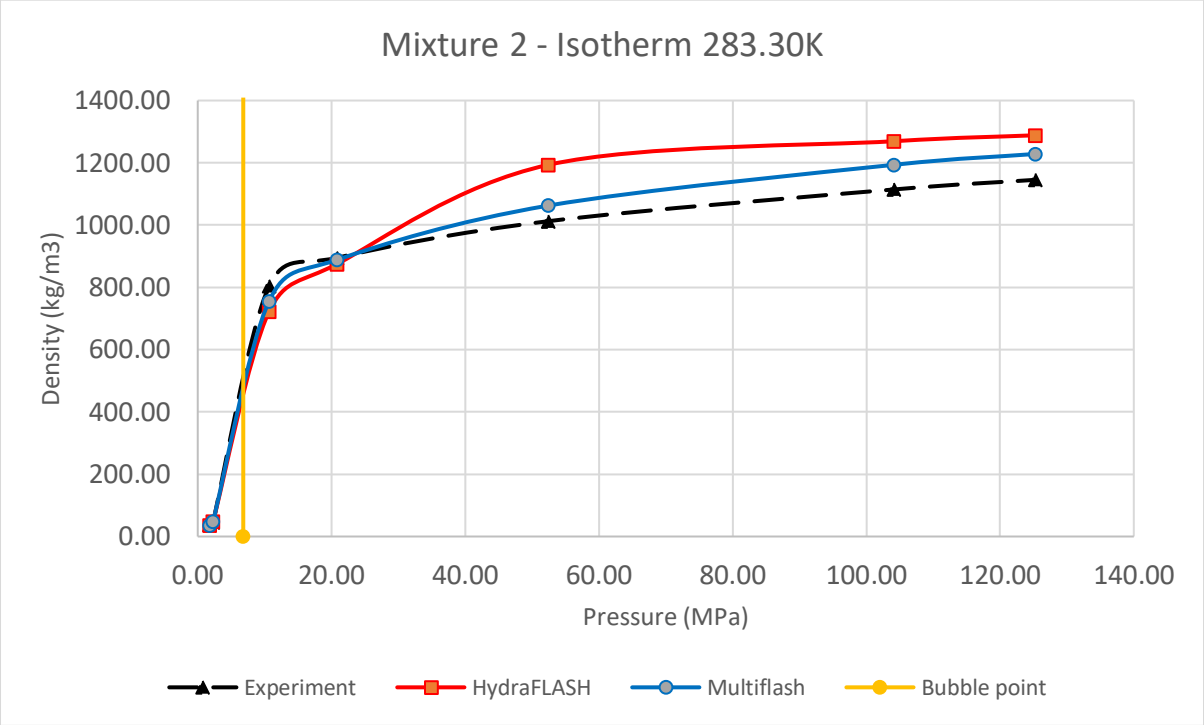

Figure 19 Density results for Mixture 2, Isotherm 283.30 K with saturation pressure at 6.8 MPa

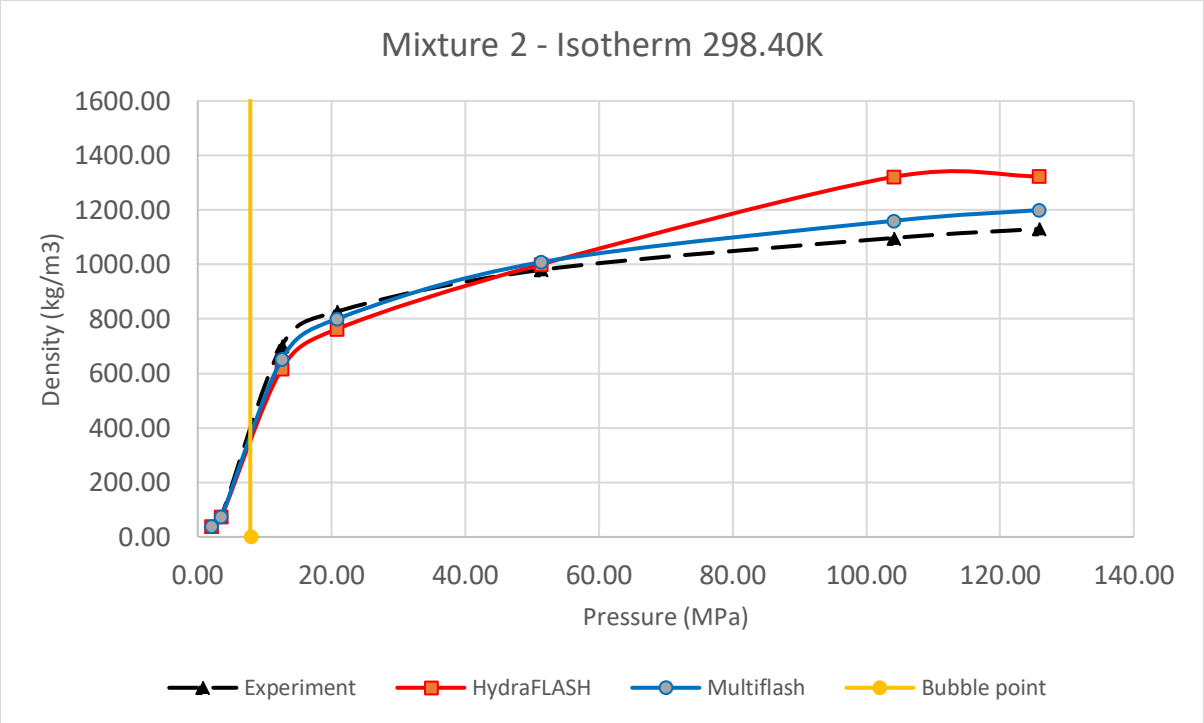

Figure 20 Density results for Mixture 2, Isotherm 298.40 K with saturation pressure at 8.1 MPa

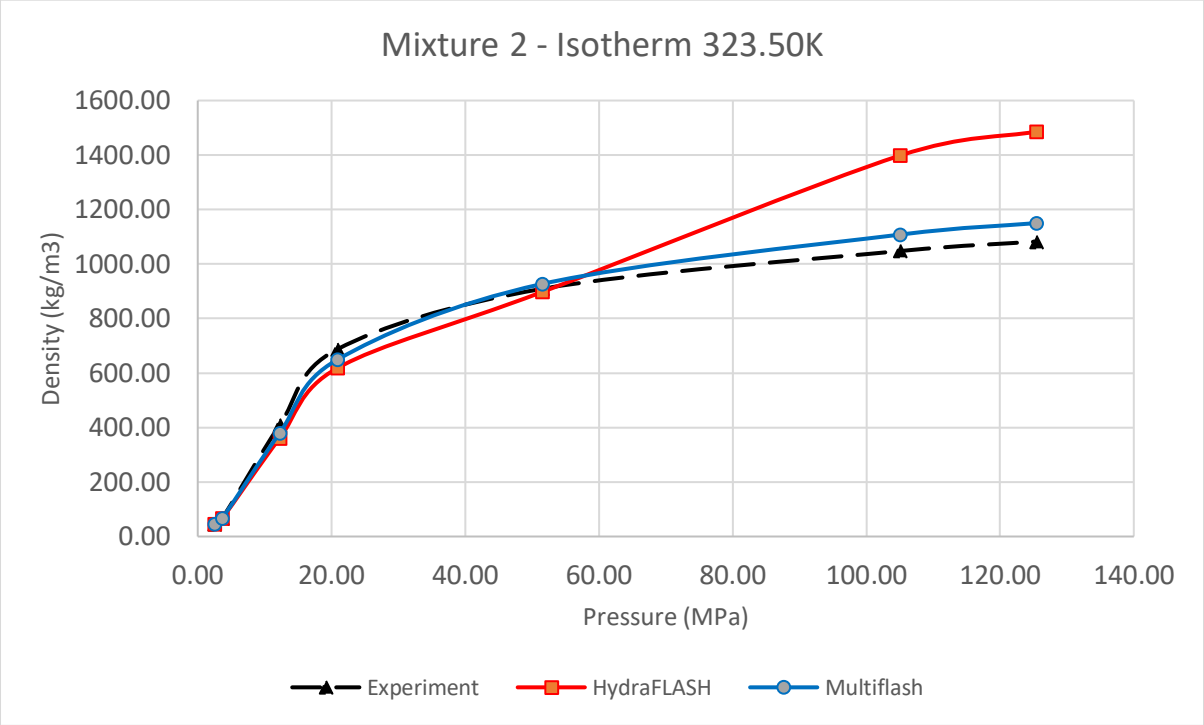

Figure 21 Density results for Mixture 2, Isotherm 323.50 K

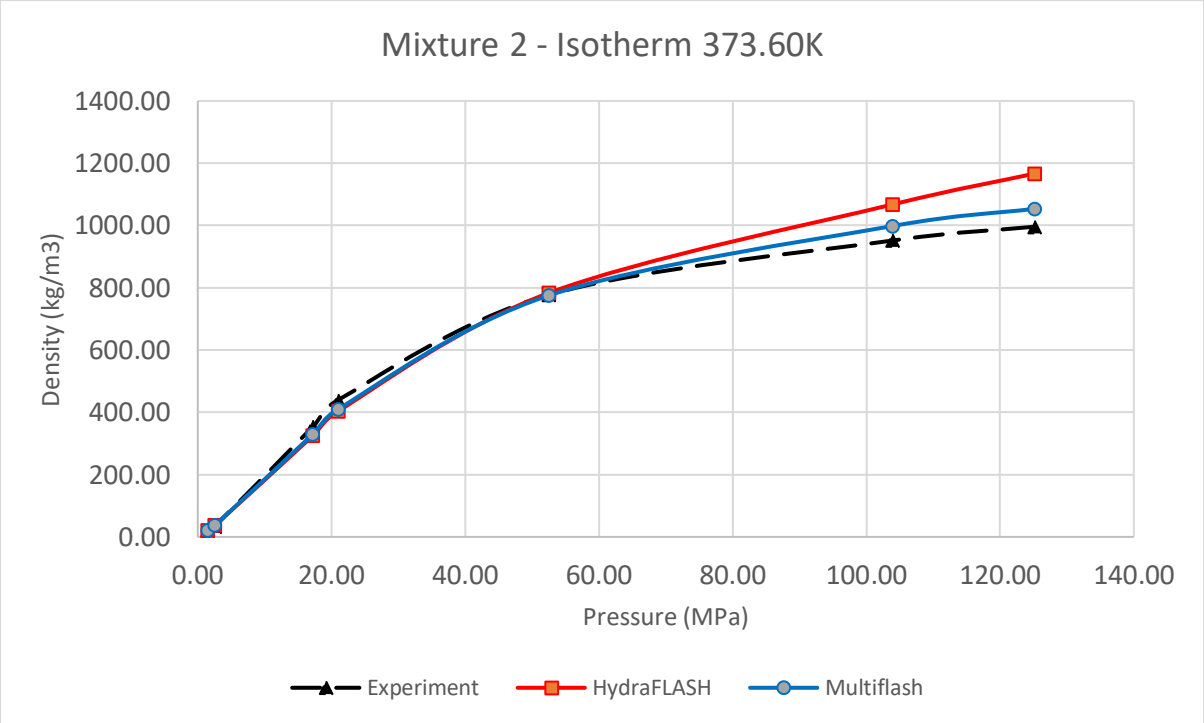

Figure 22 Density results for Mixture 2, Isotherm 373.60 K

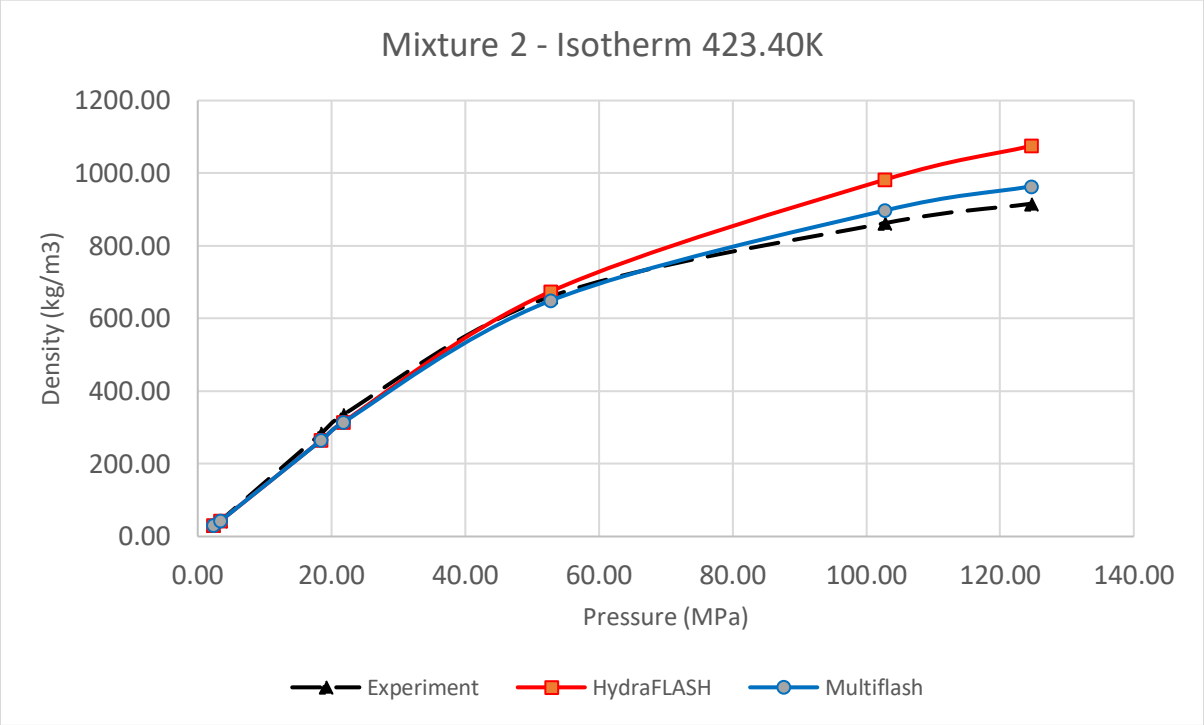

Figure 23 Density results for Mixture 2, Isotherm 423.40 K

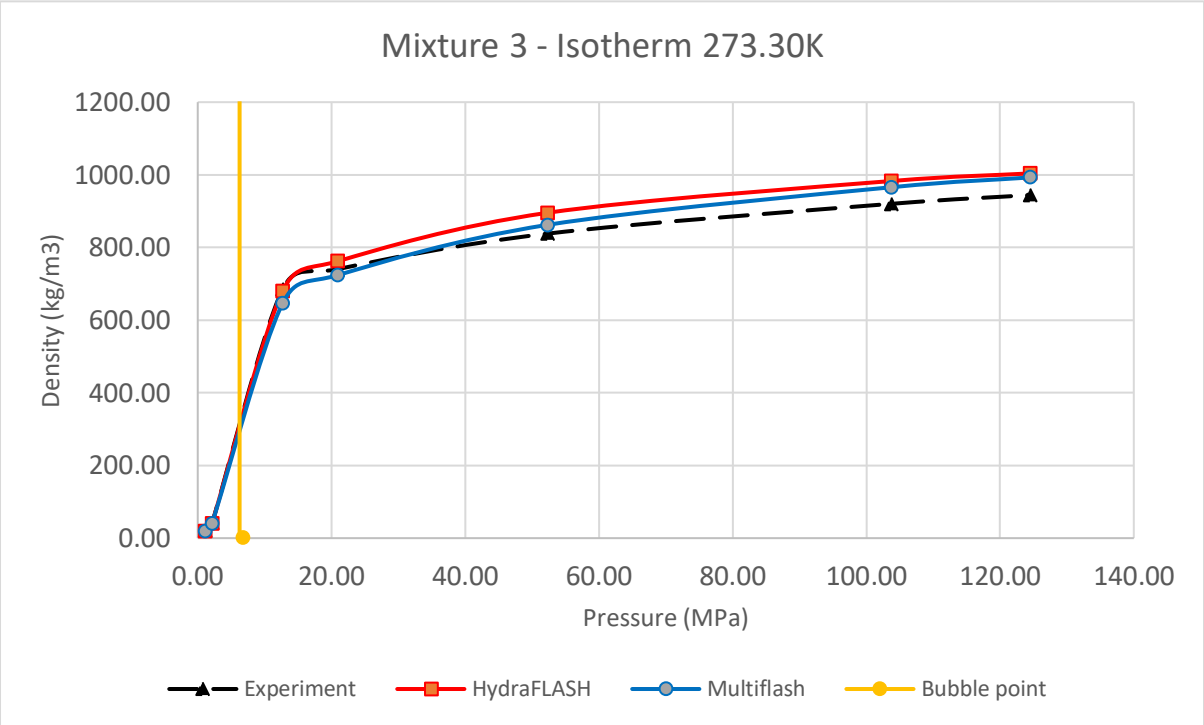

Figure 24 Density results for Mixture 3, Isotherm 273.30 K with saturation pressure at 6.8 MPa

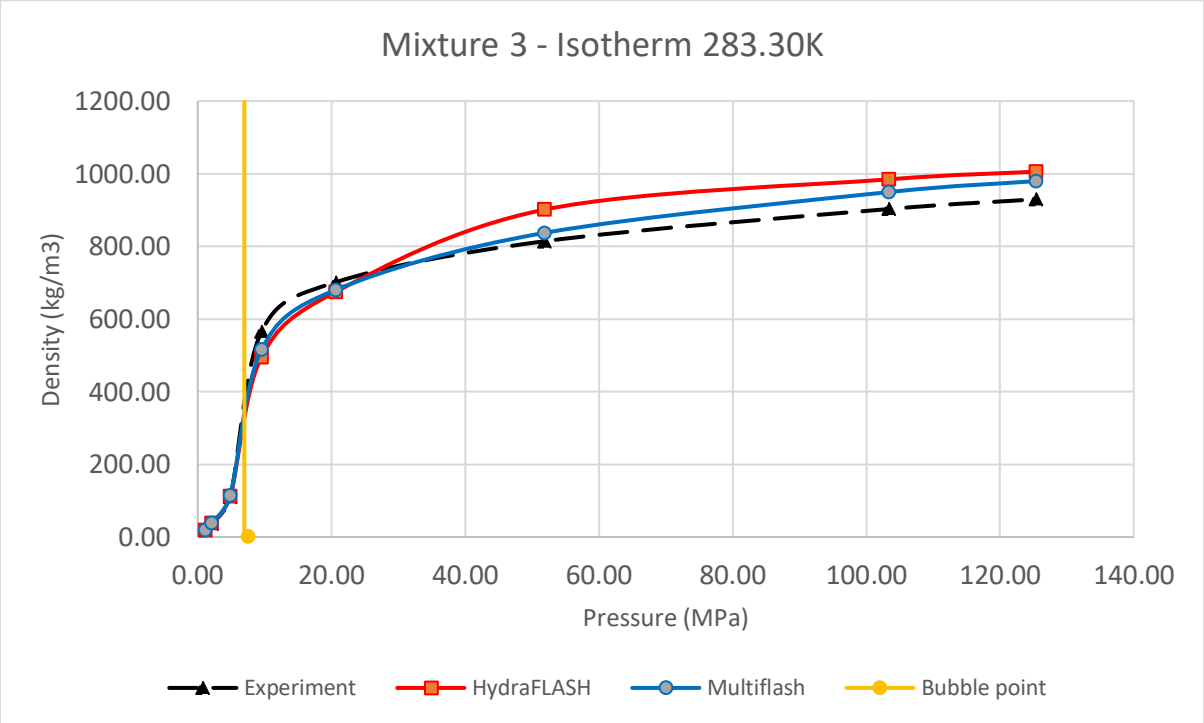

Figure 25 Density results for Mixture 3, Isotherm 283.30 K with saturation pressure at 7.54 MPa

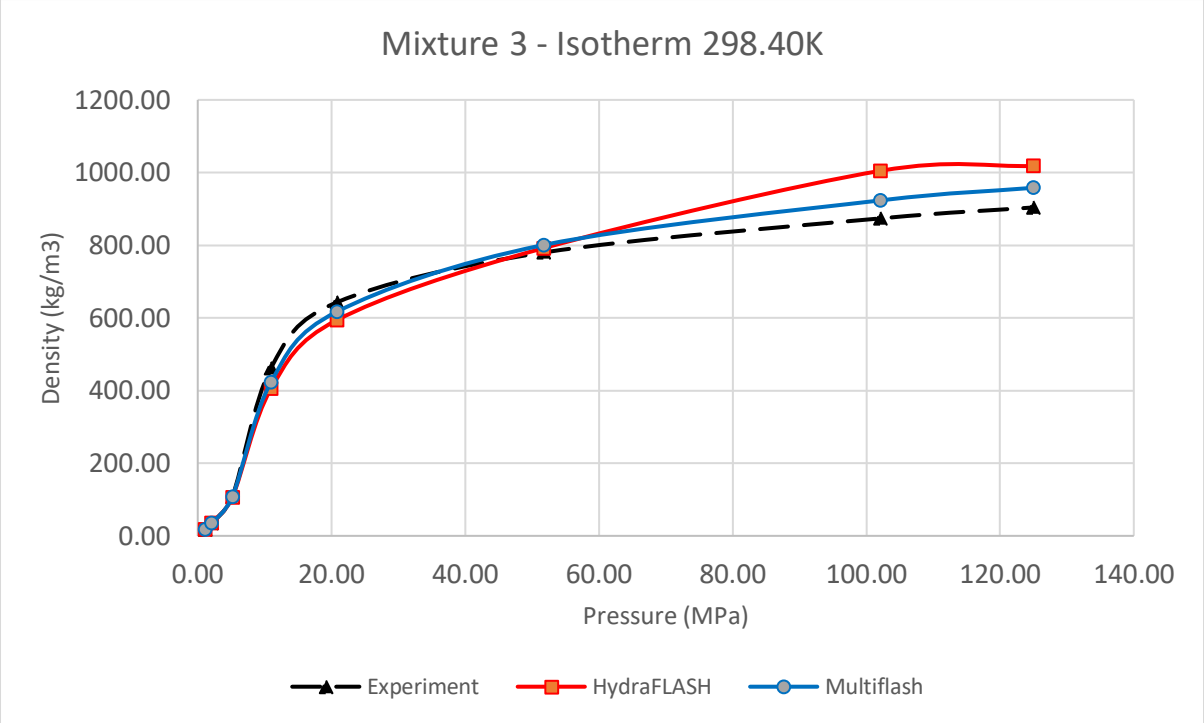

Figure 26 Density results for Mixture 3, Isotherm 298.40 K

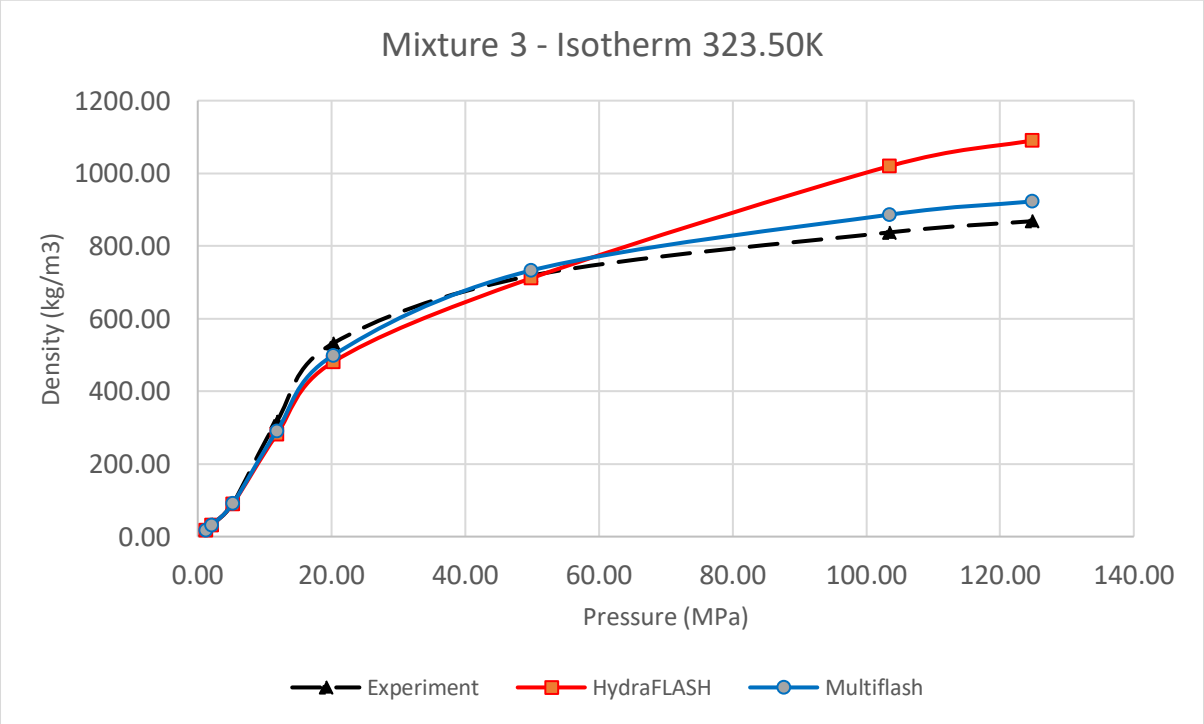

Figure 27 Density results for Mixture 3, Isotherm 323.50 K

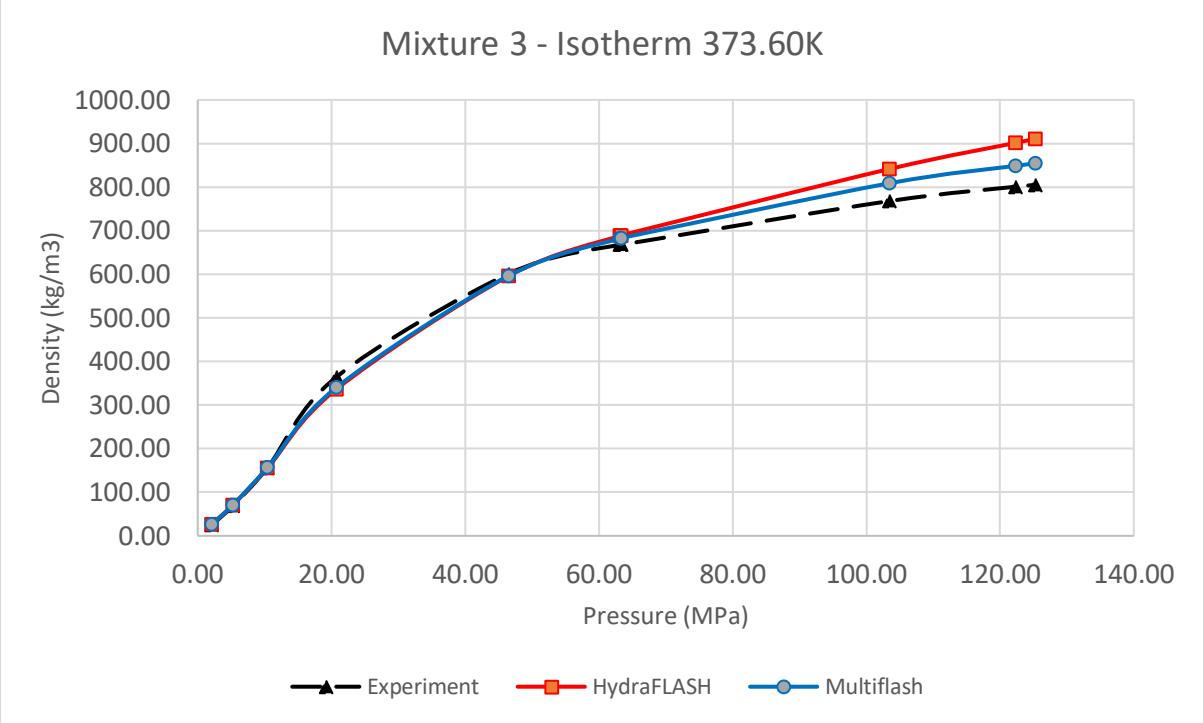

Figure 28 Density results for Mixture 3, Isotherm 373.60 K

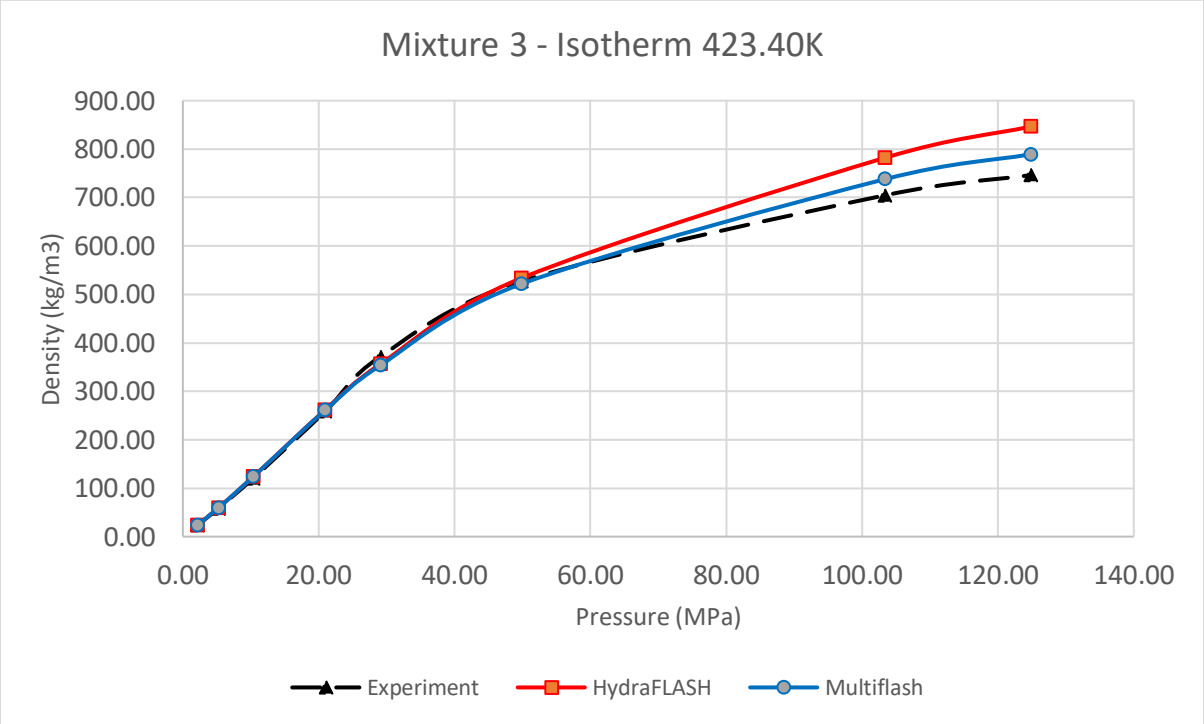

Figure 29 Density results for Mixture 3, Isotherm 423.40 K

3.2. Density of binary CO_2-CH_4 mixture

Accurate prediction of density data for the binary CO_2−CH_4 system is very important for the process of natural gas purification and CCS processes. In those processes, the major compositions of the fluid are carbon dioxide and methane (Liu, et al., 2017). In this part of the project, densities of the CO_2−CH_4 binary system with CO_2 mole fractions ranging from 0.2017 to 0.8988 were calculated in two commercial software programs, at temperatures between 313 K and 353 K and pressures of 3−18 MPa. Another density calculations were performed in order to get a more soild judgement on density predictions for both software programs. We will see that calculations were identical as with multi-component mixtures.

3.2.1. Experimental data

Binary mixtures were obtained from Liu et al. work (Liu, et al., 2017). Their compositions are presented in Table 5.

Table 5 CO_2-CH_4 binary mixtures (mole fraction)

Components	Mixture 1	Mixture 2	Mixture 3
CO_2	0.2017	0.6015	0.8988
CH_4	0.7983	0.3985	0.1012

A magnetic suspension balance was used for measuring density data of binary CO_2–CH_4 mixture in this study. This method for density measurement is based on the Archimedes' principle. The fluid density was calculated by weighing the sinker in the measured fluid, whose volume is known. Double-walled thermostatic jacket surrounds the measuring cell and is connected with a refrigerated/heating circulator which controls the temperature of the target gas in the measuring cell. Resistance thermometer is used for temperature detection. The target gas is pressurized and stabilized by the piston container and pump, and measured by a pressure sensor, with operating pressure up to 20 MPa. In order to ensure the accuracy of measurement, mass and volume of the sinker was calibrated before experiment (Liu, et al., 2017).

3.2.2. Results

Cubic-Plus-Association Equation of State is again applied in both software programs. Results are numerically shown in Tables 6–8. Graphical description of obtained data is depicted in Figures 30–38. Although both softwares showed good agreement with the experimental data, generally for lower pressures HydraFLASH works better, while for higher pressures, Multiflash has an advantage. This is the practice which is already spotted at calculating densities for multicomponent systems. Interestingly, for mixture with the lowest percent of CO_2 (Mixture 1), HydraFLASH has better matching until 5 MPa pressure, while for the higher concentration of CO_2 (Mixture 2 and 3), better matching extends until 10 MPa. Worst results for both softwares is noticed at highest concentration of CO2 (Mixture 3). Relative average deviation for this mixture was 3.44% for HydraFLASH, and 2.48% for Multiflash. For Mixture 1, relative average deviations was 1.04% and 0.58%, while for Mixture 2, 1.35% and 1.25%, respectively.

Table 6 Density results for 0.2017 CO_2 mixture

Conditions		Density (kg/m^3)			Absolute Error ρexp -ρmod (kg/m^3)		Relative Error (ρexp-ρmod)/ρexp (%)	
T (K)	P (MPa)	ρexp	ρmodhydra	ρmodmulti	HydraFLASH	Multiflash	HydraFLASH	Multiflash
313	4	35.71	35.76	35.86	0.05	0.14	**0.14**	0.41
313	5	45.48	45.46	45.61	0.02	0.14	**0.03**	0.31
313	6	55.52	55.45	55.68	0.07	0.16	**0.13**	0.29
313	7	65.96	65.70	66.03	0.26	0.07	0.39	**0.10**
313	8	76.61	76.19	76.63	0.42	0.02	0.54	**0.02**
313	9	87.63	86.88	87.44	0.75	0.19	0.86	**0.21**
313	10	98.79	97.72	98.43	1.07	0.36	1.08	**0.36**
313	11	110.19	108.65	109.52	1.54	0.67	1.40	**0.61**
313	12	121.58	119.61	120.65	1.97	0.92	1.62	**0.76**
313	15	155.93	152.04	153.67	3.89	2.25	2.49	**1.45**
313	18	188.70	182.64	184.91	6.06	3.79	3.21	**2.01**
333	4	33.07	33.04	33.12	0.03	0.05	**0.08**	0.16
333	5	41.85	41.81	41.94	0.04	0.09	**0.10**	0.21
333	6	50.92	50.76	50.95	0.16	0.03	0.31	**0.06**
333	7	60.17	59.88	60.14	0.29	0.03	0.49	**0.05**
333	8	69.46	69.13	69.48	0.34	0.01	0.48	**0.02**
333	9	79.05	78.49	78.94	0.56	0.11	0.70	**0.14**
333	10	88.82	87.94	88.50	0.88	0.32	0.99	**0.37**
333	11	98.61	97.44	98.12	1.17	0.49	1.18	**0.49**
333	12	108.44	106.95	107.76	1.49	0.68	1.37	**0.63**
333	15	138.03	135.21	136.46	2.82	1.57	2.05	**1.14**

333	18	166.84	162.36	164.11	4.48	2.73	2.68	**1.64**
353	4	30.58	30.77	30.83	0.18	0.25	**0.60**	0.81
353	6	46.94	46.96	47.10	0.02	0.16	**0.04**	0.35
353	9	72.33	71.96	72.29	0.37	0.04	0.51	**0.05**
353	12	98.59	97.35	97.94	1.24	0.65	1.26	**0.66**
353	15	125.02	122.53	123.43	2.49	1.59	1.99	**1.27**
353	18	150.55	146.95	148.19	3.60	2.36	2.39	**1.57**

Table 7 Density results for 0.6015 CO_2 mixture

Conditions		Density (kg/m^3)			Absolute Error ρexp -ρmod (kg/m^3)		Relative Error (ρexp-ρmod)/ρexp (%)	
T (K)	P (MPa)	ρexp	ρmod$_{hydra}$	ρmod$_{multi}$	HydraFLASH	Multiflash	HydraFLASH	Multiflash
313	4	56.42	57.07	57.35	0.65	0.94	**1.15**	1.66
313	5	73.05	73.78	74.26	0.73	1.21	**1.00**	1.66
313	6	90.96	91.69	92.44	0.74	1.48	**0.81**	1.63
313	7	110.30	110.89	111.98	0.59	1.69	**0.54**	1.53
313	8	130.85	131.45	132.99	0.60	2.14	**0.46**	1.64
313	9	153.28	153.37	155.48	0.09	2.20	**0.06**	1.43
313	10	177.42	176.56	179.34	0.86	1.92	**0.49**	1.08
313	11	202.91	200.74	204.33	2.17	1.42	1.07	**0.70**
313	12	229.13	225.50	229.99	3.63	0.85	1.59	**0.37**
313	15	308.15	297.75	305.13	10.40	3.02	3.37	**0.98**
313	18	375.86	359.05	368.97	16.81	6.88	4.47	**1.83**
333	4	51.39	52.14	52.37	0.75	0.98	**1.46**	1.91
333	5	65.94	66.79	67.17	0.84	1.22	**1.28**	1.85
333	6	81.34	82.14	82.72	0.80	1.38	**0.99**	1.70
333	7	97.41	98.22	99.04	0.81	1.63	**0.83**	1.68
333	8	114.28	115.02	116.15	0.73	1.86	**0.64**	1.63
333	9	131.93	132.51	134.00	0.57	2.07	**0.43**	1.57
333	10	150.60	150.63	152.55	0.02	1.95	**0.02**	1.30
333	11	169.87	169.27	171.69	0.60	1.82	**0.35**	1.07
333	12	189.96	188.30	191.27	1.66	1.31	0.88	**0.69**
333	15	251.32	245.79	250.63	5.53	0.69	2.20	**0.27**
333	18	310.35	299.96	306.68	10.39	3.66	3.35	**1.18**
353	3	35.14	35.48	35.57	0.34	0.43	**0.98**	1.22
353	6	74.99	74.95	75.32	0.05	0.33	**0.06**	0.44
353	9	119.45	118.37	119.29	1.08	0.16	0.90	**0.13**
353	10	135.16	133.61	134.78	1.55	0.39	1.15	**0.29**
353	12	167.98	164.94	166.66	3.04	1.32	1.81	**0.78**
353	15	219.08	212.79	215.51	6.29	3.56	2.87	**1.63**
353	18	269.80	259.50	263.27	10.30	6.53	3.82	**2.42**

Table 8 Density results for 0.8988 CO_2 mixture

Conditions		Density (kg/m^3)			Absolute Error ρexp -ρmod (kg/m^3)		Relative Error (ρexp-ρmod)/ρexp (%)	
T (K)	P (MPa)	ρexp	ρmodhydra	ρmodmulti	HydraFLASH	Multiflash	HydraFLASH	Multiflash
313	6	128.66	129.71	131.19	1.04	2.53	**0.81**	1.97
313	7	163.20	164.08	166.51	0.88	3.31	**0.54**	2.03
313	8	206.75	206.75	210.73	0.00	3.99	**0.00**	1.93
313	9	265.24	261.92	268.65	3.33	3.40	**1.25**	1.28
313	10	344.18	331.45	342.55	12.74	1.63	3.70	**0.47**
313	11	432.06	401.52	416.98	30.54	15.08	7.07	**3.49**
313	12	506.07	456.77	475.32	49.30	30.74	9.74	**6.07**
313	15	624.64	558.65	583.00	65.99	41.64	10.56	**6.67**
313	18	683.03	620.13	648.02	62.90	35.01	9.21	**5.13**
333	4	67.86	68.41	68.80	0.55	0.94	**0.80**	1.38
333	5	88.52	89.10	89.76	0.58	1.24	**0.65**	1.40
333	6	111.00	111.73	112.79	0.74	1.80	**0.66**	1.62
333	7	136.15	136.68	138.29	0.54	2.14	**0.39**	1.57
333	8	164.58	164.35	166.70	0.23	2.12	**0.14**	1.29
333	9	196.34	195.14	198.50	1.21	2.16	**0.61**	1.10
333	10	232.81	229.30	234.02	3.51	1.21	1.51	**0.52**
333	11	274.20	266.65	273.09	7.55	1.11	2.75	**0.41**
333	12	319.54	306.15	314.60	13.40	4.94	4.19	**1.55**
333	15	456.32	418.55	432.79	37.77	23.53	8.28	**5.16**
333	18	552.63	502.31	520.33	50.32	32.31	9.11	**5.85**
353	4	61.90	62.59	62.83	0.69	0.93	**1.12**	1.51
353	6	99.47	99.81	100.41	0.34	0.94	**0.34**	0.95
353	9	165.76	165.20	166.84	0.56	1.08	**0.34**	0.65
353	12	250.22	242.87	246.35	7.35	3.87	2.94	**1.55**
353	15	346.06	327.26	333.18	18.80	12.87	5.43	**3.72**
353	18	437.70	406.22	414.41	31.48	23.29	7.19	**5.32**

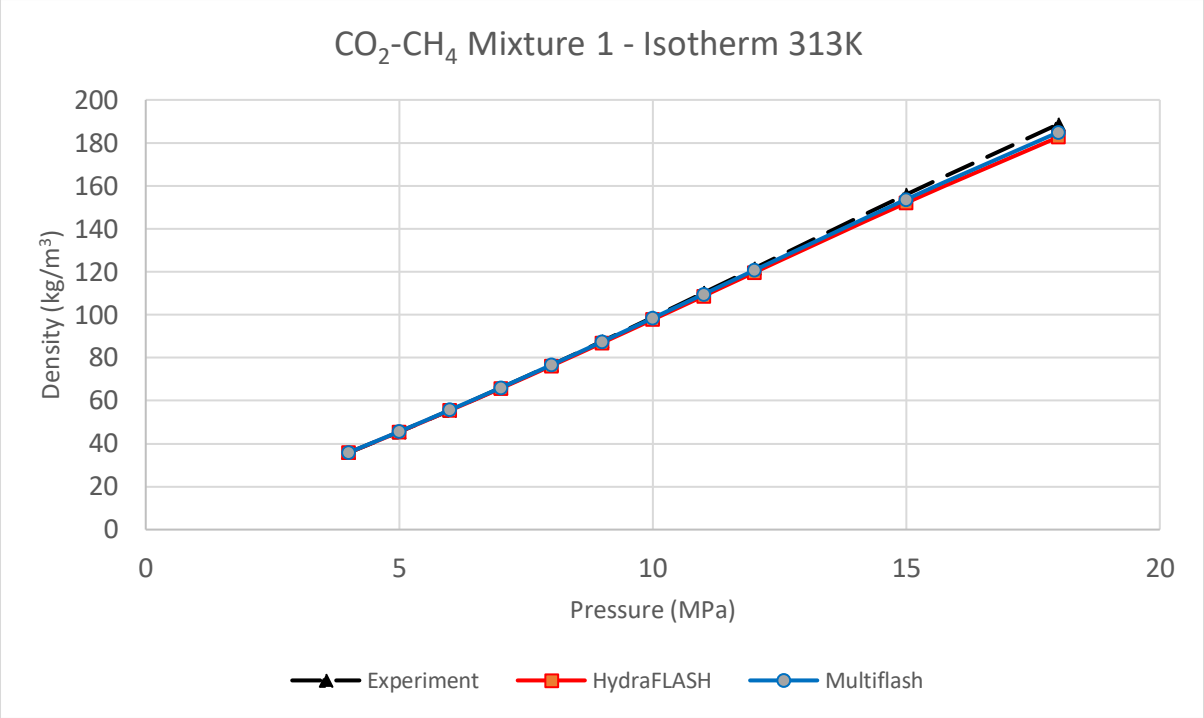

Figure 30 Density results for binary CO_2-CH_4 Mixture 1 - Isotherm 313K

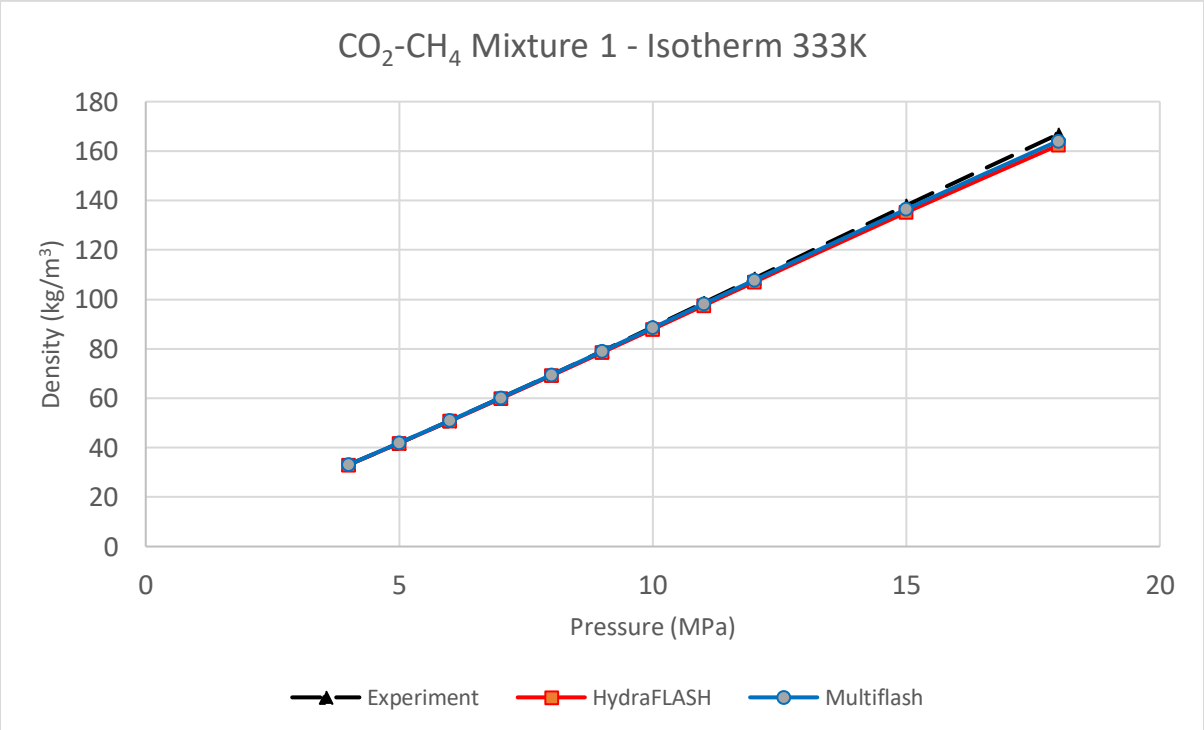

Figure 31 Density results for binary CO_2-CH_4 Mixture 1 - Isotherm 333K

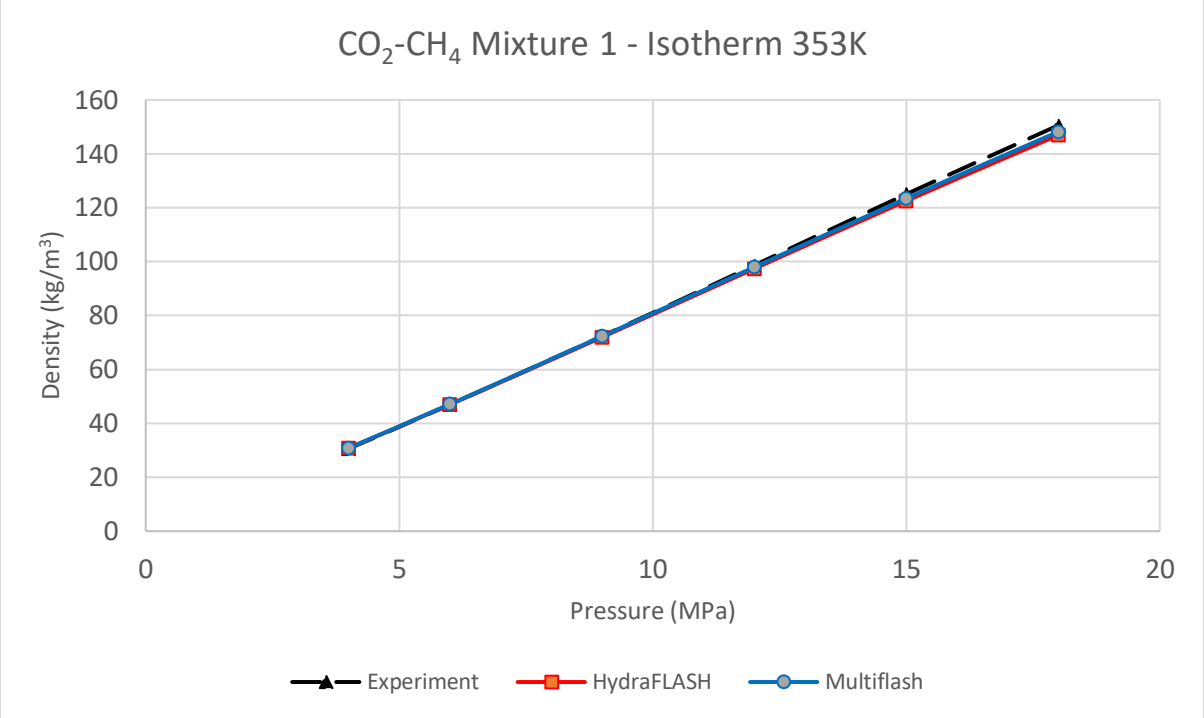

Figure 32 Density results for binary CO_2-CH_4 Mixture 1 - Isotherm 353K

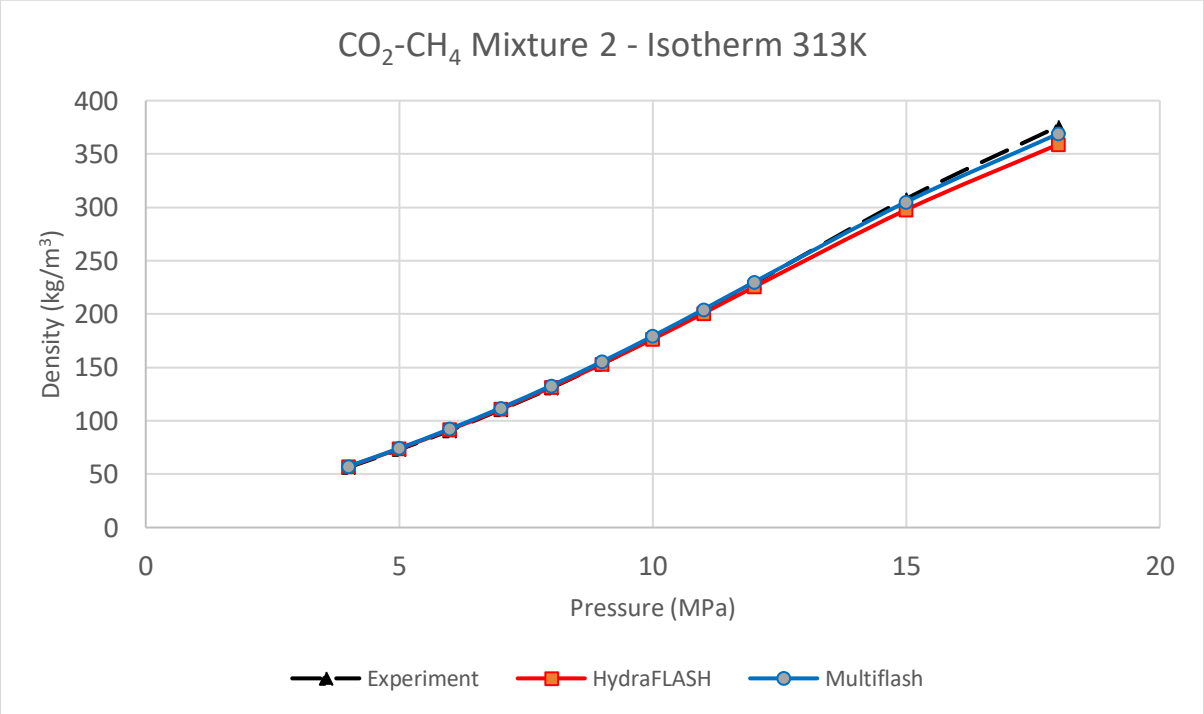

Figure 33 Density results for binary CO_2-CH_4 Mixture 2 - Isotherm 313K

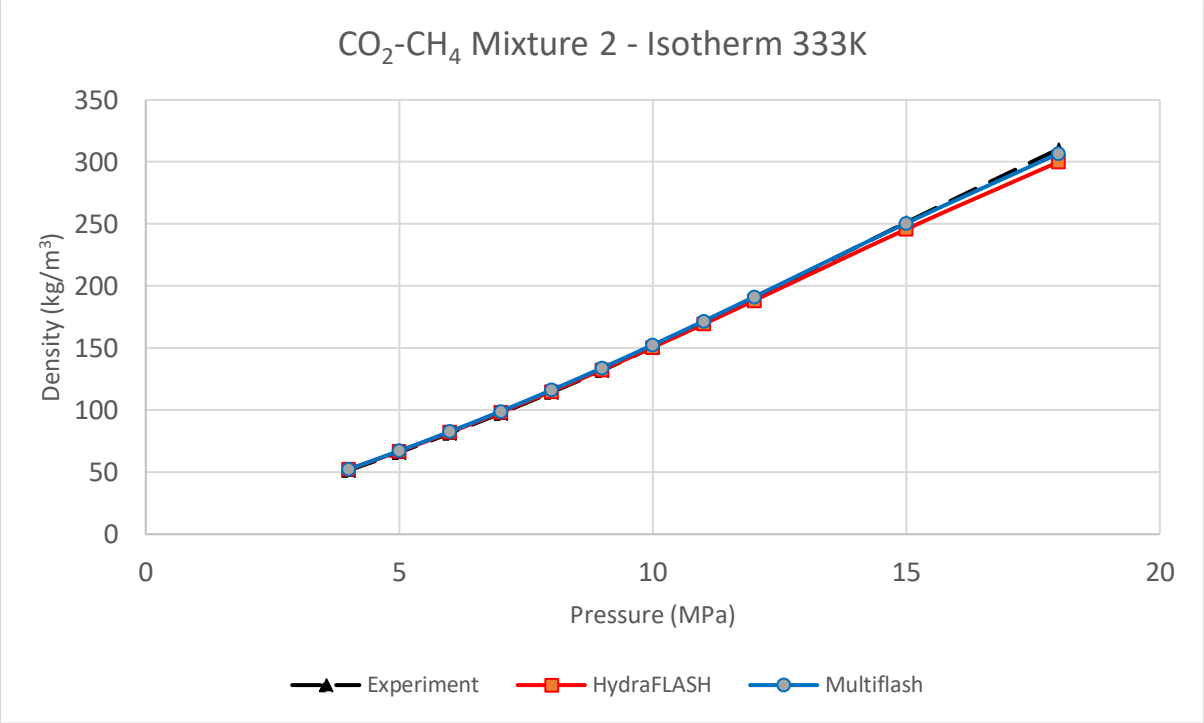

Figure 34 Density results for binary CO_2-CH_4 Mixture 2 - Isotherm 333K

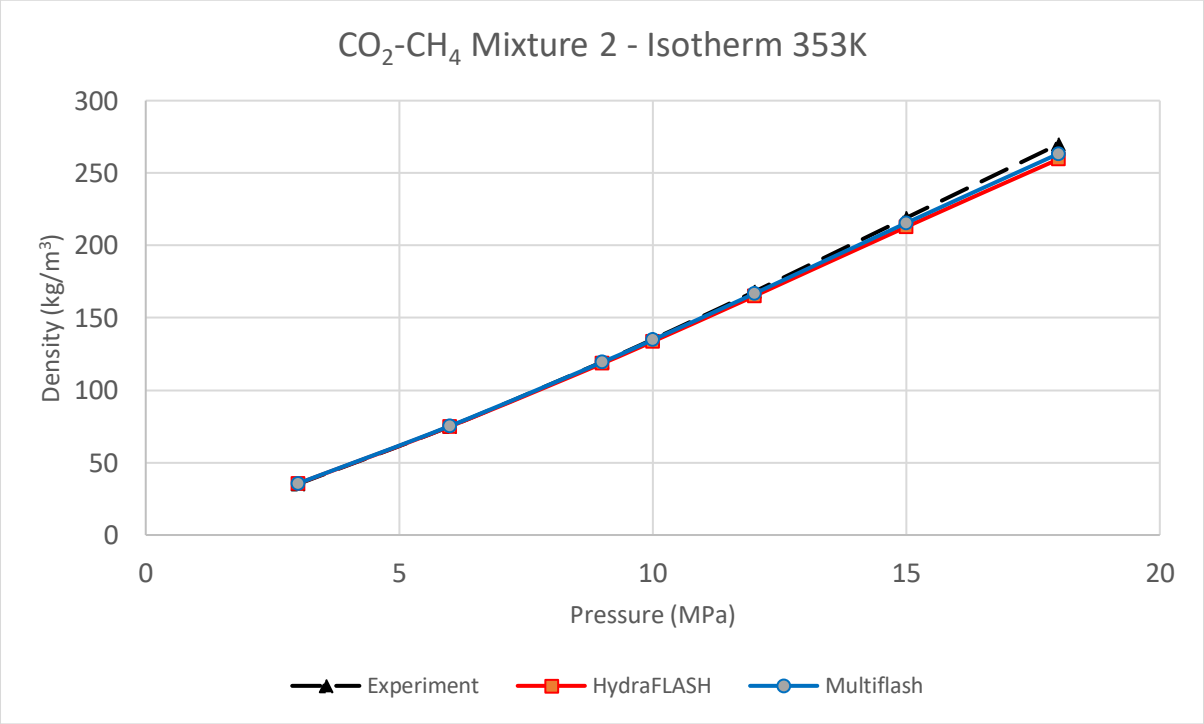

Figure 35 Density results for binary CO_2-CH_4 Mixture 2 - Isotherm 353K

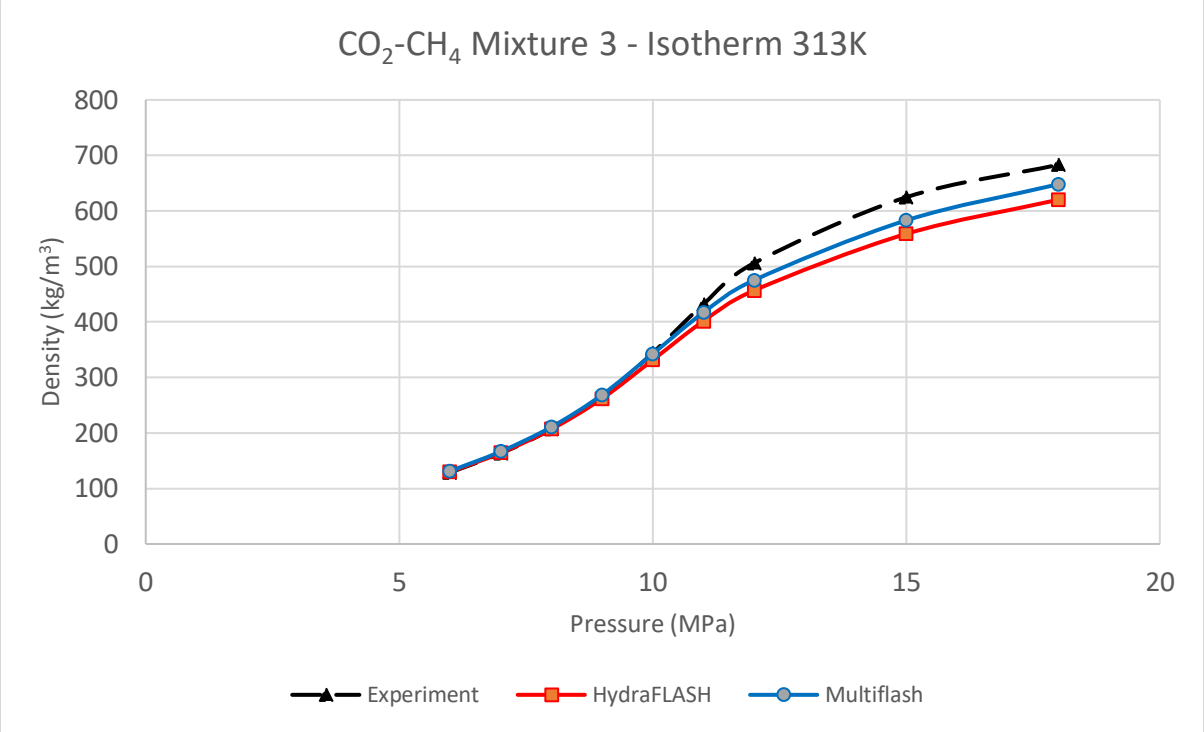

Figure 36 Density results for binary CO_2-CH_4 Mixture 3 - Isotherm 313K

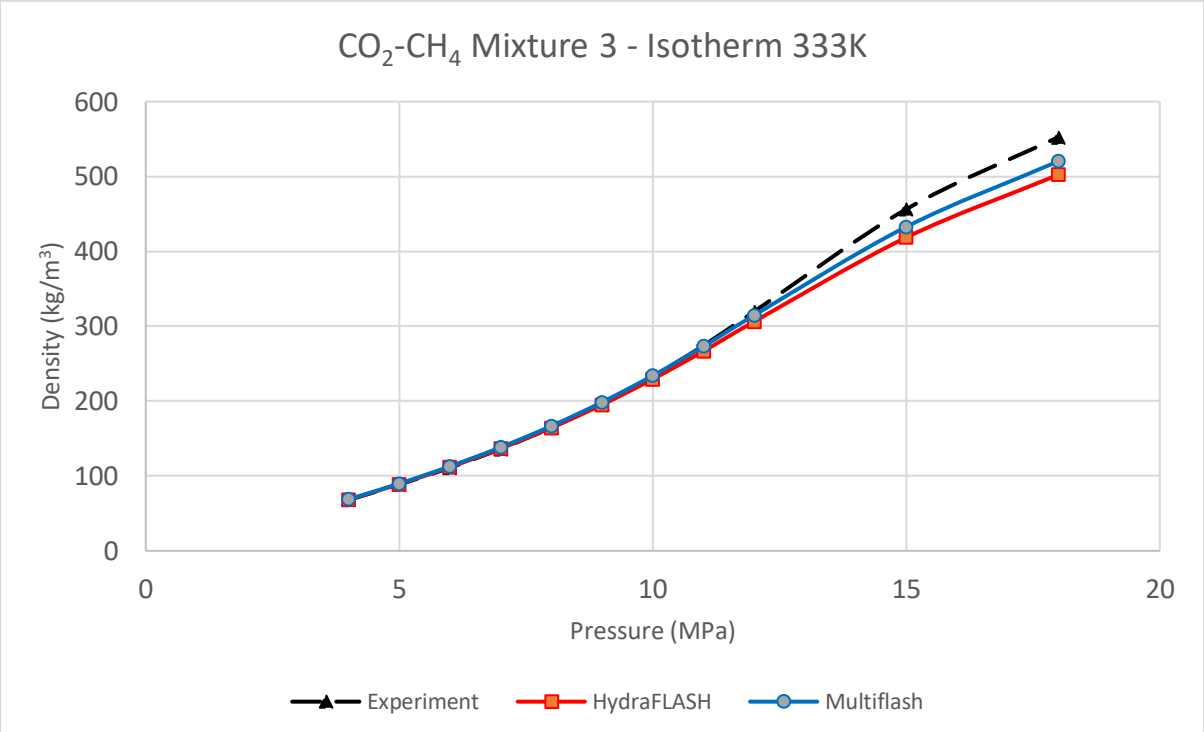

Figure 37 Density results for binary CO_2-CH_4 Mixture 3 - Isotherm 333K

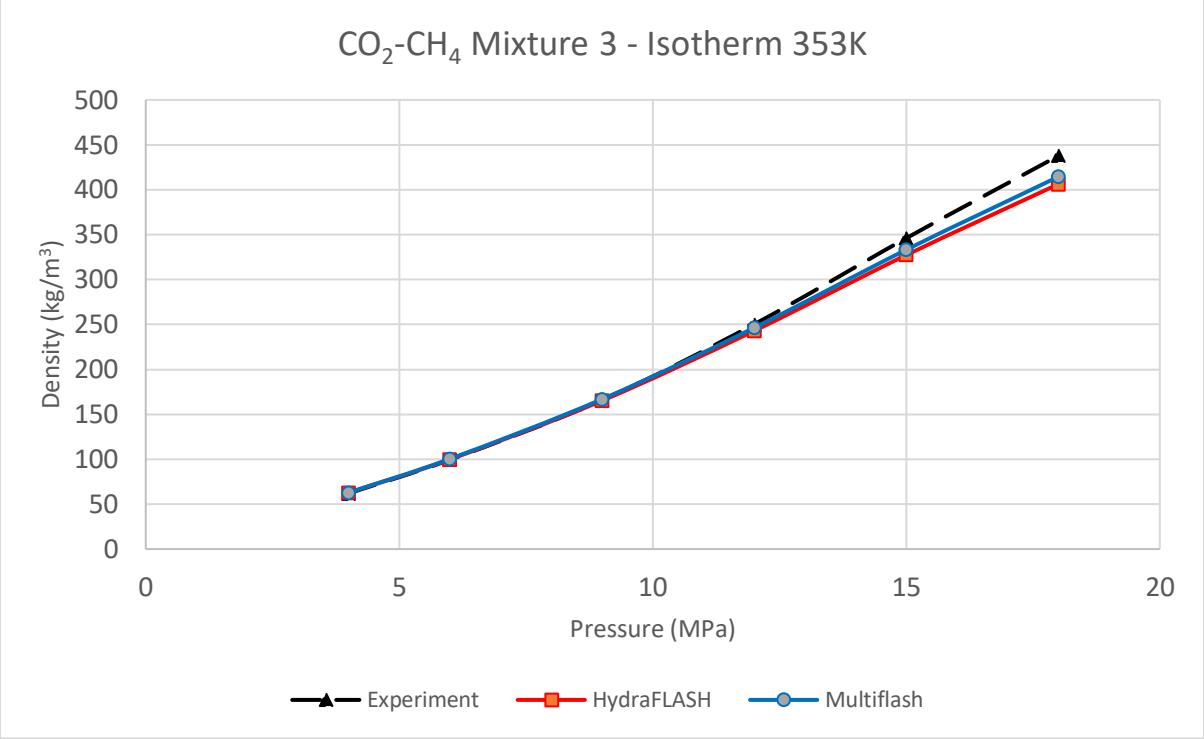

Figure 38 Density results for binary CO_2-CH_4 Mixture 3 - Isotherm 353K

4. Speed of sound

The speed of sound is a term which describes the velocity of sound waves passing through a medium/phase. The sound velocity depends on the medium (for instance, sound waves go faster through the water than through the air), and properties of the medium, such as temperature. Sound velocity measurements for CO_2-rich mixtures could provide important information for the development of mixture models which are applicable to processes of CO_2 capture, transportation and storage.

In the design of pipeline transport systems for compressed CO_2, it is significantly important to model the propagation of shock waves in the fluid, as they have significant role in mechanics of pipeline fractures. Design of pipeline for transport of CO_2 must be optimized to ensure cost-effectiveness and safety. The sound velocity is a valuable and key thermodynamic property to gain information about several features of transport, such as detecting and monitoring of gas bubbles in the dense phase and depressurization and leak checking, as speed of sound determines how fast the pressure will drop. The role of impurities is very important in pipeline failure scenarios and also in flow metering application.

During the storage of CO_2, the fluid is in supercritical phase, because of the conditions inside geologic reservoirs. Hence, the speed of sound can be used for monitoring the formation of bubbles if leakage occurs. Also, knowledge of speed of sound would be useful for estimating seismic properties of hydrocarbon reservoirs, for optimizing enhanced oil recovery processes and for monitoring CO_2 plumes in depleted reservoirs and saline aquifers.

4.1. Experimental data

In this chapter, three binary mixtures of CO_2 and propane were implemented. They are taken from C.-W. Lin and J. P. M. Trusler work (Lin & Trusler, 2012). Their following compositions are below (Table 9):

Table 9 Composition of binary CO_2 - propane mixture (mole fraction)

Components	Mixture 1	Mixture 2	Mixture 3
CO_2	0.93757	0.96828	0.99073
C_3H_8	0.06243	0.03172	0.00927

Important thing when measuring speed of sound of CO_2 is right choice of doping agent. Function of doping agent is to reduce relaxation time, in order to allow sensitive measurement of the sound speed at frequency where the pure fluid alone would be acoustically opaque. In this study, propane was chosen as doping agent, as it is very efficient in catalyzing vibration-translation energy transfer and in reducing the sound absorption coefficient (Lin & Trusler, 2012).

In this experiment, a low frequency (2 MHz) dual-path ultrasonic cell was used. Scheme of ultrasonic cell is shown in Figure 39.

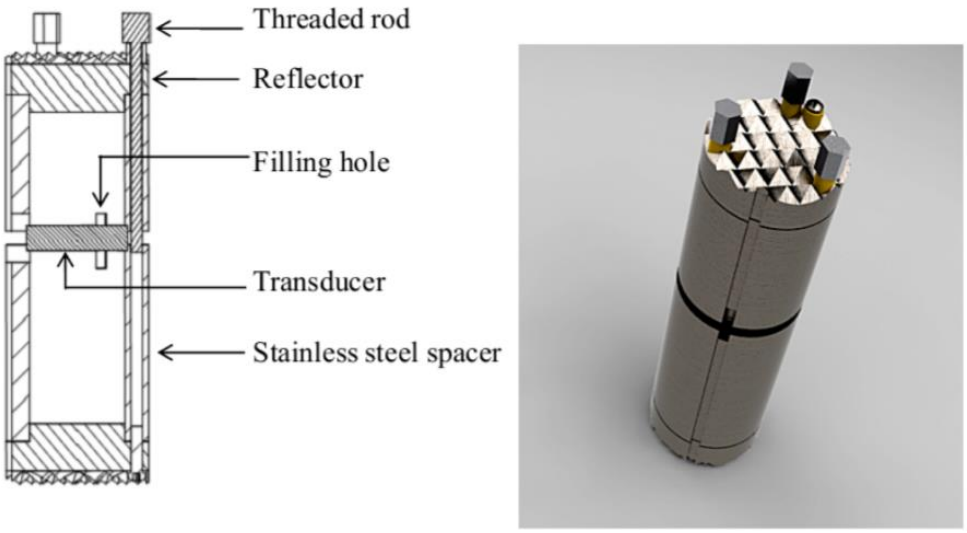

Figure 39 Dual-path ultrasonic cell. Source: (Lin & Trusler, 2012)

Cell consists of piezoceramic transducer, two stainless-steel spacer tubes of different length and two stainless-steel reflectors. Transducer is coated with gold on

both sides in order to avoid electrical contact. In order to initiate measurement, function generator generates 10 V peak-to-peak five cycles tone bust with 2 MHz frequency. After that, two ultrasonic pulses go in opposite directions along path which is filled with fluid. After they were being reflected at the ends of acoustic path, pulses return back to the transducer. Signal was being recorded by high-speed digital oscilloscope (Lin & Trusler, 2012).

4.2. Results

For these calculations, Cubic Plus Association (CPA) EoS was used and set up as a model in both software. Results are presented in Tables 10–12. Both software packages showed an excellent agreement with experimental data. However, HydraFLASH showed better performance in mostly all ranges of pressures and temperatures and its results were closer to sound velocity data from experiment. Only for two isotherms (298 K and 323 K) Multiflash results were more accurate in comparison to another software. The relative average deviation (%RAD) for HydraFLASH was 0.08% for all three mixtures, which is considered as an outstanding performance. However, Multiflash provided slightly poorer performance, with relative average deviation of 0.12%, 0.11% and 0.11%, respectively.

Table 10 Mixture 1 Speed of sound results

Conditions		Speed of sound (m/s)			Absolute Error Cexp-Cmod (m/s)		Relative Error (Cexp-Cmod)/Cexp (%)	
T (K)	P (MPa)	Experiment	HydraFLASH	Multiflash	HydraFLASH	Multiflash	HydraFLASH	Multiflash
248.88	8.00	799.40	638.32	570.19	161.08	229.21	**0.20**	0.29
248.88	15.00	855.40	692.87	617.25	162.53	238.15	**0.19**	0.28
248.88	25.00	924.80	763.89	678.88	160.91	245.92	**0.17**	0.27
248.88	50.00	1056.80	905.71	809.99	151.09	246.81	**0.14**	0.23
248.88	75.00	1159.30	1049.48	924.08	109.82	235.22	**0.09**	0.20
248.88	100.00	1246.20	1172.79	1028.92	73.41	217.28	**0.06**	0.17
248.88	125.00	1320.10	1289.21	1127.86	30.89	192.24	**0.02**	0.15
248.88	150.00	1385.80	1398.96	1222.69	13.16	163.11	**0.01**	0.12
248.88	175.00	1447.10	1510.83	1314.48	63.73	132.62	**0.04**	0.09
273.25	8.00	614.80	510.35	505.64	104.45	109.16	**0.17**	0.18
273.25	15.00	699.70	577.31	565.77	122.39	133.93	**0.17**	0.19
273.25	25.00	787.40	657.80	636.34	129.60	151.06	**0.16**	0.19
273.25	50.00	946.50	816.84	775.81	129.66	170.69	**0.14**	0.18
273.25	75.00	1062.20	950.91	892.16	111.29	170.04	**0.10**	0.16
273.25	100.00	1155.20	1072.02	997.15	83.18	158.05	**0.07**	0.14

273.25	125.00	1236.30	1186.12	1095.26	50.18	141.04	**0.04**	0.11
273.25	150.00	1305.40	1294.19	1188.68	11.21	116.72	**0.01**	0.09
273.25	175.00	1369.60	1400.07	1278.71	30.47	90.89	**0.02**	0.07
273.25	200.00	1428.50	1501.09	1366.15	72.59	62.35	**0.05**	0.04
298.18	8.00	388.50	369.38	430.17	19.12	41.67	**0.05**	0.11
298.18	15.00	538.70	470.93	529.30	67.78	9.40	0.13	**0.02**
298.18	25.00	659.00	564.53	619.18	94.47	39.82	0.14	**0.06**
298.18	50.00	846.60	732.30	775.65	114.30	70.95	0.14	**0.08**
298.18	75.00	975.10	865.59	898.43	109.51	76.67	0.11	**0.08**
298.18	100.00	1076.70	985.75	1006.55	90.95	70.15	0.08	**0.07**
298.18	125.00	1162.30	1098.03	1106.20	64.27	56.10	0.06	**0.05**
298.18	150.00	1236.70	1202.60	1200.27	34.10	36.43	**0.03**	0.03
298.18	175.00	1302.70	1303.91	1290.34	1.21	12.36	**0.00**	0.01
298.18	200.00	1364.50	1403.95	1377.39	39.44	12.89	0.03	**0.01**
323.19	15.00	381.40	374.43	409.33	6.97	27.93	**0.02**	0.07
323.19	25.00	541.20	486.16	516.95	55.04	24.25	0.10	**0.04**
323.19	50.00	758.50	662.55	679.28	95.96	79.22	0.13	**0.10**
323.19	75.00	897.60	796.28	800.32	101.32	97.28	0.11	**0.11**
323.19	100.00	1005.20	913.96	905.21	91.24	99.99	**0.09**	0.10
323.19	125.00	1095.70	1022.95	1001.16	72.75	94.54	**0.07**	0.09
323.19	150.00	1173.90	1125.70	1091.36	48.20	82.54	**0.04**	0.07
323.19	175.00	1243.40	1225.52	1177.53	17.88	65.87	**0.01**	0.05
323.19	200.00	1307.50	1320.04	1260.70	12.54	46.80	**0.01**	0.04
348.18	25.00	446.80	426.32	424.09	20.48	22.71	**0.05**	0.05
348.18	50.00	682.30	607.57	585.13	74.73	97.17	**0.11**	0.14
348.18	75.00	830.60	738.54	702.16	92.06	128.44	**0.11**	0.15
348.18	100.00	943.70	853.88	802.69	89.82	141.01	**0.10**	0.15
348.18	125.00	1037.10	961.07	894.29	76.03	142.81	**0.07**	0.14
348.18	150.00	1117.70	1060.82	980.23	56.88	137.47	**0.05**	0.12
348.18	175.00	1189.80	1156.21	1062.25	33.59	127.55	**0.03**	0.11
348.18	200.00	1254.30	1249.17	1141.38	5.13	112.92	**0.00**	0.09
373.12	25.00	385.00	388.75	373.31	3.75	11.69	**0.01**	0.03
373.12	50.00	618.80	564.62	526.81	54.18	91.99	**0.09**	0.15
373.12	75.00	772.60	692.66	640.21	79.94	132.39	**0.10**	0.17
373.12	100.00	889.40	804.77	737.37	84.64	152.03	**0.10**	0.17
373.12	125.00	985.60	908.80	825.70	76.80	159.90	**0.08**	0.16
373.12	150.00	1069.00	1005.85	908.47	63.15	160.53	**0.06**	0.15
373.12	175.00	1141.60	1098.71	987.38	42.89	154.22	**0.04**	0.14
373.12	200.00	1208.70	1188.41	1063.47	20.29	145.23	**0.02**	0.12

Table 11 Mixture 2 Speed of sounds results

Conditions		Speed of sound (m/s)			Absolute Error Cexp-Cmod (m/s)		Relative Error (Cexp-Cmod)/Cexp (%)	
T (K)	P (MPa)	Experiment	HydraFLASH	Multiflash	HydraFLASH	Multiflash	HydraFLASH	Multiflash
249.03	7.92	797.20	639.72	570.07	157.48	227.13	**0.20**	0.28
249.03	15.00	852.80	695.26	618.61	157.54	234.19	**0.18**	0.27
249.03	25.00	922.30	764.43	678.97	157.87	243.33	**0.17**	0.26
249.03	50.00	1052.60	898.62	807.64	153.98	244.96	**0.15**	0.23
249.03	75.00	1155.30	1043.24	919.75	112.06	235.55	**0.10**	0.20
249.03	100.00	1239.60	1163.45	1022.83	76.15	216.77	**0.06**	0.17
249.03	125.00	1312.10	1277.15	1120.15	34.95	191.95	**0.03**	0.15
249.03	150.00	1377.40	1387.11	1213.46	9.71	163.94	**0.01**	0.12
273.34	8.01	610.50	511.19	510.85	99.31	99.65	**0.16**	0.16
273.34	15.00	694.40	578.67	571.98	115.73	122.42	**0.17**	0.18
273.34	25.00	785.00	657.03	641.82	127.97	143.18	**0.16**	0.18
273.34	50.00	942.80	812.80	780.00	130.00	162.80	**0.14**	0.17
273.34	75.00	1058.90	943.83	895.36	115.07	163.54	**0.11**	0.15
273.34	100.00	1149.40	1061.89	999.52	87.52	149.88	**0.08**	0.13
273.34	125.00	1229.30	1173.43	1096.91	55.87	132.39	**0.05**	0.11
273.34	150.00	1293.70	1279.42	1189.70	14.28	104.00	**0.01**	0.08
273.34	175.00	1360.30	1382.90	1279.18	22.60	81.12	**0.02**	0.06
273.34	200.00	1417.30	1482.53	1366.13	65.23	51.17	**0.05**	0.04
298.14	15.00	532.20	471.15	542.30	61.05	10.10	0.11	**0.02**
298.14	25.00	654.50	563.46	633.90	91.04	20.60	0.14	**0.03**
298.14	50.00	841.60	728.99	792.68	112.61	48.92	0.13	**0.06**
298.14	75.00	969.00	860.26	917.11	108.74	51.89	0.11	**0.05**
298.14	100.00	1070.00	976.86	1026.70	93.14	43.30	0.09	**0.04**
298.14	125.00	1154.10	1085.05	1127.76	69.05	26.34	0.06	**0.02**
298.14	150.00	1228.90	1188.53	1223.22	40.38	5.68	0.03	**0.00**
298.14	175.00	1294.10	1289.30	1314.70	4.80	20.60	**0.00**	0.02
298.14	200.00	1354.10	1383.97	1403.20	29.87	49.10	**0.02**	0.04
323.09	25.00	534.80	484.46	523.00	50.34	11.80	0.09	**0.02**
323.09	50.00	752.60	659.20	686.85	93.40	65.75	0.12	**0.09**
323.09	75.00	890.20	789.52	808.53	100.68	81.67	0.11	**0.09**
323.09	100.00	1000.10	905.23	913.88	94.87	86.22	0.09	**0.09**
323.09	125.00	1088.70	1011.36	1010.27	77.34	78.43	**0.07**	0.07
323.09	150.00	1164.30	1112.09	1100.92	52.21	63.38	**0.04**	0.05
323.09	175.00	1234.80	1207.61	1187.56	27.19	47.24	**0.02**	0.04
323.09	200.00	1296.50	1300.83	1271.24	4.33	25.26	**0.00**	0.02
348.09	30.00	504.80	466.94	462.51	37.86	42.29	**0.07**	0.08
348.09	50.00	675.20	604.06	583.87	71.14	91.33	**0.11**	0.14
348.09	75.00	823.00	732.05	700.37	90.95	122.63	**0.11**	0.15
348.09	100.00	937.30	845.48	800.32	91.82	136.98	**0.10**	0.15
348.09	125.00	1029.00	949.89	891.37	79.11	137.63	**0.08**	0.13
348.09	150.00	1109.40	1047.16	976.82	62.24	132.58	**0.06**	0.12
348.09	175.00	1178.60	1142.25	1058.38	36.35	120.22	**0.03**	0.10
348.09	200.00	1243.80	1231.10	1137.09	12.70	106.71	**0.01**	0.09
373.12	35.00	488.80	462.80	438.87	26.00	49.93	**0.05**	0.10
373.12	50.00	611.60	561.00	522.21	50.60	89.39	**0.08**	0.15

373.12	75.00	764.50	685.66	634.66	78.84	129.84	**0.10**	0.17
373.12	100.00	881.30	795.45	730.93	85.85	150.37	**0.10**	0.17
373.12	125.00	976.50	897.14	818.43	79.36	158.07	**0.08**	0.16
373.12	150.00	1057.90	992.70	900.42	65.20	157.48	**0.06**	0.15
373.12	175.00	1131.50	1083.93	978.60	47.57	152.90	**0.04**	0.14
373.12	200.00	1196.40	1171.84	1054.00	24.57	142.40	**0.02**	0.12

Table 12 Mixture 3 Speed of sound results

Conditions		Speed of sound (m/s)			Absolute Error Cexp-Cmod (m/s)		Relative Error (Cexp-Cmod)/Cexp (%)	
T (K)	P (Mpa)	Experiment	HydraFLASH	Multiflash	HydraFLASH	Multiflash	HydraFLASH	Multiflash
251.21	8.05	786.80	633.55	568.32	153.25	218.48	**0.19**	0.28
251.21	15.00	844.20	687.21	615.78	156.99	228.42	**0.19**	0.27
251.21	25.00	913.80	755.76	675.78	158.04	238.02	**0.17**	0.26
251.21	50.00	1045.70	882.53	803.31	163.17	242.39	**0.16**	0.23
251.21	75.00	1143.20	1029.34	914.21	113.86	228.99	**0.10**	0.20
251.21	100.00	1230.80	1146.89	1016.10	83.91	214.70	**0.07**	0.17
251.21	125.00	1299.10	1258.78	1112.27	40.32	186.83	**0.03**	0.14
251.21	150.00	1366.30	1364.29	1204.48	2.01	161.82	**0.00**	0.12
273.39	8.07	614.00	516.09	518.04	97.91	95.96	**0.16**	0.16
273.39	15.00	698.10	581.62	577.96	116.48	120.14	**0.17**	0.17
273.39	25.00	787.20	658.13	647.25	129.07	139.95	**0.16**	0.18
273.39	50.00	941.20	811.04	784.56	130.17	156.64	**0.14**	0.17
273.39	75.00	1055.90	939.41	899.33	116.49	156.57	**0.11**	0.15
273.39	100.00	1145.50	1056.16	1003.04	89.34	142.46	**0.08**	0.12
273.39	125.00	1225.50	1164.73	1100.07	60.77	125.43	**0.05**	0.10
273.39	150.00	1292.30	1269.82	1192.60	22.48	99.70	**0.02**	0.08
273.39	175.00	1354.80	1370.58	1281.88	15.78	72.92	**0.01**	0.05
273.39	200.00	1410.80	1466.99	1368.70	56.19	42.10	0.04	**0.03**
298.14	25.00	653.90	563.07	647.47	90.83	6.43	0.14	**0.01**
298.14	50.00	837.80	726.24	808.78	111.56	29.02	0.13	**0.03**
298.14	75.00	965.00	854.43	935.18	110.57	29.82	0.11	**0.03**
298.14	100.00	1064.00	970.90	1046.59	93.10	17.41	0.09	**0.02**
298.14	125.00	1147.90	1077.40	1149.44	70.50	1.54	0.06	**0.00**
298.14	150.00	1220.20	1177.41	1246.69	42.79	26.49	0.04	**0.02**
298.14	175.00	1285.60	1275.89	1340.00	9.71	54.40	**0.01**	0.04
298.14	200.00	1346.20	1370.94	1430.37	24.74	84.17	**0.02**	0.06
323.09	30.00	590.10	524.51	568.56	65.59	21.54	0.11	**0.04**
323.09	50.00	747.00	657.14	693.76	89.86	53.24	0.12	**0.07**
323.09	75.00	886.10	784.84	816.23	101.26	69.87	0.11	**0.08**
323.09	100.00	992.60	898.47	922.26	94.13	70.34	0.09	**0.07**
323.09	125.00	1080.50	1003.59	1019.29	76.92	61.21	0.07	**0.06**
323.09	150.00	1157.20	1102.19	1110.61	55.01	46.59	0.05	**0.04**
323.09	175.00	1224.10	1197.51	1197.97	26.59	26.13	0.02	**0.02**
323.09	200.00	1288.40	1289.50	1282.40	1.10	6.00	0.00	**0.00**
348.09	50.00	672.70	602.25	583.29	70.45	89.41	**0.10**	0.13
348.09	75.00	816.90	727.03	699.48	89.87	117.42	**0.11**	0.14
348.09	100.00	931.10	838.56	799.10	92.54	132.00	**0.10**	0.14
348.09	125.00	1023.20	941.82	889.84	81.38	133.36	**0.08**	0.13

348.09	150.00	1101.40	1037.97	975.01	63.43	126.39	**0.06**	0.11
348.09	175.00	1171.40	1129.28	1056.34	42.12	115.06	**0.04**	0.10
348.09	200.00	1236.70	1219.02	1134.86	17.68	101.84	**0.01**	0.08
373.12	50.00	607.50	559.45	519.10	48.05	88.40	**0.08**	0.15
373.12	75.00	763.80	679.99	630.90	83.81	132.90	**0.11**	0.17
373.12	100.00	874.40	788.85	726.56	85.55	147.84	**0.10**	0.17
373.12	125.00	970.30	889.34	813.50	80.96	156.80	**0.08**	0.16
373.12	150.00	1051.50	982.36	894.96	69.14	156.54	**0.07**	0.15
373.12	175.00	1121.20	1072.15	972.65	49.05	148.55	**0.04**	0.13
373.12	200.00	1188.30	1158.86	1047.60	29.44	140.70	**0.02**	0.12

5. Solubility of CO_2 in aqueous phases

Accurate knowledge of CO_2 solubility in aqueous phases is a very important property when designing an efficient Carbon Capture and Storage (CCS) processes. Once the CO_2 has been captured, it needs to be safely and permanently stored. Currently, CO_2 storage in depleted oil and gas fields or deep saline aquifers is considered to be the best method for CO_2 storage. This is mainly because of their huge storage capacities and the fact that some of the infrastructure needed for CO_2 injection already exists, as it is made for the oil and gas industry. For geological storage of CO_2, CO_2 must be compressed to a supercritical state and pumped into brine aquifers, in order to be stored by structural and pore-scale trapping, dissolution into brine, and mineral precipitation. Additionally, CO_2 dissolution into brine is a crucial mechanism of CO_2 enhanced oil recovery as it improves sweep efficiency and increases oil displacement. The efficiency of CO_2 dissolution in brine as a trap directly depends on temperature, pressure, and chemical composition. Besides use for geological storage and for enhanced oil recovery, exact predictions of CO_2 solubility in fluids is crucial for design, control and optimization of numerous industrial processes like gas sweetening and decontamination of wastewaters containing dissolved acid gases.

In this part of thesis, calculation of the solubility of CO_2 in water and single salt aqueous solution will be presented. Firstly, the solubility of CO_2 in water was calculated in a pressure range up to 5 MPa and for different isotherms, ranging from 298.15 K, up to 393.15 K. The solubility of CO_2 in water was calculated in both software packages and compared against the available experimental data to validate the model. Secondly, CO_2 solubility in a salt aqueous solution (single salt NaCl) was calculated in both software, in a pressure range up to 39 MPa and for different isotherms up to 423.19 K. Results were again compared and discussed.

5.1. Solubility of CO_2 in water

As the concentration of aqueous CO_2 in solution is significant for estimation amount of carbon dioxide that can be stored, knowledge of the solubility of CO_2 in pure water and salt solutions is required. The solubility of CO_2 in water is a lot higher than solubility of hydrocarbon components in water, and that is a factor that cannot be neglected in the simulation process (Klins, 1984). Under reservoir conditions, water and CO_2 are two immiscible fluids, which generally means that the CO_2-rich fluid will flood on top of the water-rich fluid, due to a difference in density. However, at the contact between the two fluids, dissolution of CO_2 into the water, as well as dissolution of water into the CO_2, can take place. The properties of these mixtures can be modelled using proper equations of state.

5.1.1. Experimental data

Experimental data of CO_2 solubility in pure water was taken from Lucile et al work (Lucile, et al., 2012). The measurements of CO_2 solubility were done with an apparatus through a static method. Scheme of the experimental equipment is shown in Figure 40. FT01 and FT02 are mass flowmeters; RD is rupture disc; EC stands for equilibrium cell; TB is thermostatted bath; P is pressure transducer or manometer and T is for the temperature probes. Apparatus is based on a Hastelloy C276 well-stirred equilibrium cell with a double jacket with volume of 2400 cm^3, and operating pressures up to 6 MPa and temperature ranging from 293 K to 393 K. Thermostatted bath is regulating the temperature. On the top of the apparatus, there is a heating resistance, which allows minimizing thermal gradient, because volume cell is large, and therefore thermal gradient could exist. Temperature is measured at three points: in the vapor phase, at the vapor-liquid interface, and in the liquid phase through three 100 Ω platinum probes. Pressure is measured with pressure transducer (Lucile, et al., 2012).

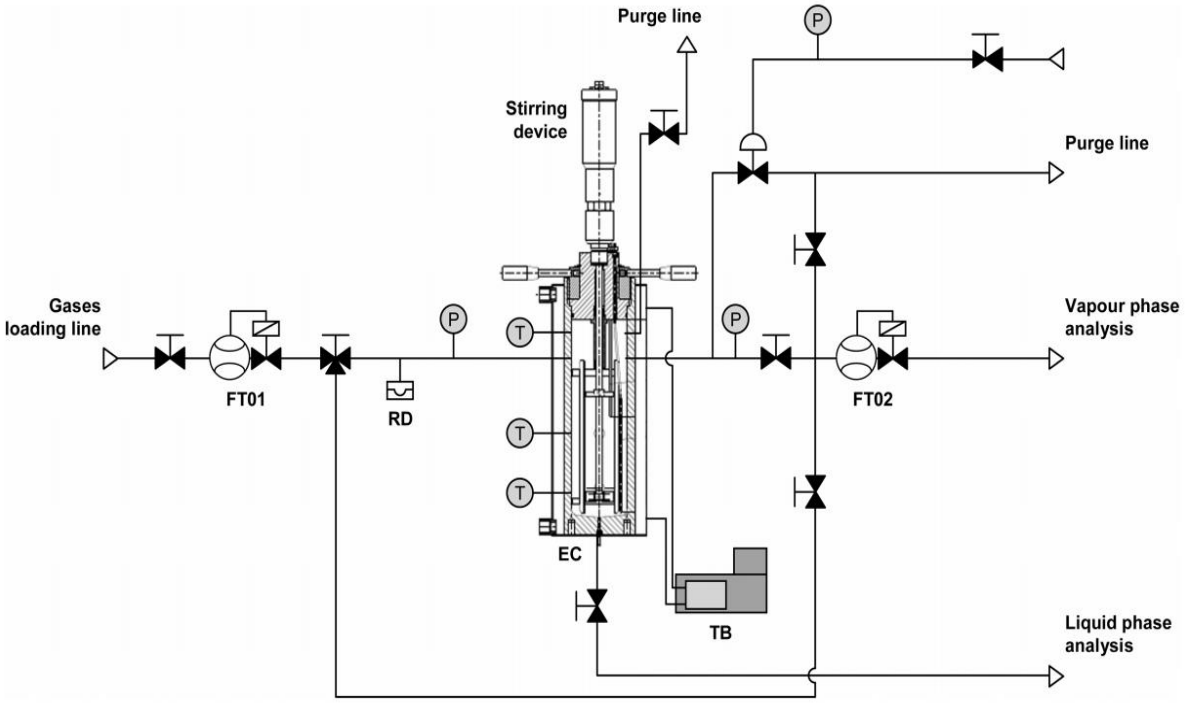

Figure 40 Scheme of the experimental equipment. Source: (Lucile, et al., 2012)

There are two mass flowmeters. First one is located on the gas loading line and it measures gas volume loaded in the cell. The second one allows control of gas flow in the gas phase analyzer. The stiring device ensures the homogeneity of the two phases. The equilibrium cell and lines are purged using a vacuum pump, before introducing aqueous solution. Solvent is loaded in the cell and then the gas is set up to the desired pressure, as well as desired temperature. Stirring starts with 700 rpm which is enough for gas aspiration through the stirrer, and contact area between two phases is increasing. Once the cell is loaded, samples are analyzed by ion chromatography, until CO_2 concentration in water no longer differs (Lucile, et al., 2012). It is well known that solubility of carbon dioxide in pure water increases as the pressure increases and decreases when the temperature decreases.

5.1.2. Results

Results are showed in Table 13 and Figures 41–45. For this calculations, CPA EoS is used and therefore, in both software packages, CPA EoS model was set up.

The relative average deviations (%RAD) of results in comparison with the experimental data were found to be 0.12% for HydraFLASH and 0.04% for Multiflash,

respectively. For HydraFLASH, big deviations were observed mostly at high pressures, confirming limits of HydraFLASH software in solubility prediction at high pressures when tuned over a wide pressure range. HydraFLASH provided best results at lower temperatures, more precisely isotherms 298.15 K and 323.15 K, and moderate pressures, between 2 MPa and 4 MPa, which is clearly seen at Figures 42 and 43. At higher pressures and temperatures, Multiflash provides better results.

Table 13 Results of CO_2 solubility in water

Conditions		Solubility CO2, X (mole fraction)			Absolute Error Xexp-Xmod (mole fraction)		Relative Error (Xexp-Xmod)/Xexp (%)	
T (K)	P (MPa)	Experiment	HydraFLASH	Multiflash	HydraFLASH	Multiflash	HydraFLASH	Multiflash
298.15	0.61	0.00362	0.00312	0.00334	0.00050	0.00028	0.14	**0.08**
298.15	0.98	0.00534	0.00496	0.00533	0.00038	0.00001	0.07	**0.00**
298.15	1.97	0.00985	0.00967	0.01041	0.00018	0.00056	**0.02**	0.06
298.15	3.01	0.01470	0.01419	0.01533	0.00051	0.00063	**0.03**	0.04
298.15	4.04	0.01880	0.01818	0.01972	0.00062	0.00092	**0.03**	0.05
298.15	4.73	0.02220	0.02053	0.02233	0.00167	0.00013	0.08	**0.01**
323.15	0.60	0.00214	0.00174	0.00197	0.00040	0.00017	0.19	**0.08**
323.15	1.05	0.00331	0.00303	0.00344	0.00028	0.00013	0.08	**0.04**
323.15	2.06	0.00616	0.00580	0.00661	0.00037	0.00045	**0.06**	0.07
323.15	2.98	0.00895	0.00814	0.00933	0.00082	0.00038	0.09	**0.04**
323.15	4.09	0.01130	0.01072	0.01237	0.00058	0.00107	**0.05**	0.09
323.15	4.12	0.01160	0.01079	0.01245	0.00081	0.00085	**0.07**	0.07
323.15	5.02	0.01390	0.01268	0.01470	0.00122	0.00080	0.09	**0.06**
348.15	0.54	0.00126	0.00104	0.00120	0.00022	0.00006	0.18	**0.05**
348.15	1.00	0.00241	0.00197	0.00227	0.00044	0.00014	0.18	**0.06**
348.15	2.03	0.00467	0.00396	0.00460	0.00071	0.00007	0.15	**0.01**
348.15	3.10	0.00688	0.00590	0.00689	0.00098	0.00001	0.14	**0.00**
348.15	4.03	0.00859	0.00747	0.00878	0.00112	0.00019	0.13	**0.02**
348.15	5.14	0.01060	0.00922	0.01089	0.00138	0.00029	0.13	**0.03**
373.15	0.99	0.00175	0.00146	0.00168	0.00029	0.00007	0.17	**0.04**
373.15	2.01	0.00359	0.00306	0.00354	0.00053	0.00005	0.15	**0.01**
373.15	3.05	0.00541	0.00461	0.00536	0.00080	0.00005	0.15	**0.01**
373.15	4.04	0.00697	0.00602	0.00702	0.00095	0.00005	0.14	**0.01**
373.15	5.03	0.00857	0.00734	0.00860	0.00123	0.00003	0.14	**0.00**
393.15	0.96	0.00141	0.00113	0.00130	0.00028	0.00011	0.20	**0.08**
393.15	2.03	0.00326	0.00267	0.00307	0.00059	0.00019	0.18	**0.06**
393.15	3.05	0.00487	0.00407	0.00471	0.00080	0.00016	0.16	**0.03**
393.15	4.03	0.00617	0.00536	0.00623	0.00081	0.00006	0.13	**0.01**
393.15	4.83	0.00715	0.00637	0.00742	0.00078	0.00027	0.11	**0.04**

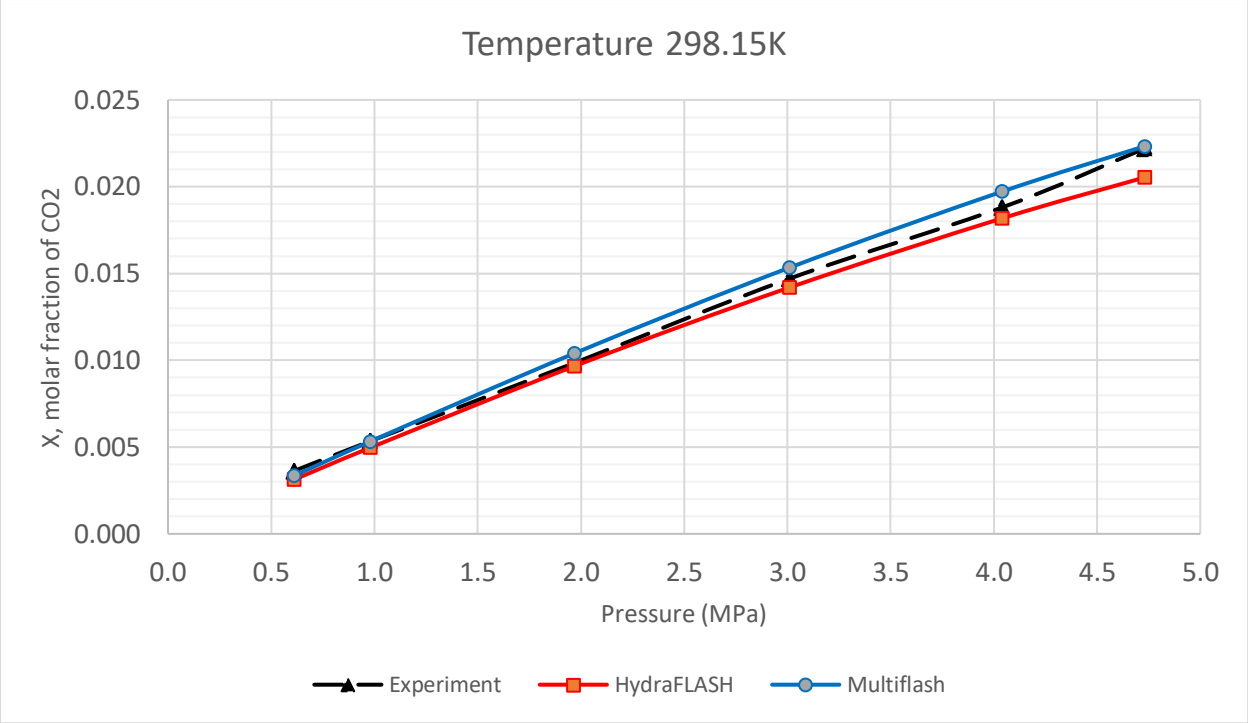

Figure 41 CO_2 solubility in water - Isotherm 298.15K

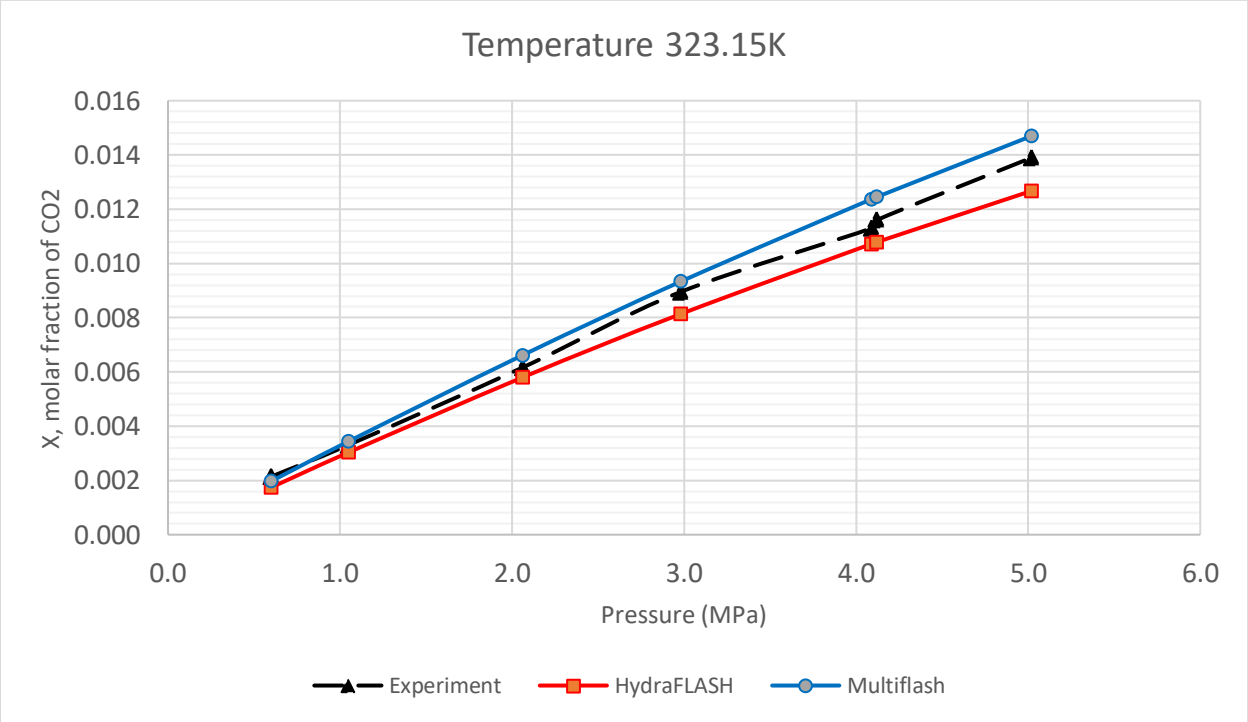

Figure 42 CO_2 solubility in water - Isotherm 323.15K

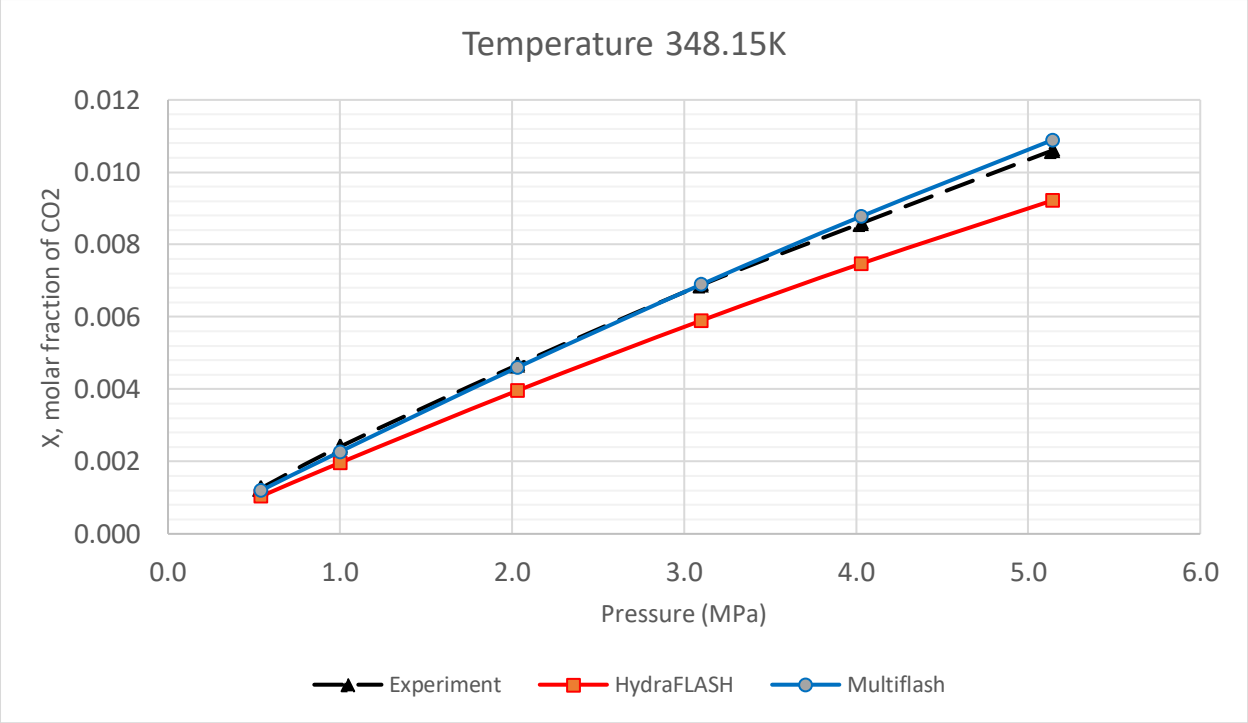

Figure 43 CO_2 solubility in water - Isotherm 348.15K

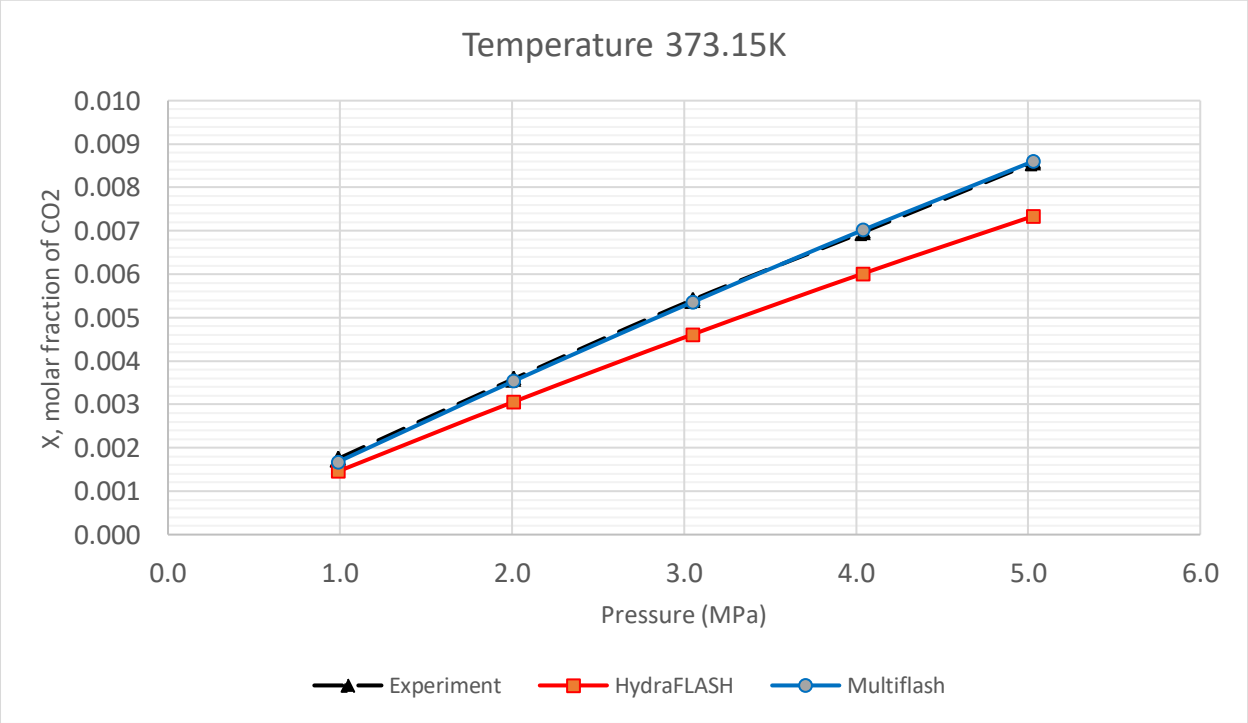

Figure 44 CO_2 solubility in water - Isotherm 373.15K

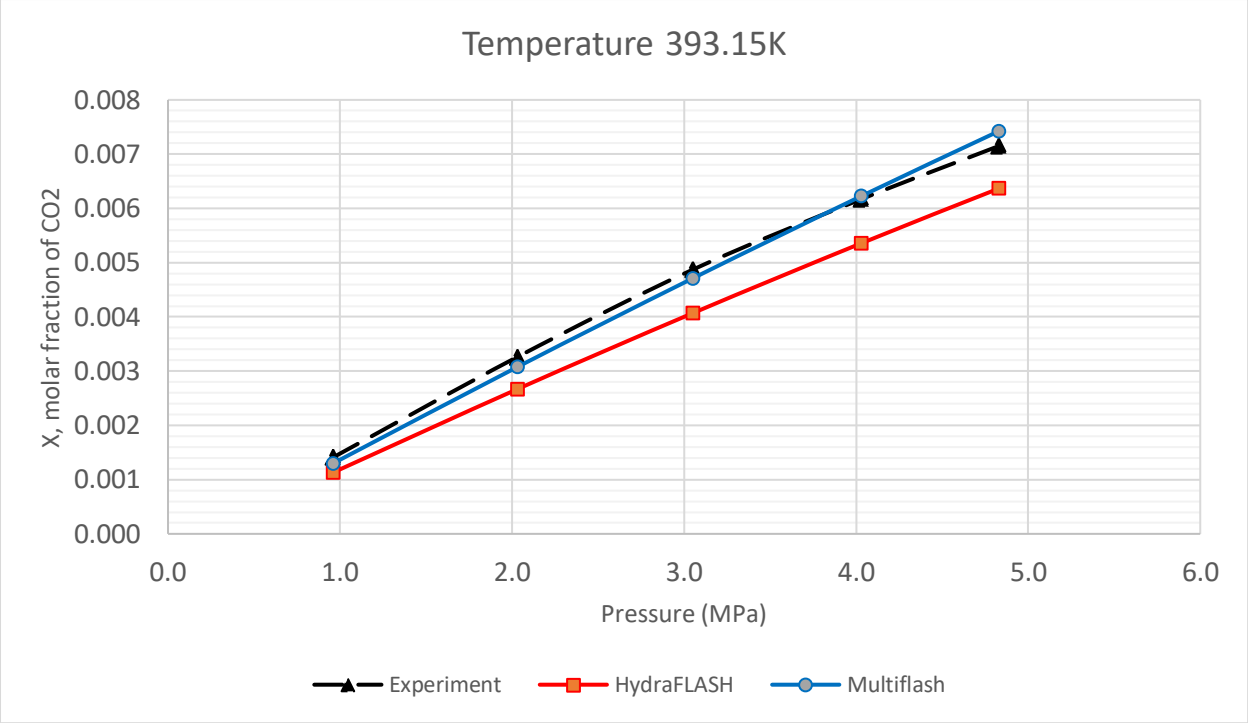

Figure 45 CO_2 solubility in water - Isotherm 393.15K

5.2. Solubility of CO_2 in salt aqueous solution

In this part of work, the solubility of CO_2 in salt aqueous solution (single salt NaCl) was calculated at pressures up 39 MPa and different isotherms up to 423.19 K. Many CO_2 solubility models are built on simple NaCl solutions. However, brines, are not that simple, as they often contain a complex mixture of ions including HCO^{3-}, Ca^{2+}, Mg^{2+}, K^{+}, and $SO4^{2-}$, in addition to organic acids and anions which are found in deep reservoirs (Gilbert, Bennett, Wolfe, Zhang, & Romanak, 2016).

5.2.1. Experimental data

The experimental setup from Ahmadi and Chapoy work is schematically presented in Figure 46. For mixing of CO_2-aqueous phase system, pneumatic rocking system was used. The measurement cell is 300 ml titanium cylindrical, which operates at pressures up to 68 MPa. Vessel is mounted on an adjustable rotary axis of the rocking system. Operating temperatures range from 203.15 K to 423.15 K (Ahmadi & Chapoy, 2018).

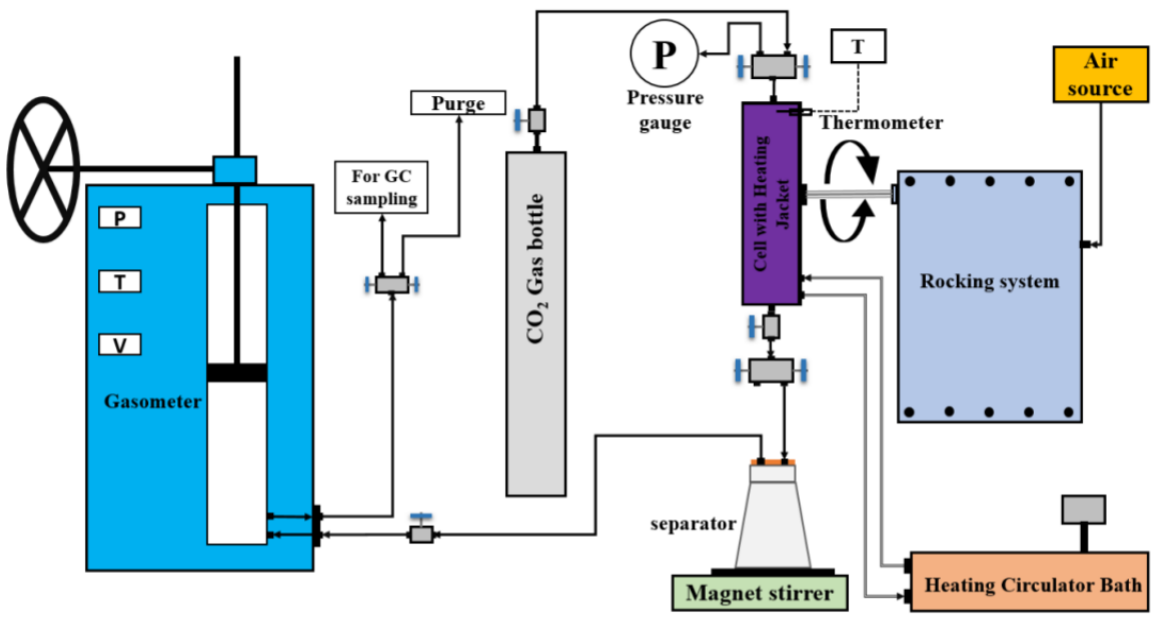

Figure 46 Schematic diagram of the solubility measurement setup. Source: (Ahmadi & Chapoy, 2018)

Temperature of the system is controlled by Heating Circulator Bath (HCB). Measurement cell is covered by heating jacked which is connected to HCB, while platinum-Resistance thermometer (PRT) is mounted on the body of the heating jacket in order to measure the temperature of the cell. Pressure is measured by pressure transducer. For measuring solubility of CO_2 at specified temperature and pressure, gasometer of maximum capacity of 4000 cm^3 is used (Ahmadi & Chapoy, 2018).

5.2.2. Results

For calculating solubility of CO_2 in salt aqueous solution, models were set up in both software. Since the Multiflash cannot load CPA model when NaCl is present, Redlich–Kwong-Soave "Advanced", commonly known as RKSA EoS model was used instead. In HydraFLASH, sCPA model was regularly set up.

Results are presented in Table 14 and Figures 47–50. Clearly, HydraFLASH software provided better results in terms of agreement with experimental data experimental data. Possible reason for this is usage of different EoS used in softwares. Obviously, RKSA EoS does not produce accurate results at lower temperatures, as it is shown in Figures 47 and 48. However, at higher temperatures, RKSA model could

provide almost equally good results, as sCPA EoS does, if not even better, which is clearly seen at Figures 49 and 50. Relative average deviation (%RAD) for HydraFLASH was estimated to 0.08%, while for Multiflash is 0.20%.

Table 14 Results of CO_2 solubility in salt aqueous phase

Conditions		Solubility CO_2, X (mole fraction)			Absolute Error X_{exp}-X_{mod} (mole fraction)		Relative Error (X_{exp}-X_{mod})/X_{exp} (%)	
T (K)	P (MPa)	Experiment	HydraFLASH	Multiflash	HydraFLASH	Multiflash	HydraFLASH	Multiflash
303.16	1.63	0.00527	0.00587	0.00356	0.00060	0.00171	**0.11**	0.32
303.16	6.61	0.01649	0.01820	0.01056	0.00171	0.00593	**0.10**	0.36
303.16	8.68	0.01804	0.01940	0.01120	0.00136	0.00684	**0.08**	0.38
303.16	20.52	0.01913	0.02174	0.01254	0.00261	0.00659	**0.14**	0.34
303.16	35.39	0.02096	0.02363	0.01368	0.00267	0.00728	**0.13**	0.35
323.20	1.76	0.00443	0.00425	0.00295	0.00018	0.00148	**0.04**	0.33
323.20	6.26	0.01192	0.01253	0.00846	0.00061	0.00346	**0.05**	0.29
323.20	10.72	0.01540	0.01656	0.01100	0.00116	0.00440	**0.08**	0.29
323.20	18.17	0.01708	0.01866	0.01231	0.00158	0.00477	**0.09**	0.28
323.20	38.86	0.01975	0.02169	0.01431	0.00194	0.00544	**0.10**	0.28
373.19	1.93	0.00232	0.00248	0.00219	0.00016	0.00013	0.07	**0.05**
373.19	8.17	0.00860	0.00923	0.00805	0.00063	0.00055	0.07	**0.06**
373.19	22.90	0.01561	0.01676	0.01432	0.00115	0.00129	**0.07**	0.08
373.19	38.81	0.01877	0.02018	0.01712	0.00141	0.00165	**0.07**	0.09
423.19	2.42	0.00244	0.00204	0.00222	0.00040	0.00022	0.16	**0.09**
423.19	5.43	0.00498	0.00511	0.00533	0.00013	0.00035	**0.03**	0.07
423.19	9.25	0.00879	0.00847	0.00874	0.00032	0.00005	0.04	**0.01**
423.19	24.34	0.01720	0.01729	0.01749	0.00009	0.00029	**0.01**	0.02
423.19	36.95	0.01999	0.02150	0.02157	0.00151	0.00158	**0.08**	0.08

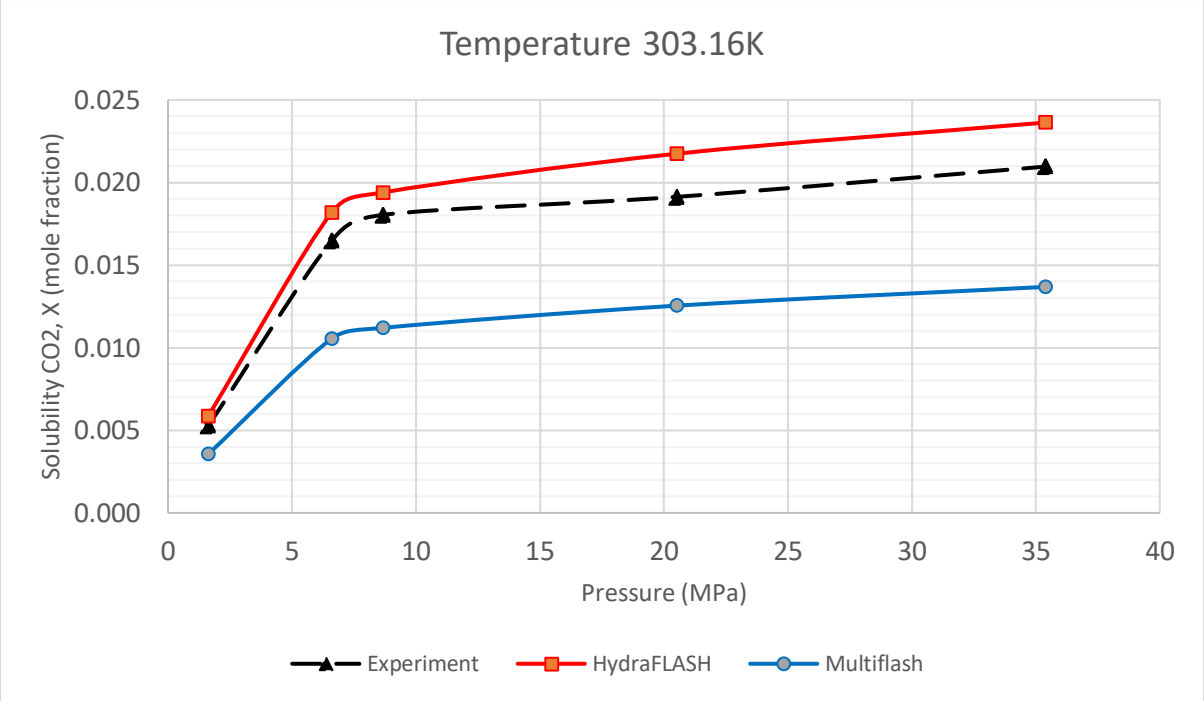

Figure 47 CO_2 solubility in salt aqueous phase - Isotherm 303.16K

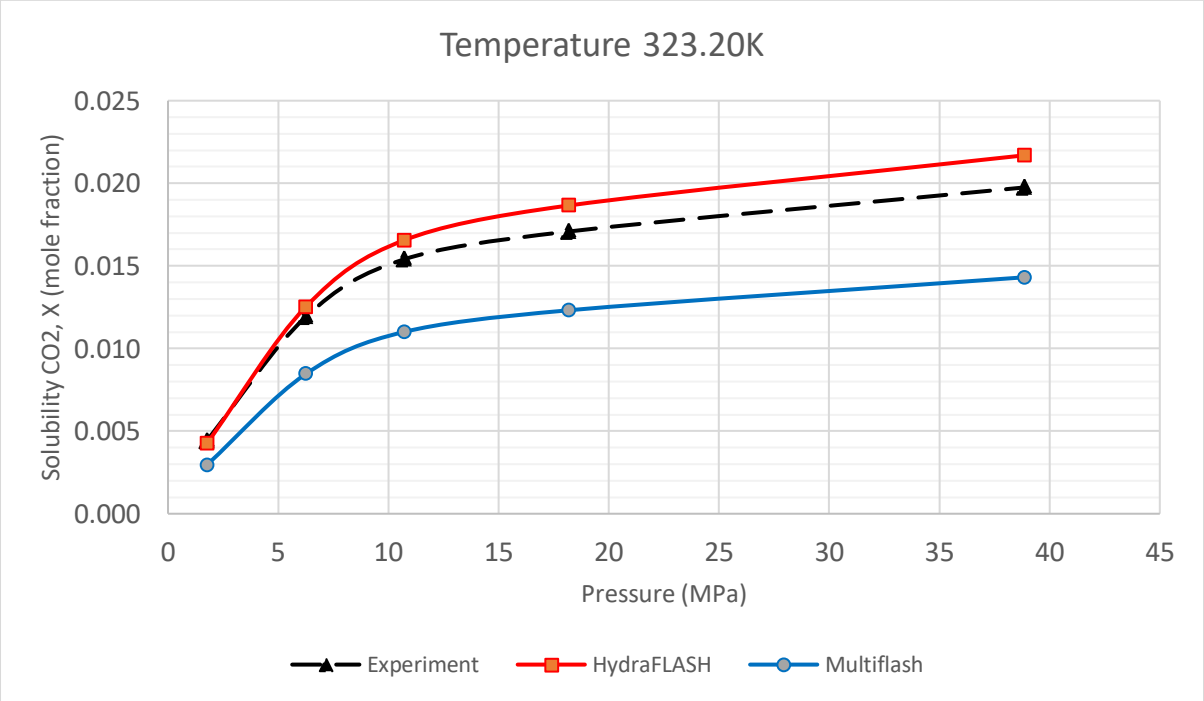

Figure 48 CO_2 solubility in salt aqueous phase - Isotherm 323.20K

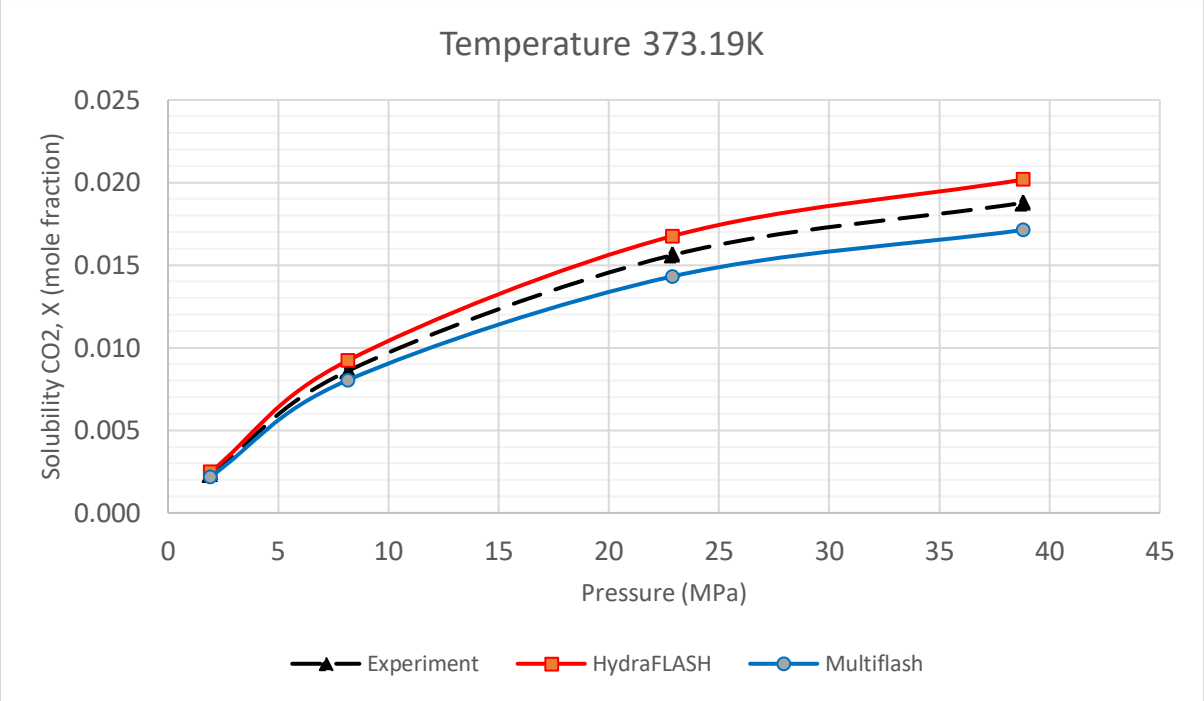

Figure 49 CO_2 solubility in salt aqueous phase - Isotherm 373.19K

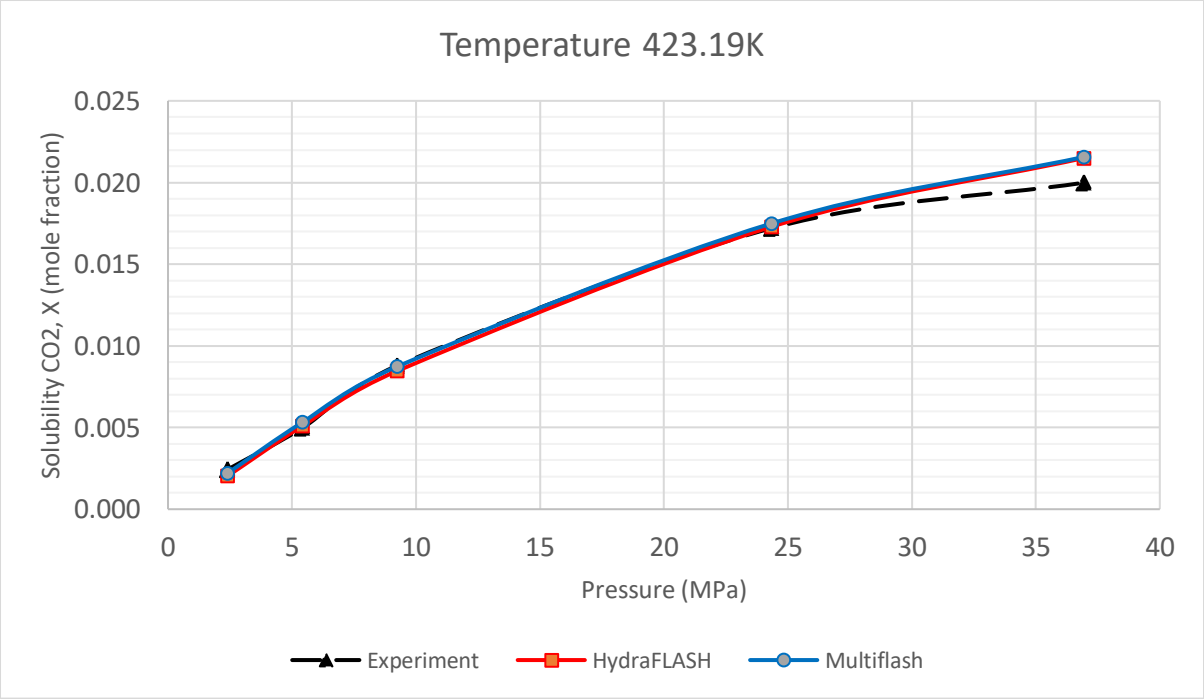

Figure 50 CO_2 solubility in salt aqueous phase - Isotherm 423.19K

6. Hydrate dissociation data

One of the main causes of transportation pipelines blockage, besides deposition of waxes and asphaltenes, is the formation of gas hydrates. Risk of hydrate formation and possible blockage in transportation pipelines is one of the most significant topics in the study of flow assurance. Gas hydrate blockage occurs at certain temperature and pressure conditions in pipeline, in the presence of water. If the blockage entirely fills the pipeline, capacity of transportation is immediately lost. In order to stop and prevent hydrate formation and blockage of pipelines, free and dissolved water should be removed from the system, high temperature and low pressure should be maintained, as well as usage of additives that act as hydrate inhibitors.

Gas hydrates are commonly known as clathrate hydrates or clathrates. Gas hydrate is a structure in which one of the components, which is known as a host, forms cages which surround molecules of another component, which is known as a guest. Generally, gas hydrates form one of three crystal structures. Those structures are shown in Figure 51, and they are: cubic structure I, cubic structure II, and the hexagonal structure H. The form of the hydrate structure depends on the gas (guest) which is contained in the hydrate cavities.

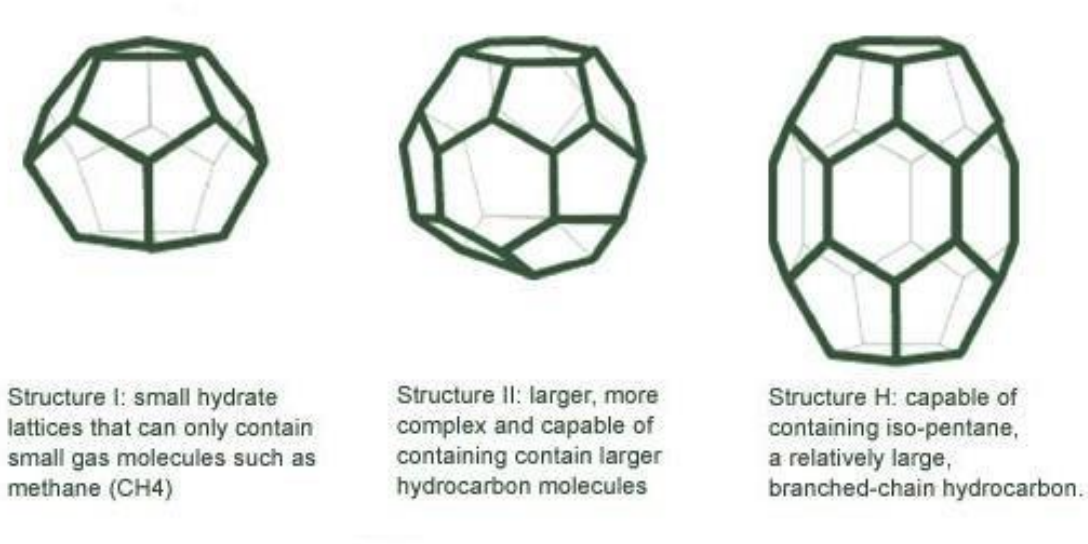

Figure 51 Gas hydrate structure types. Source: (Fakharian, Ganji, Naderifar, & Mofrad, 2010)

Although gas hydrates were primarily studied because of the risk of pipeline blockage during natural gas transport, recently they became also important for Carbon Capture and Storage (CCS) purposes. Capture and storage of CO_2 in the form of gas hydrates has been suggested as a possible method to reduce CO_2 emissions. There are two approaches for this. The first one is based on methane hydrate reservoirs that exist under permafrost and in continental and margin sediments can be used to store CO_2, while the second approach is based on forming gas hydrate from power plant flue gas, with the expectation that more CO_2 than N_2 will enter the hydrate phase, providing the possibility to separate and capture CO_2 after hydrate formation (Hassanpouryouzband, et al., 2019).

6.1. Hydrate dissociation data in presence of methanol/ethylene glycol

One of the major problems during the production of natural gas from CO_2-rich gas reservoirs is their big predisposition to form gas hydrates. Gas hydrates are the main problem of flow assurance in gas production, particularly in deep water gas reservoirs where hydrate formation cause pipeline blockage and raise safety concerns. Since the carbon-dioxide is more suitable to form gas hydrates in comparison to the methane, it is quite imperative that CO_2-rich gas mixtures are more predisposed to form gas hydrates than natural gas. One of the common methods to prevent formation of gas hydrates, is to make sure that working condition in the pipeline are not in the area of the hydrate formation condition. This is generally done by pipeline insulation or constant pipeline heating. Other options are dehydration of the natural gas and more often used injection of hydrate inhibitors.

Produced gas carries a notable amount of water in vapor form. Presence of different types of salts, reduces the ability for gas hydrates formation. However, when saline water inhibition is insufficient, aqueous solution of methanol and ethylene glycol will be injected into the pipeline, creating a system that includes both inhibitors and salts. Regarding to this, proper knowledge for gas hydrate dissociation condition in the presence of salt and inhibitors (methanol/ethylene glycol in this project) is needed as to

prevent formation of gas hydrates. This provides projection of safe and economical plant design, production and processing facilities, and pipeline operations (Nasir, Lau, Lal, & Sabil, 2014).

6.1.1. Experimental data

For this part of the project, CO_2-rich gas mixture in the existence of two different mass fractions of methanol and ethylene glycol is used for calculation of hydrate dissociation conditions. CO_2-rich gas mixture is used with following composition (Table 15). Mixture composition and experimental data is taken from Qazi Nasir study (Nasir, Lau, Lal, & Sabil, 2014).

Table 15 CO_2-rich Gas mixture (mole fraction)

Components	Mole fraction
CO_2	0.70353
N_2	0.03096
CH_4	0.26551

In this experiment, isochoric pressure search method was used for measuring hydrate dissociation condition. Scheme of experimental apparatus is shown in Figure 52. Apparatus consists of a high pressure equilibrium sapphire cell with 60 cm^3 volume, maximum working pressure of 20 MPa, and temperature range of 253.15 K to 338.15 K (Nasir, Lau, Lal, & Sabil, 2014).

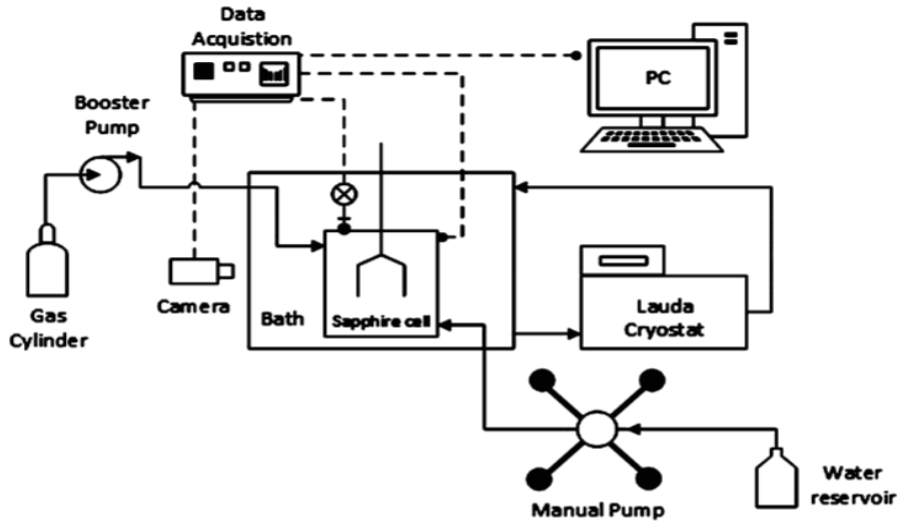

Figure 52 Schematic diagram of the experimental apparatus. Source: (Nasir, Lau, Lal, & Sabil, 2014)

The temperature inside the cell is controlled by DLK45 thermostats and ethanol circulation is used for cooling. Magnetic torque stirrer inside the equilibrium cell is used for proper mixing of sample inside the equilibrium cell. The gas sample from gas cylinder is transported to the equilibrium sapphire cell using air booster pump (compressor) which maximum outlet pressure is 31 MPa. Deonized water from water reservoir is transferred to the equilibrium with usage of manual pump. Lastly, camera is used for monitoring any possible changes that could happen to the sample in the equilibrium cell. First, temperature and pressure are set outside the hydrate stability boundary zone. After that, temperature of the system is decreasing until hydrate is formed, which is noticed as a quick drop in pressure at almost constant temperature. Completion of hydrate formation is supposed to be when there is no more change in temperature and pressure over time (Nasir, Lau, Lal, & Sabil, 2014).

6.1.2. Results

Results of hydrate dissociation predictions obtained from both HydraFLASH and Multiflash software are collected and compared with the experimental data. In both software programs, CPA EoS was successfully applied. Results are presented in Tables 16 and 17, and graphically shown in Figures 53–56. Both software showed an excellent agreement with experimental data. However, in the presence of methanol, HydraFLASH provides better results, while in the presence of ethylene glycol, Multiflash works slightly better in matching experimental data. In the presence of methanol, relative average deviation (%RAD) for HydraFLASH was 0.06%, while for Multiflash it was 0.07%. When ethylene glycol is present, %RAD is 0.05% and 0.03%, respectively.

We can conclude that while both software give fairly good results for hydrate dissociation data, HydraFLASH will be a better choice when methanol is present as inhibitor in temperature range between 272 K and 283 K, while Multiflash will provide better data in presence of ethylene glycol, in similar temperature range.

Table 16 Results of Hydrate Dissociation Data in presence of methanol

Conditions		Hydrate Dissociation Pressure (MPa)			Absolute Error Pexp -Pmod (MPa)		Relative Error (Pexp-Pmod)/Pexp (%)	
MeOH (mass fraction)	T (K)	Experiment	HydraFLASH	Multiflash	HydraFLASH	Multiflash	HydraFLASH	Multiflash
0.10	279.35	3.35	3.68	3.59	0.33	0.24	0.10	**0.07**
0.10	281.35	4.84	4.83	4.68	0.01	0.16	**0.00**	0.03
0.10	282.75	6.19	5.99	5.77	0.20	0.42	**0.03**	0.07
0.10	283.25	7.30	6.51	6.25	0.79	1.05	**0.11**	0.14
0.20	272.55	2.97	2.80	2.83	0.17	0.14	0.06	**0.05**
0.20	275.45	4.22	4.12	4.09	0.10	0.13	**0.02**	0.03
0.20	277.45	5.89	5.60	5.48	0.29	0.41	**0.05**	0.07
0.20	278.15	6.94	6.33	6.15	0.61	0.79	**0.09**	0.11

Table 17 Results of Hydrate Dissociation Data in presence of ethylene glycol

Conditions		Hydrate Dissociation Pressure (MPa)			Absolute Error Pexp -Pmod (MPa)		Relative Error (Pexp-Pmod)/Pexp (%)	
MEG (mass fraction)	T (K)	Experiment	HydraFLASH	Multiflash	HydraFLASH	Multiflash	HydraFLASH	Multiflash
0.10	279.45	3.21	3.38	3.31	0.17	0.10	0.05	**0.03**
0.10	282.35	4.87	4.99	4.85	0.12	0.02	0.02	**0.00**
0.10	283.85	6.10	6.29	6.08	0.19	0.02	0.03	**0.00**
0.10	284.15	7.18	6.61	6.39	0.57	0.79	**0.08**	0.11
0.20	276.85	3.12	3.32	3.27	0.20	0.15	0.06	**0.05**
0.20	279.45	4.62	4.72	4.61	0.10	0.01	0.02	**0.00**
0.20	281.35	5.86	6.37	6.17	0.51	0.31	0.09	**0.05**
0.20	281.85	6.92	6.97	6.73	0.05	0.19	**0.01**	0.03

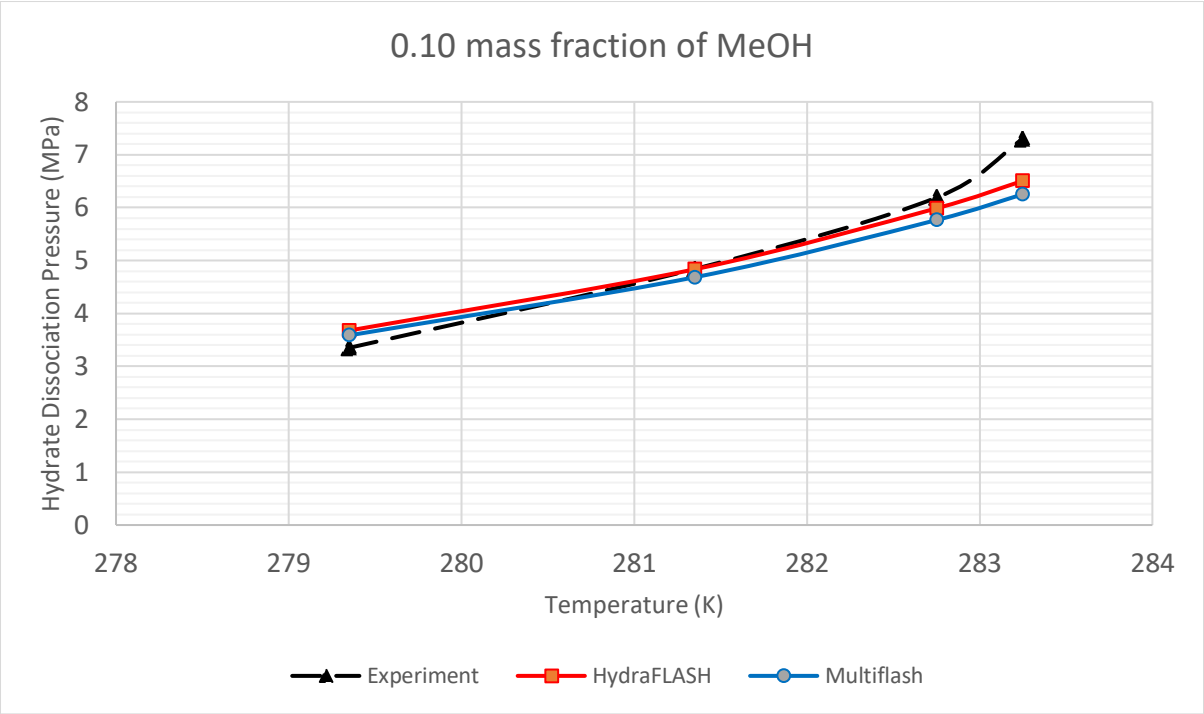

Figure 53 Hydrate Dissociation Data - 0.10 mass fraction of MeOH

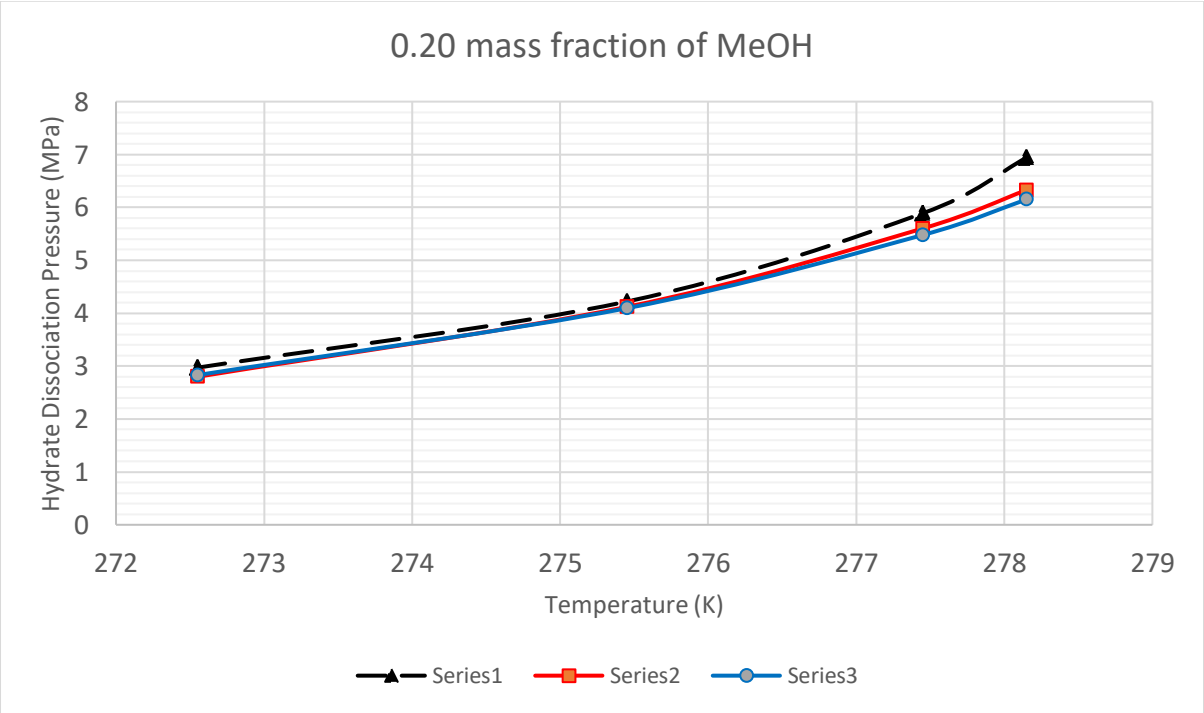

Figure 54 Hydrate Dissociation Data - 0.20 mass fraction of MeOH

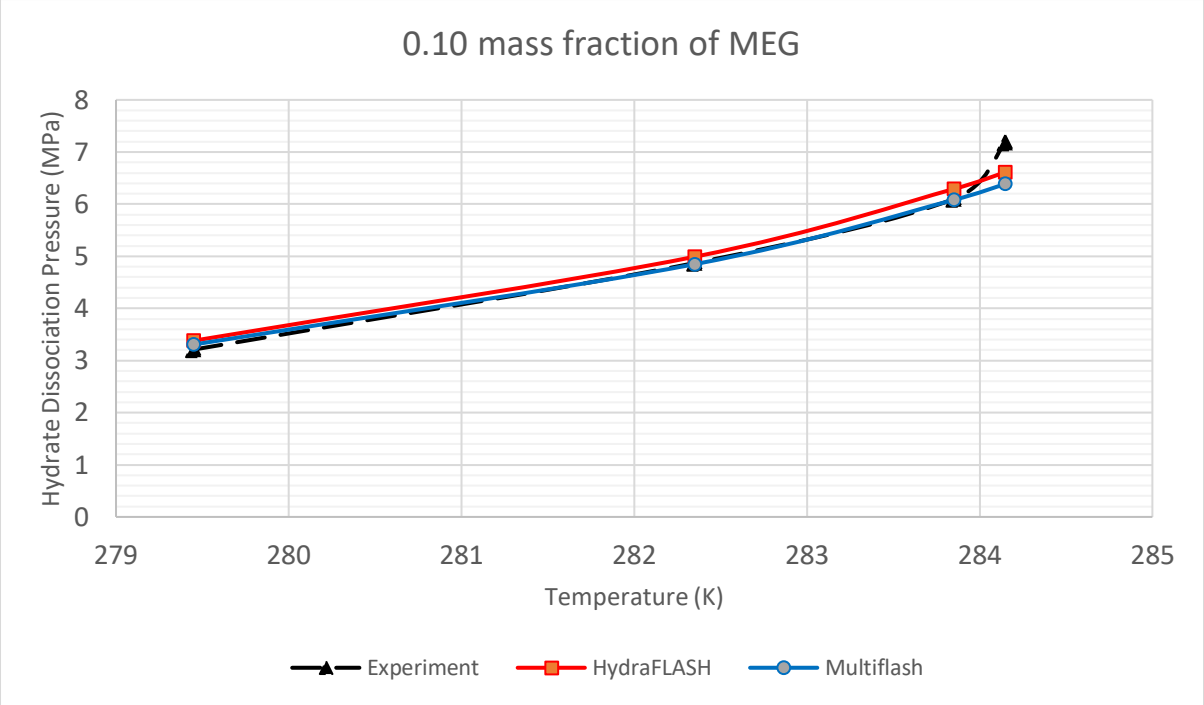

Figure 55 Hydrate Dissociation Data - 0.10 mass fraction of MEG

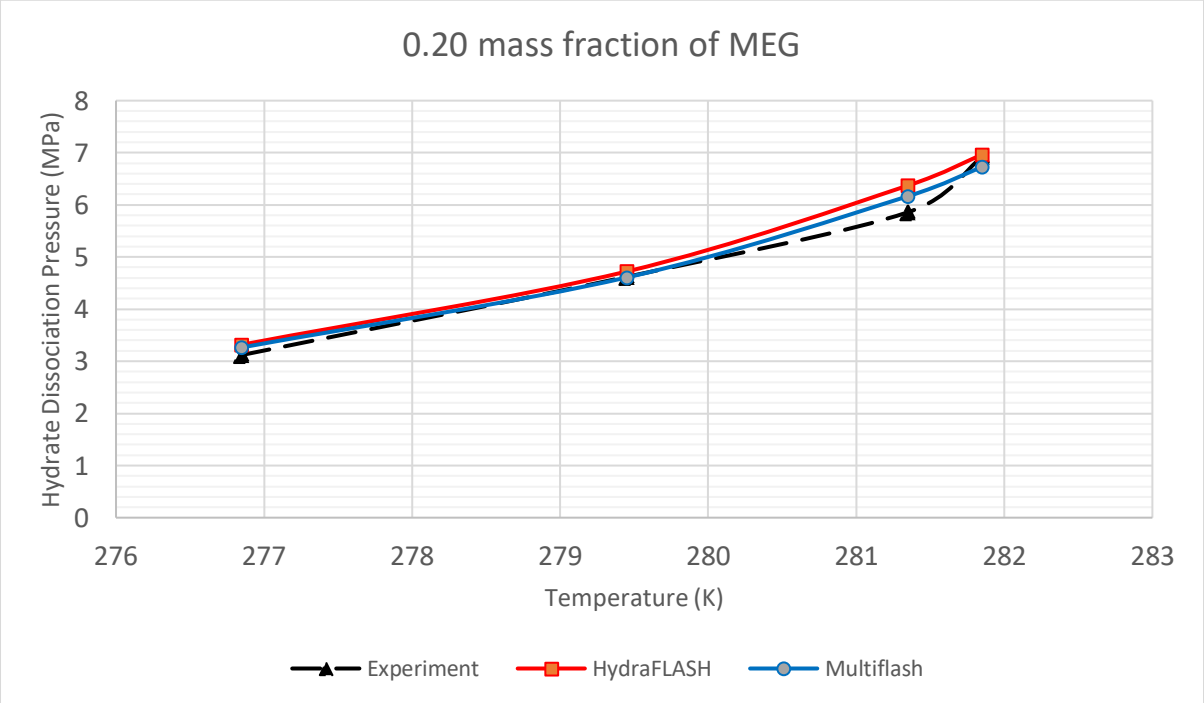

Figure 56 Hydrate Dissociation Data - 0.20 mass fraction of MEG

6.2. Hydrate dissociation data in presence of water

Formation of gas hydrates is one of the main characteristics of the water–carbon dioxide system. A correct description of thermodynamic properties of this system needs a compatible description of both fluid (liquid, vapor, and supercritical fluid) and solid phase (ice, dry ice, and hydrates) and of their phase equilibrium. It is well-known that CO_2 forms sI gas hydrates, under the specific conditions of temperature and pressure.

6.2.1. Experimental data

For hydrate dissociation data in the presence of water, binary synthetic mixtures from Chapoy et al. study were used (Chapoy, Burgass, Tohidi, & Alsiyabi, 2015). Molar compositions of mixtures used in this study are shown below in Table 18. Impurities presented are mostly common impurities which exists during the CCS processes. Deionized water was used in all hydrate tests.

Table 18 Composition of synthetic binary mixtures

Impurity	CO_2	Mole fraction
Nitrogen	balance	0.046
Methane		0.059
Carbon monoxide		0.059
Oxygen		0.053
Argon		0.050

During the experiment, a reliable isochoric step-heating method was used to calculate hydrate dissociation points. In Figure 57 is presented apparatus which is used to measure the phase equilibrium conditions. The equilibrium setup consists of a piston-type variable volume with volume of 300 mL, titanium cylindrical pressure vessel with mixing ball, which is mounted on a horizontal pivot with associated stand for pneumatic controlled rocking mechanism. Adequate mixing of the cell fluids is ensured by rocking of the cell at constant rate and subsequent movement of the mixing ball. Cell volume and pressure, is adjusted by injecting or withdrawal of liquid behind the moving piston. Working temperature of rig ranges between 203.15 K and 453.15 K, and maximum

operating pressure is 70 MPa. Temperature of the system is controlled by circulating coolant from a cryostat within a jacket surrounding the cell (Chapoy, Burgass, Tohidi, & Alsiyabi, 2015).

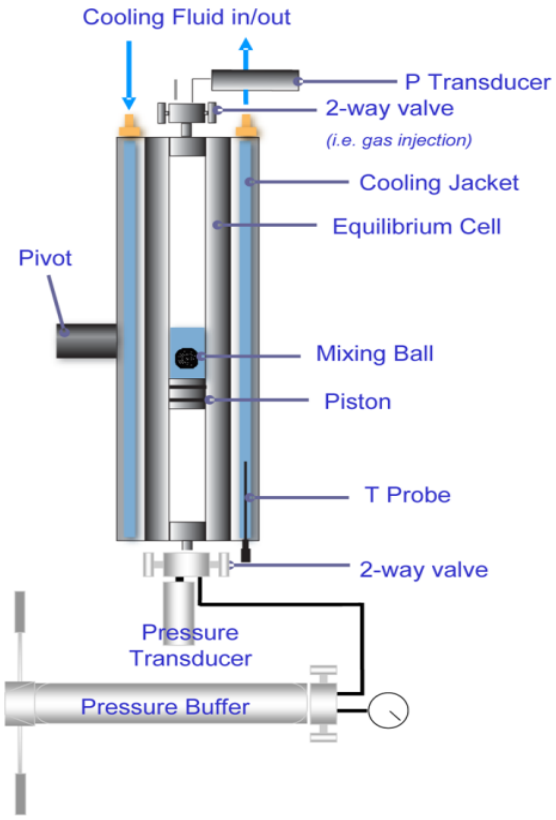

Figure 57 Schematic illustration of equilibrium rig used for measuring saturation pressure. Source: (Chapoy, Burgass, Tohidi, & Alsiyabi, 2015)

The equilibrium cell and pipework are well insulated, in order to ensure constant temperature. The temperature is measured and monitored by platinum resistance thermometers which are located in the cooling jacket of the cell. Quartzdyne pressure transducer with an accuracy of ± 0.03 MPa was used for monitoring the pressure. The weight of the injected fluids (i.e., water and the multicomponent CO_2 fluid) are recorded before any measurements, so the overall feed composition can be calculated (Chapoy, Burgass, Tohidi, & Alsiyabi, 2015). The core of the equipment for measuring the water content is originally described by Chapoy A. (Haghighi, Chapoy, Burgass, & Tohidi, 2011). Equipment includes an equilibrium cell and a device for water content measurement of equilibrated fluids passed from the cell. Setup for measuring water content consists of a heated line, a tunable diode laser adsorption spectroscope (TDLAS) and a flow meter (Chapoy, Burgass, Tohidi, & Alsiyabi, 2015).

6.2.2. Results

By studying the phase envelopes produced by both software for different binary mixtures, there are clearly some differences in phase regions that leads to less accurate results. For binary mixture CO_2–Ar, phase envelope is shown below in Figures 58 and 59. Clearly, it can be seen that third point in Multiflash software is in two phase region, while in HydraFLASH is in single liquid phase, which produced different results of HydraFLASH software related to experimental data. However, since these predictions were compared with only one set of data, there is a possibility that experimental data is inaccurate. Also, the error is within the uncertainty of the experimental data, so it cannot be concluded that either HydraFLASH or Multiflash has more accurate results. In Figures 60–67 phase envelopes of other binary mixtures are shown.

All mixtures were successfully implemented in both software and CPA EoS model was set up. Results of hydrate dissociation data are shown in Tables 19–23 and graphically presented in Figures 68–72. It can be clearly seen that HydraFLASH provided better results in matching experimental data. In CO_2–CH_4 and CO_2–CO mixtures, HydraFLASH produced better matching than Multiflash software for all experimental temperatures and pressures (Tables 19 and 21). Relative average deviations (%RAD) from experimental data for both mixtures, were 0.03% and 0.09% for HydraFLASH, and 0.08% and 0.51% for Multiflash, respectively.

In regard to the rest of mixtures, there are some conditions in which Multiflash works better than HydraFLASH and vice versa. For mixture CO_2–N_2, Multiflash results were quantitatively much closer to data from experiment. Those values were measured at isotherms of 279.65 K, 283.64 K, 287.40 K and 288.55 K (Table 20). Relative average deviation for CO_2–N_2 mixture was 0.12% for HydraFLASH and 0.04% for Multiflash. Interestingly, in mixtures between carbon dioxide and oxygen, and carbon dioxide and argon, HydraFLASH offers better matching at lower temperatures (isotherms between 275 K and 282 K), while at higher temperatures (above 284 K), Multiflash showed better agreement (Tables 22 and 23).

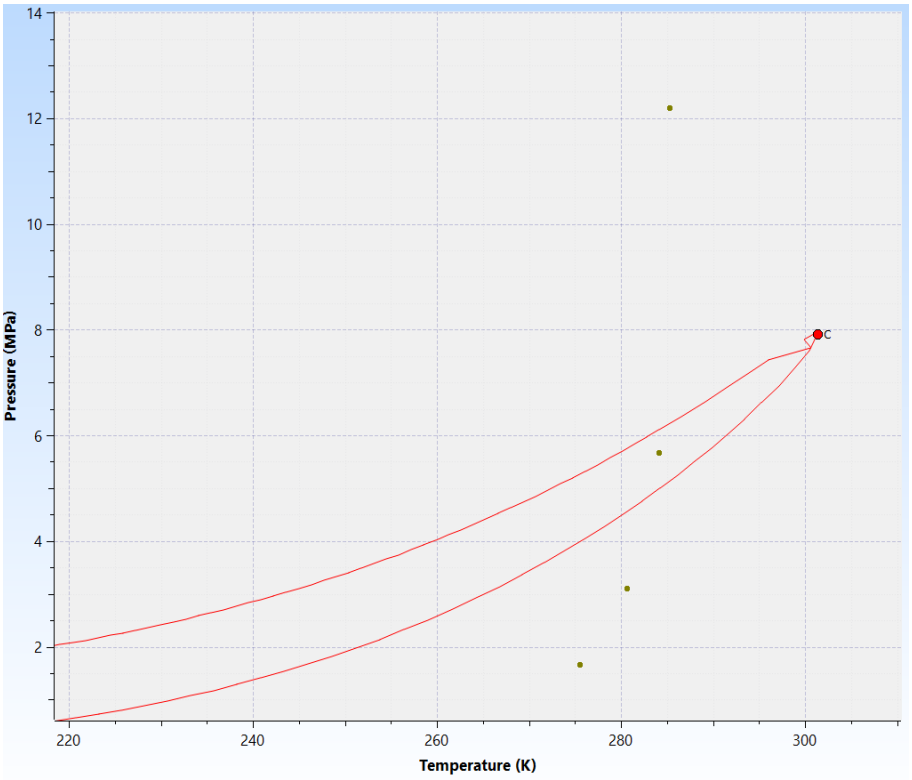

Figure 58 Phase envelope of CO_2-Ar binary mixture in Multiflash software with added result points

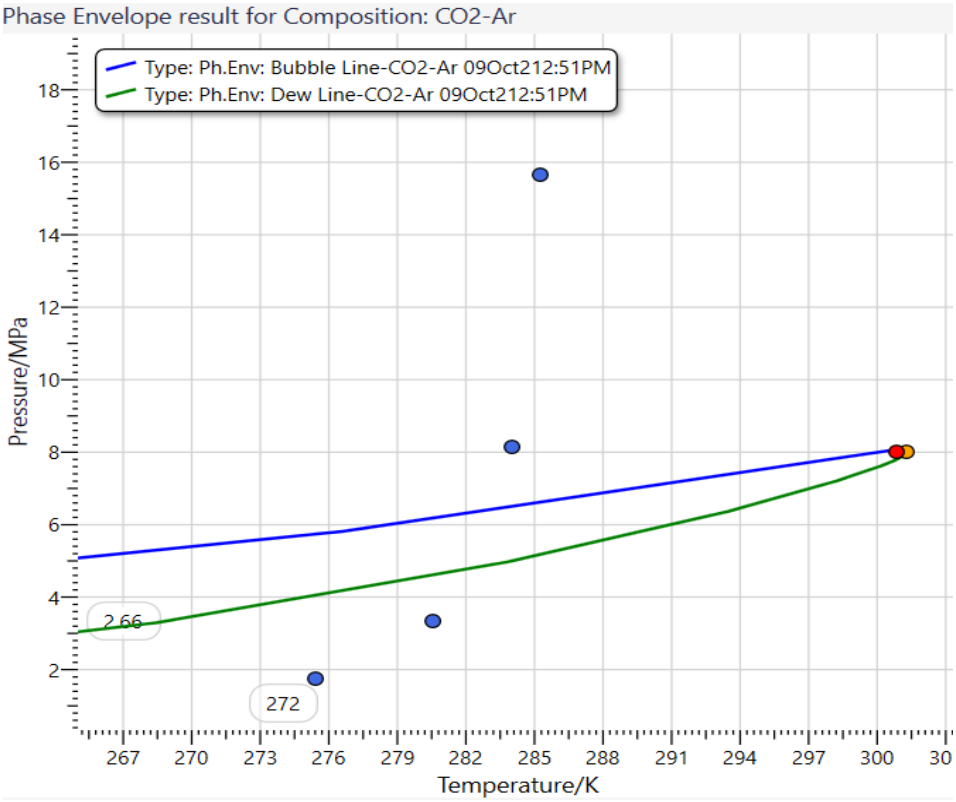

Figure 59 Phase envelope of CO_2-Ar binary mixture in HydraFLASH software with added result points

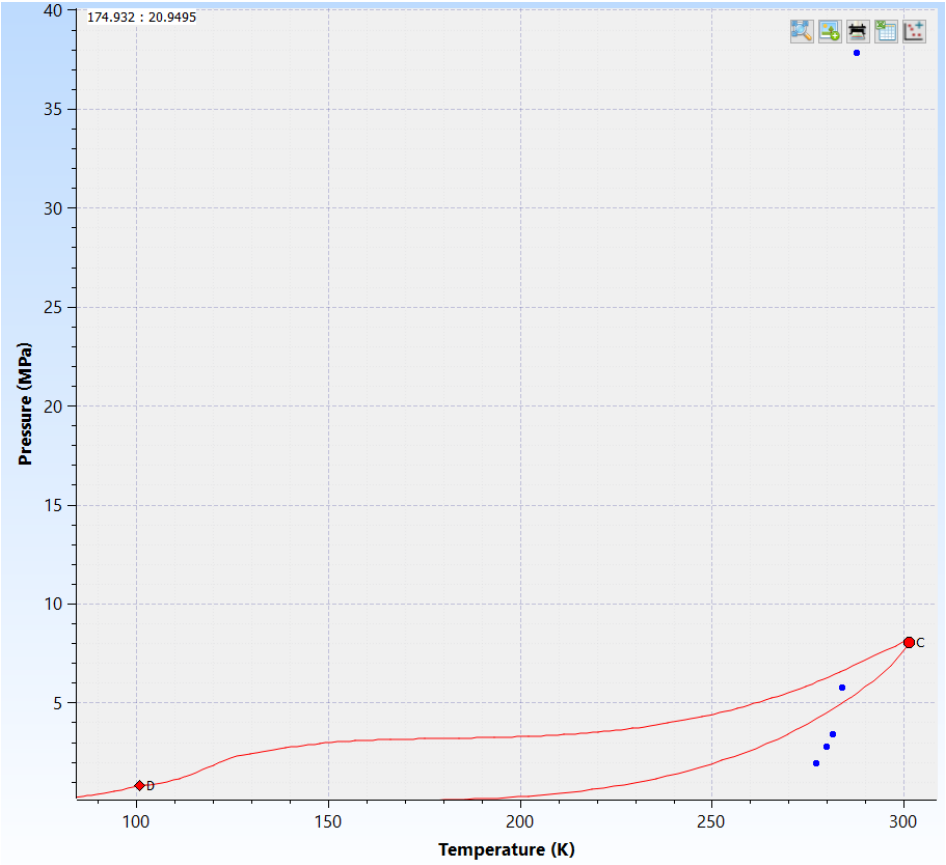

Figure 60 Phase envelope of CO2-N2 binary mixture in Multiflash software with added result points

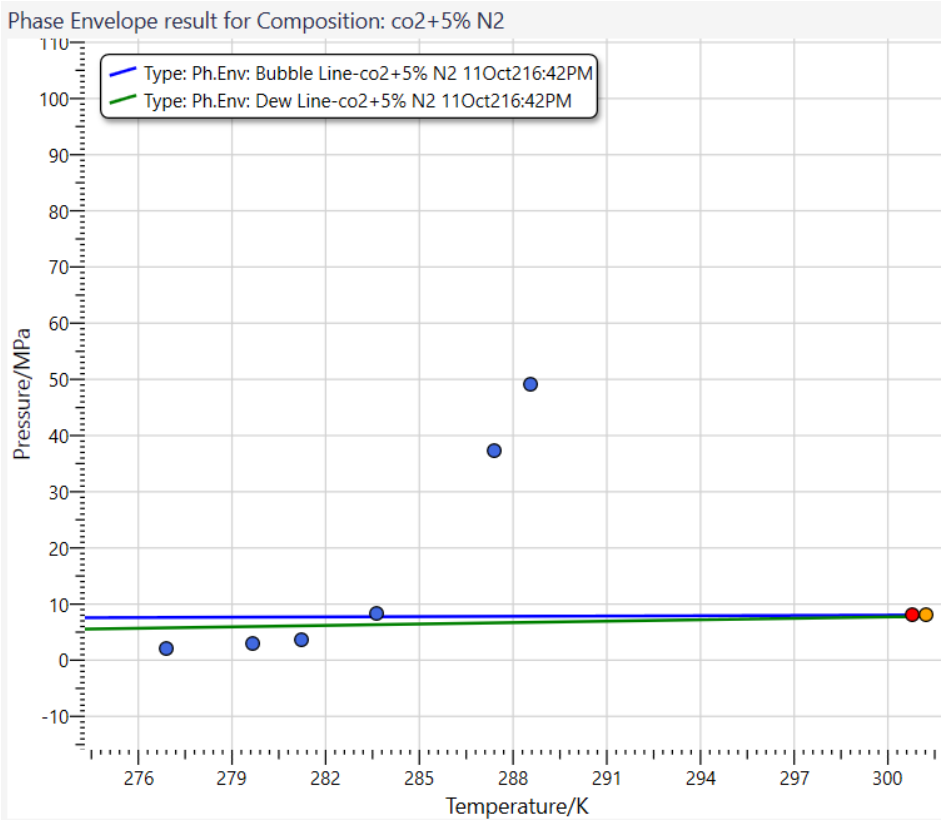

Figure 61 Phase envelope of CO2-N2 binary mixture in HydraFLASH software with added result points

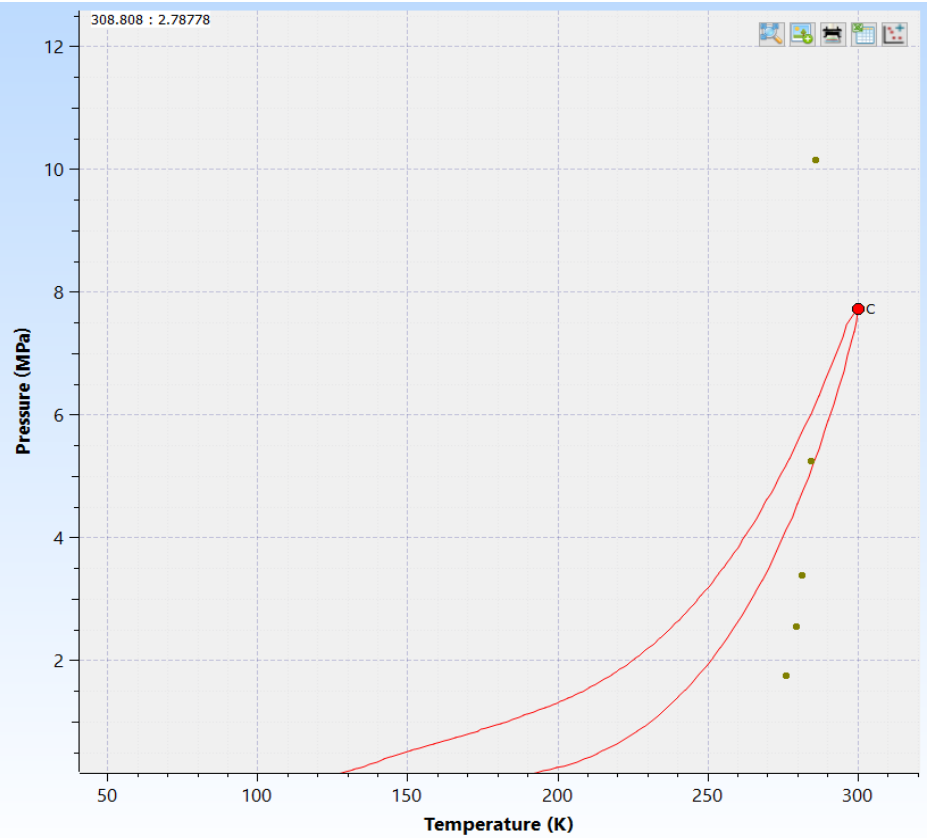

Figure 62 Phase envelope of CO2-CH4 binary mixture in Multiflash software with added result points

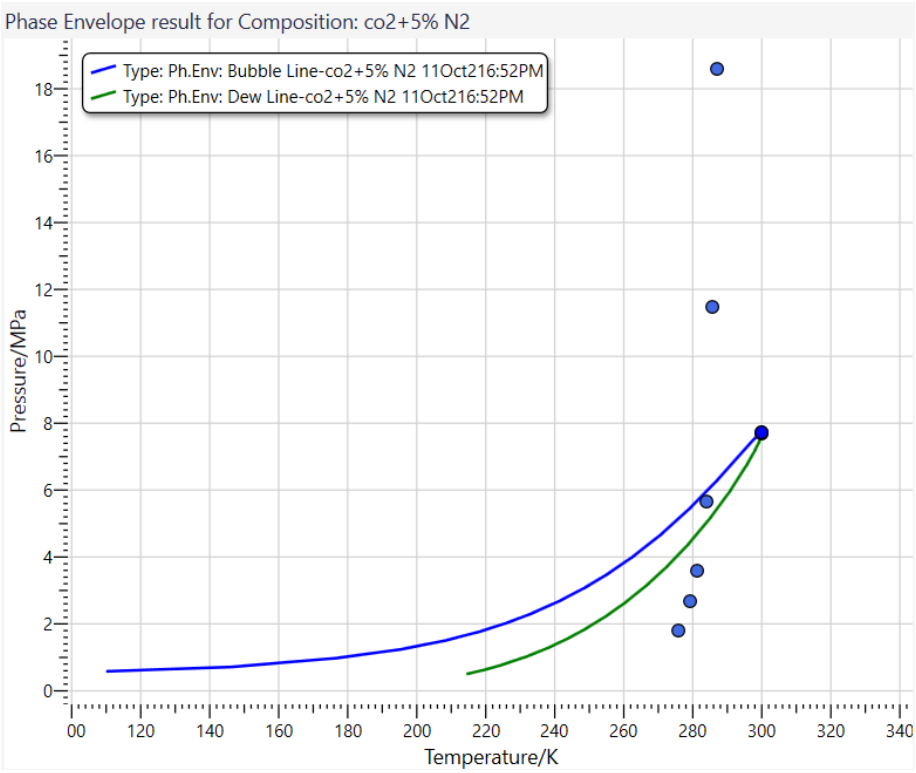

Figure 63 Phase envelope of CO2-CH4 binary mixture in HydraFLASH software with added result points

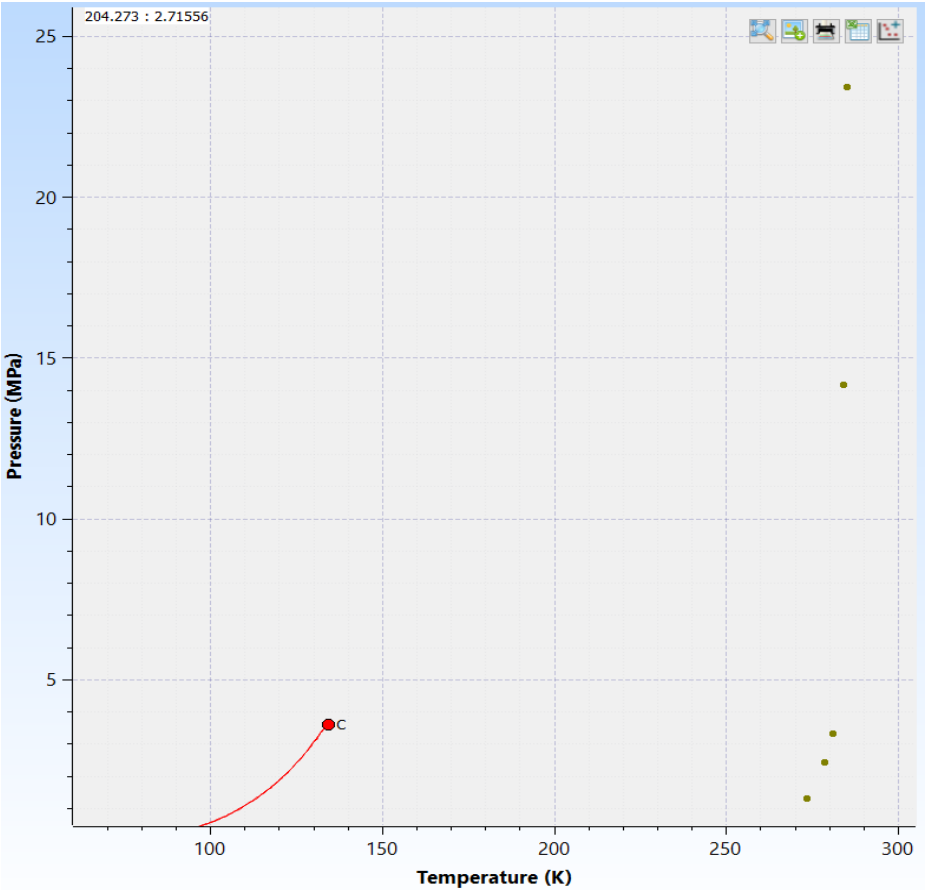

Figure 64 Phase envelope of CO2-CO binary mixture in Multiflash software with added result points

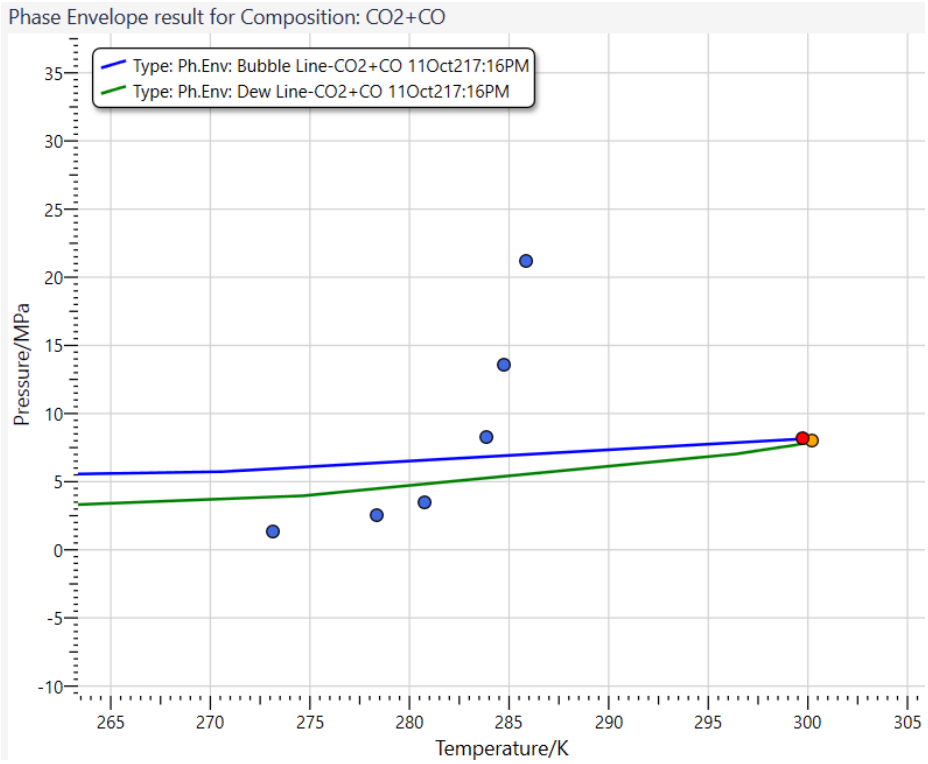

Figure 65 Phase envelope of CO2-CO binary mixture in HydraFLASH software with added result points

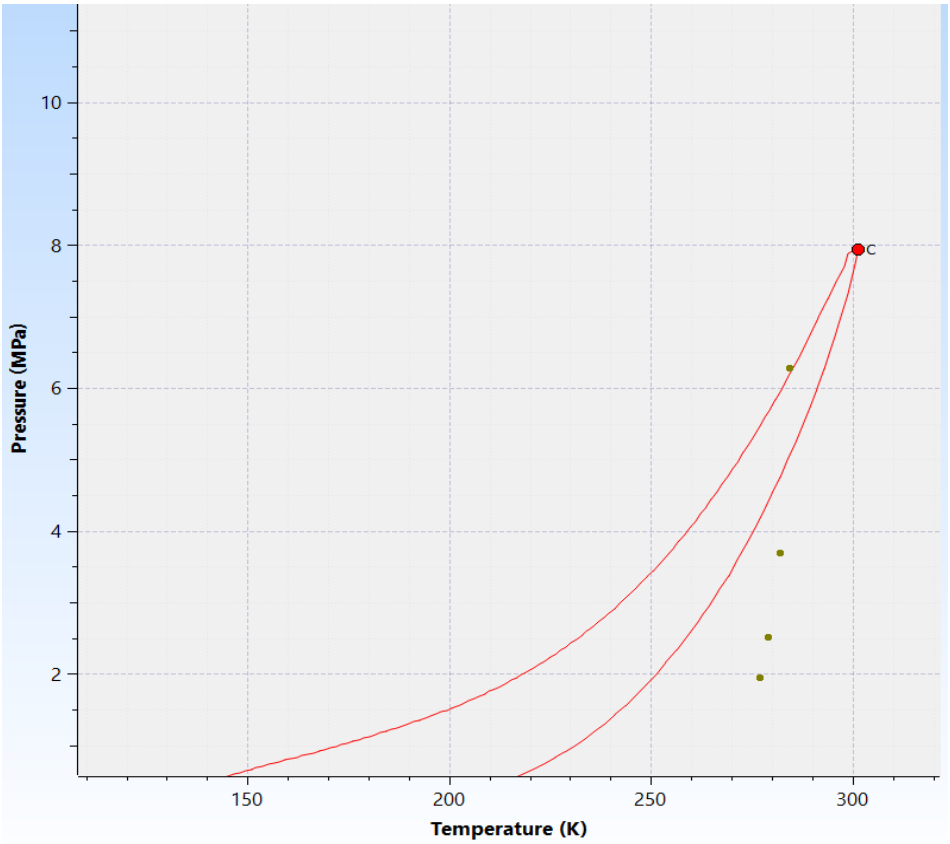

Figure 66 Phase envelope of CO2-O2 binary mixture in Multiflash software with added result points

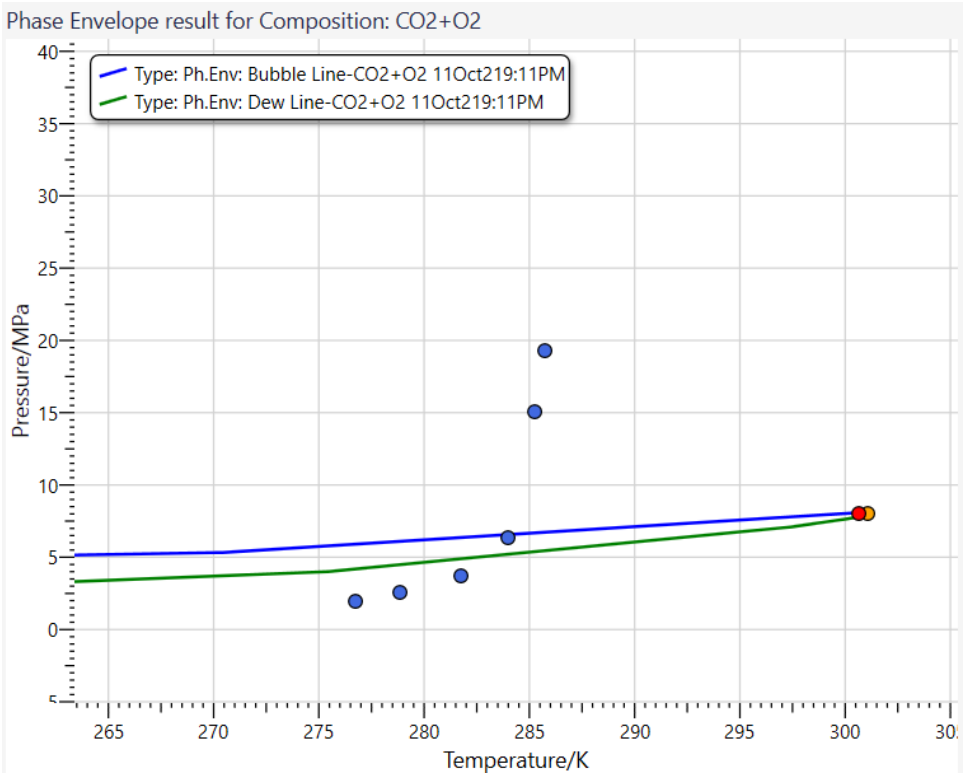

Figure 67 Phase envelope of CO2-O2 binary mixture in HydraFLASH software with added result points

Table 19 Results of Hydrate Dissociation Data in CO_2–CH_4 System

T (K)	Hydrate Dissociation Pressure (MPa)			Absolute Error Pexp -Pmod (MPa)		Relative Error (Pexp-Pmod)/Pexp (%)	
	Experiment	HydraFLASH	Multiflash	HydraFLASH	Multiflash	HydraFLASH	Multiflash
276.00	1.82	1.81	1.76	0.01	0.07	**0.00**	0.04
279.20	2.68	2.68	2.57	0.00	0.11	**0.00**	0.04
281.35	3.61	3.59	3.40	0.02	0.21	**0.01**	0.06
284.15	5.81	5.64	5.26	0.17	0.56	**0.03**	0.10
285.75	12.25	11.47	10.16	0.78	2.09	**0.06**	0.17
286.95	19.97	18.60	17.84	1.37	2.13	**0.07**	0.11

Table 20 Results of Hydrate Dissociation Data in CO_2–N_2 System

T (K)	Hydrate Dissociation Pressure (MPa)			Absolute Error Pexp -Pmod (MPa)		Relative Error (Pexp-Pmod)/Pexp (%)	
	Experiment	HydraFLASH	Multiflash	HydraFLASH	Multiflash	HydraFLASH	Multiflash
276.91	2.05	2.08	2.00	0.03	0.05	**0.01**	0.03
279.65	2.82	2.95	2.80	0.13	0.02	0.05	**0.01**
281.23	3.66	3.69	3.46	0.03	0.20	**0.01**	0.05
283.64	5.72	8.18	5.82	2.46	0.10	0.43	**0.02**
287.40	40.82	37.32	37.89	3.50	2.93	0.09	**0.07**
288.55	55.11	49.01	51.50	6.10	3.61	0.11	**0.07**

Table 21 Results of Hydrate Dissociation Data in CO_2–CO System

T (K)	Hydrate Dissociation Pressure (MPa)			Absolute Error Pexp -Pmod (MPa)		Relative Error (Pexp-Pmod)/Pexp (%)	
	Experiment	HydraFLASH	Multiflash	HydraFLASH	Multiflash	HydraFLASH	Multiflash
273.15	1.38	1.35	1.32	0.03	0.06	**0.02**	0.04
278.35	2.63	2.51	2.44	0.12	0.19	**0.05**	0.07
280.75	3.64	3.47	3.34	0.17	0.30	**0.05**	0.08
283.85	6.69	8.26	14.20	1.57	7.51	**0.23**	1.12
284.75	11.63	13.57	23.43	1.94	11.80	**0.17**	1.01
285.85	21.30	21.21	36.34	0.09	15.04	**0.00**	0.71

Table 22 Results of Hydrate Dissociation Data in CO_2–O_2 System

T (K)	Hydrate Dissociation Pressure (MPa)			Absolute Error Pexp -Pmod (MPa)		Relative Error (Pexp-Pmod)/Pexp (%)	
	Experiment	HydraFLASH	Multiflash	HydraFLASH	Multiflash	HydraFLASH	Multiflash
276.75	2.05	2.04	1.96	0.01	0.09	**0.00**	0.05
278.85	2.68	2.66	2.52	0.02	0.16	**0.01**	0.06
281.75	4.05	4.01	3.71	0.04	0.34	**0.01**	0.08
284.01	7.04	9.36	6.29	2.32	0.75	0.33	**0.11**
285.25	13.19	17.80	15.02	4.61	1.83	0.35	**0.14**
285.75	18.33	21.71	19.30	3.38	0.97	0.18	**0.05**

Table 23 Results of Hydrate Dissociation Data in CO_2–Ar System

T (K)	Hydrate Dissociation Pressure (MPa)			Absolute Error Pexp -Pmod (MPa)		Relative Error (Pexp-Pmod)/Pexp (%)	
	Experiment	HydraFLASH	Multiflash	HydraFLASH	Multiflash	HydraFLASH	Multiflash
275.45	1.72	1.74	1.67	0.02	0.05	**0.01**	0.03
280.55	3.22	3.32	3.11	0.10	0.11	**0.03**	0.03
284.05	5.81	8.13	5.68	2.32	0.13	0.40	**0.02**
285.25	11.26	15.64	12.21	4.38	0.95	0.39	**0.08**
285.65	16.07	18.53	15.20	2.46	0.87	0.15	**0.05**

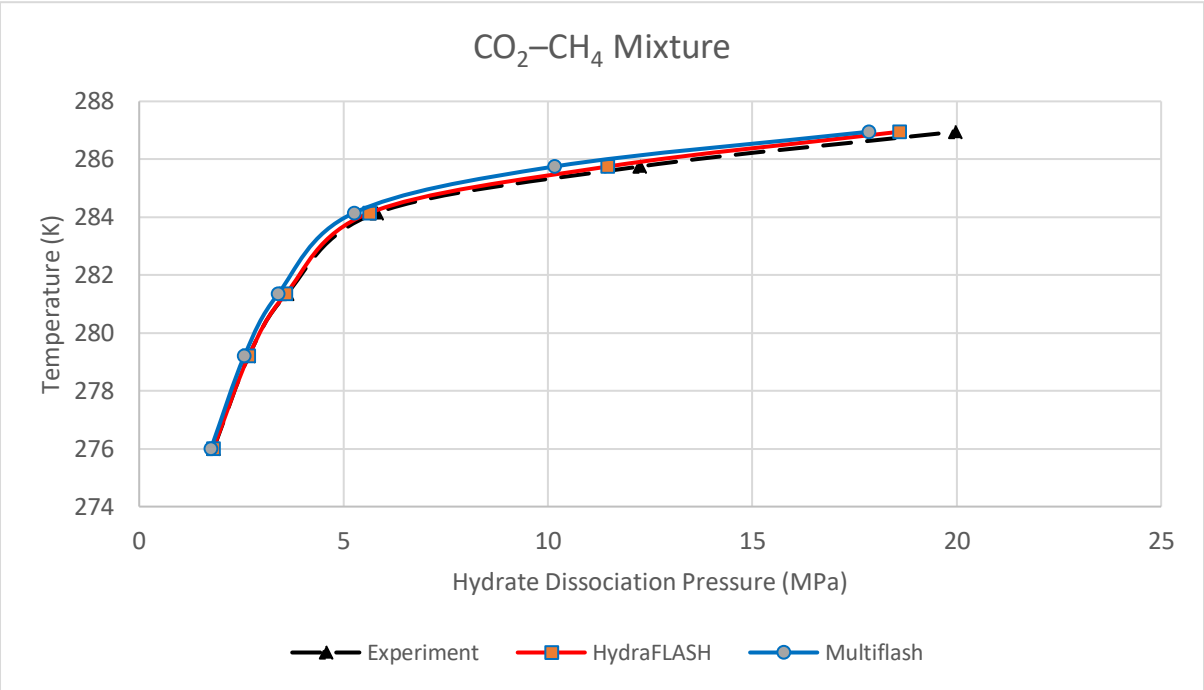

Figure 68 Hydrate Dissociation Data - CO_2–CH_4 Mixture

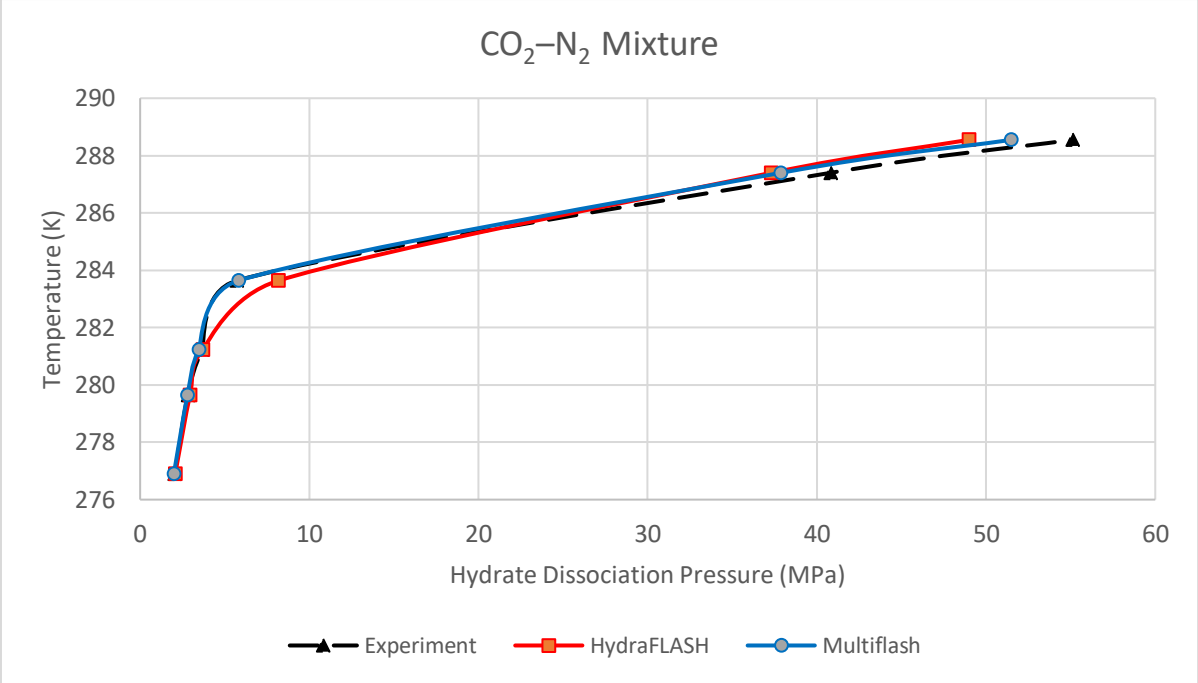

Figure 69 Hydrate Dissociation Data - CO_2–N_2 Mixture

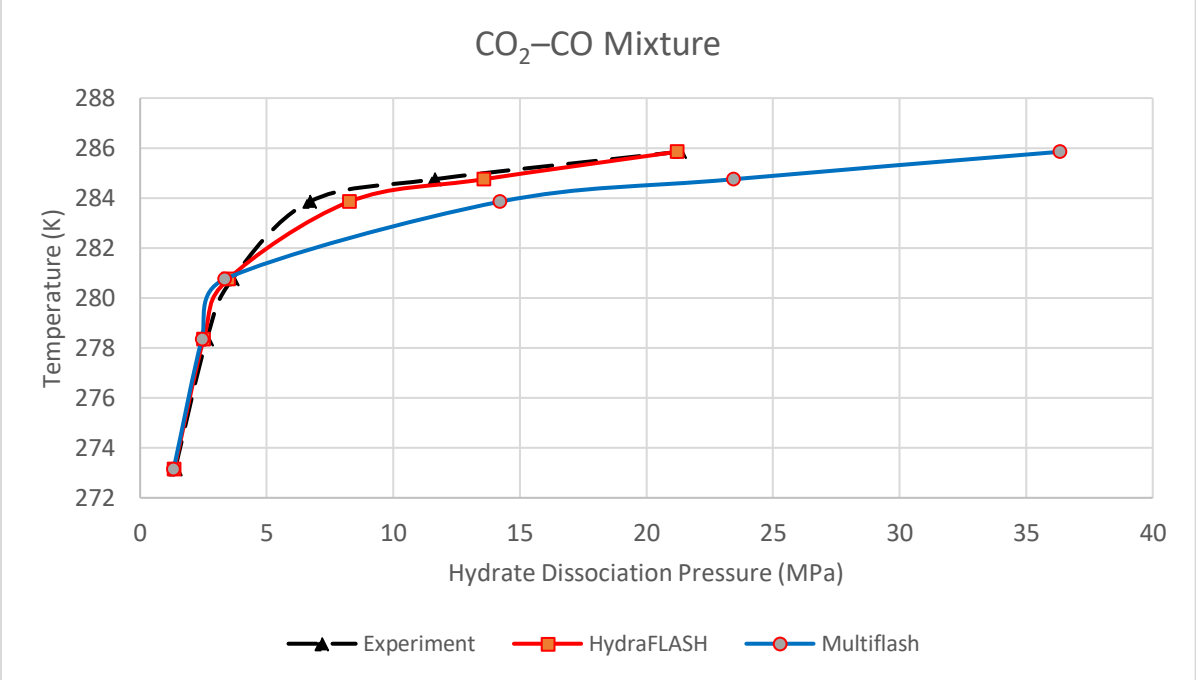

Figure 70 Hydrate Dissociation Data - CO_2–CO Mixture

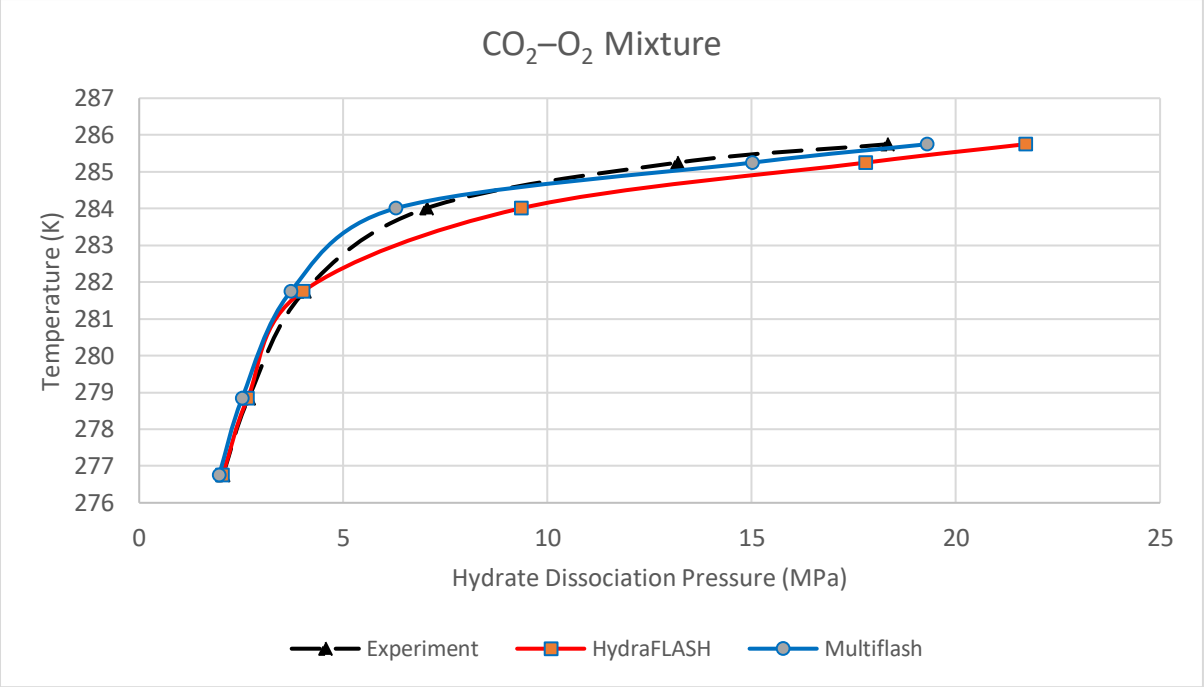

Figure 71 Hydrate Dissociation Data - CO_2–O_2 Mixture

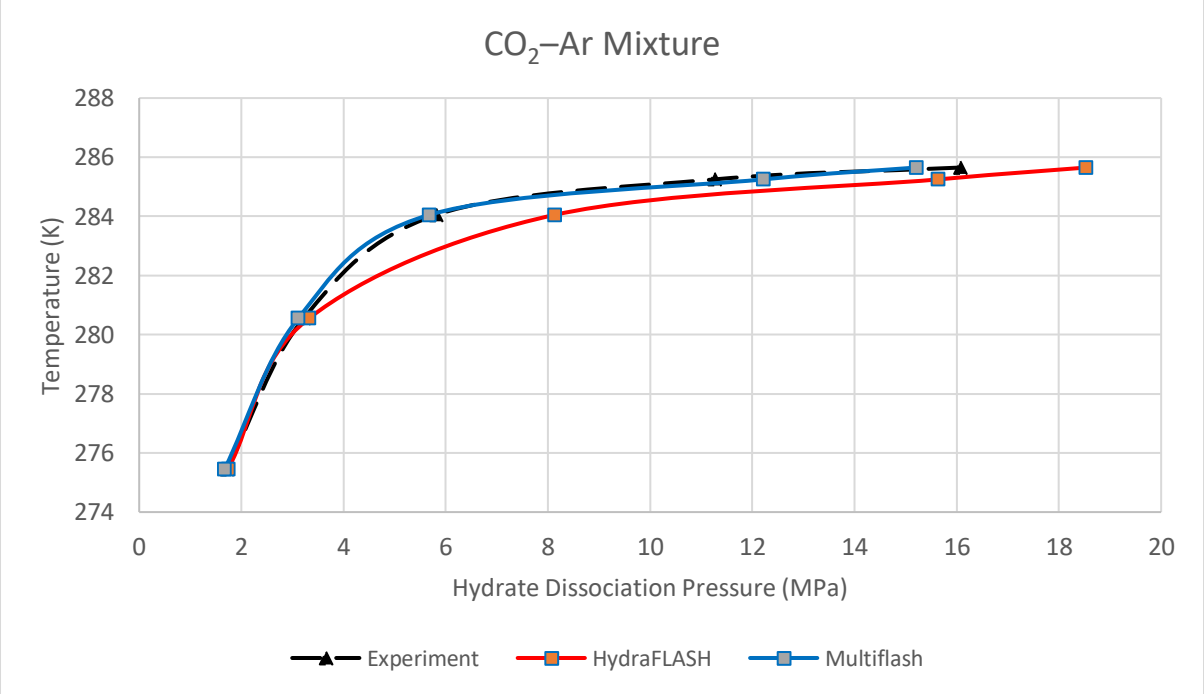

Figure 72 Hydrate Dissociation Data - CO_2–Ar Mixture

7. Conclusions

In this study, comparison of all important calculations between two commercial simulators has been made and discussed. Consideration all results, mostly both programs are producing quite similar results. The highest deviations were observed at high pressures density measurements of multicomponent mixtures (for HydraFLASH up to 9%, for Multiflash up to 5%). However, for density measurements of binary CO_2 –CH_4 components, for pressures up to 18 MPa, and three isotherms of 313 K, 333 K and 353 K, deviations in both software were very low. Additionally, very low deviations were noticed during sound velocity predictions. Generally, it can be concluded that HydraFLASH produces better results at lower pressures (up to 5 MPa) and moderate temperatures, while for very high pressures (50 MPa and more), Multiflash is superior.

Interesting fact is that during some calculations totally opposite software behaviors were observed. During predictions of solubility of CO_2 in water, it was noticed that at lower temperatures (isotherms 298 K and 323 K) HydraFLASH works better than Multiflash. But, as temperature of the system gets higher (isotherms 348 K, 373 K and 393 K) HydraFLASH results start to deviate more and more, unlike Multiflash results, which are getting more accurate at higher temperature. Similar behavior was spotted during measurement of hydrate dissociation data for binary mixtures, where accurate software results depends on composition of binary mixture. Investigating hydrate dissociation calculations of CO_2–CH_4 and CO_2–N_2 mixtures showed, almost identical results were noticed in matching experimental data in both software, but for rest of the mixtures, big variations in results were observed. For mixture CO_2–CO, Multiflash results deviation was the highest (0.51%), while for mixtures CO_2–O_2 and CO_2–Ar, HydraFLASH results showed higher deviation (0.15% and 0.20%, respectively).

In regard to the work itself in both software programs, my personal impression was that HydraFLASH software is much more user-friendly in comparison to Multiflash. Additionally, it provides very useful option to run many calculations of

different conditions of pressure and temperature at once, and helpful feature to export all results in Excel sheet, which makes collecting large sample of data much easier.

References

Ahmadi, P., & Chapoy, A. (2018). CO2 solubility in formation water under sequestration conditions. *Fluid Phase Equilibria, 463*, 80-90.

Bjørner, M., & Kontogeorgis, G. (2016). Modeling derivative properties and binary mixtures with CO2 using the CPA and the quadrupolar CPA equations of state. *Fluid Phase Equilibria, 408*, 151-169.

Chapoy, A., Burgass, R., Tohidi, B., & Alsiyabi, I. (2015). Hydrate and phase behavior modeling in CO2-rich pipelines. *Journal of Chemical and Engineering Data, 60(2)*, 447-453.

Chapoy, A., Haghighi, H., Burgess, R., & Tohidi, B. (2012). On the phase behaviours of the (carbon dioxide - water) systems at low temperatures: Experiments and modelling. *The Journal of Chemical Thermodynamics*, 6-12.

Diamantonis, N., & Economou, I. (2011). Evaluation of statistical associating fluid theory (SAFT) and perturbed chain-SAFT equations of state for the calculation of thermodynamic derivative properties of fluids related to carbon capture and sequestration. *Energy & Fuels, 25(7)*, 3334-3343.

Diamantonis, N., Boulougouris, G., Mansoor, E., Tsangaris, D., & Economou, I. (2013). Evaluation of cubic, SAFT, and PC-SAFT equations of state for the vapor-liquid equilibrium modelling of CO2 mixtures with other gases. *Industrial & Engineering Chemistry Research*, 3933-3942.

E-Education Institute, PennState. (2021). *PennState Department of Energy and Mineral Engineering*. Retrieved from Peng-Robinson EOS (1976): https://www.e-education.psu.edu/png520/m11_p2.html

E-Education Institute, PennState. (2021). *PennState Department of Energy and Mineral Engineering*. Retrieved from Soave-Redlich-Kwong EOS (1972): https://www.e-education.psu.edu/png520/m10_p5.html

EPA. (2021). *Climate Change Indicators:* . Retrieved from Greenhouse Gases: https://www.epa.gov/climate-indicators/greenhouse-gases

Fakharian, H., Ganji, H., Naderifar, A., & Mofrad, H. (2010). Mixed additives effects on methane hydrate dissociation rate. *13th Iranian National Chemical Engineering Congress & 1st International Regional Chemical and Petroleum Engineering.*

Gibbins, J., & Chalmers, H. (2008). Carbon capture and storage. *Energy policy, 36(12)*, 4317-4322.

Gilbert, K., Bennett, P., Wolfe, W., Zhang, T., & Romanak, K. (2016). CO2 solubility in aqueous solutions containing Na+, Ca2+, Cl-, SO42- and HCO3-: The effects of electrostricted water and ion hydration thermodynamics. *Applied Geochemistry, 67*, 59-67.

Gross, J., & Sadowski, G. (2001). Perturbed-chain SAFT: An equation of state based on a perturbation theory for chain molecules. *Industrial & engineering chemistry research, 40(4),* 1244-1260.

Haghighi, H., Chapoy, A., Burgass, R., & Tohidi, B. (2011). On the phase behavior of the carbon dioxide-water systems at low temperatures. *In Proceedings of the 7th International Conference on Gas Hydrate*.

Hassanpouryouzband, A., Yang, J., Tohidi, B., Chuvilin, E., Istomin, V., & Bukhanov, B. (2019). Geological CO2 capture and storage with flue gas hydrate formation in frozen and unfrozen sediments: method development, real time-scale kinetic characteristics, efficiency, and clathrate structural transition. *ACS Sustainable Chemistry and Engineering, 7(5)*, 5338-5345.

HYDRAFACT. (2021). *HydraFLASH hydrate and prediction software*. Retrieved from HYDRAFACT: http://www.hydrafact.com/index.php?page = software

IEA. (2008). *Energy Technology Analysis: CO2 Capture and Storage: A key carbon abatement option.* Paris: OECD/IEA.

IEA. (2011). *Internation Energy Agency*. Retrieved from https://www.iea.org/

IPCC. (2005). *Carbon dioxide capture and storage: Summary for policymakers and technical summary.* Bilthoven: IPCC, UNFCCC.

KBC. (2021). *Multiflash brochure*. Retrieved from KBC Global: https://www.kbc.global/software/advanced-thermodynamics/

Klins, M. (1984). *Carbon dioxide flooding; basic mechanism and project design.* Boston.

Kontogeorgis, G., Yakoumis, I., & Vlamos, P. (2000). Application of the sCPA equation of state for polymer solutions. *Computational and Theoretical Polymer Science*, 501-506.

Kontogeorgis, G., Yakoumis, V., Meijer, H., Hendriks, E., & Moorwood, T. (1999). Multicomponent phase equilibrium calculations for water-methanol-alkane mixtures. *Fluid Phase Equilibria,* 158-160.

Li, H., Wilhelmsen, Ø., & Yan, J. (2015). Properties of CO 2 Mixtures and Impacts on Carbon Capture and Storage. *Handbook of clean energy systems*, 1-17.

Lin, C., & Trusler, J. (2012). The speed of sound and derived thermodynamic properties of pure water at temperatures between (253 and 473) K and at pressures up to 400 MPa. *The Journal of chemical physics, 136(9)*, 094511.

Liu, S., Zhang, Y., Chi, Y., Song, Y., Yang, M., Liu, Y., & Lv, P. (2017). Density characteristics of CO2-CH4 binary mixtures at temperatures from (300 ti 308.15) K and pressures from (2 to 18) MPa. *The Journal of Chemical Thermodynamics, 106*, 1-9.

Lucile, F., Cézac, P., Contamine, F., Serin, J., Houssin, D., & Arpentinier, P. (2012). Solubility of carbon dioxide in water and aqueous solution containing sodium hydroxide at temperatures from (293.15 to 393.15) K and pressure up to 5 MPa: experimental measurements. *Journal of Chemical and Engineering Data, 57(3)*, 784-789.

Metz, B., Davidson, O., De Coninck, H., Loos, M., & Meyer, L. (2005). *IPCC special report on carbon dioxide capture and storage.* Cambridge: Cambridge University Press.

Nasir, Q., Lau, K., Lal, B., & Sabil, K. (2014). Hydrate dissociation condition measurement of CO2-rich mixed gas in the presence of methanol/ethylene glycol and mixed methanol/ethylene glycol+electrolyte aqueous solution. *Journal of Chemical & Engineering Data, 59(11)*, 3920-3926.

Nazeri, M., Chapoy, A., Burgass, R., & Tohidi, B. (2017). Measured densities and derived thermodynamic properties of CO2-rich mixtures in gas, liquid and supercritical phases from 273K to 423K and pressures up to 126MPA. *The Journal of Chemical Thermodynamics, 111*, 157-172.

Speranza, A., & al., e. (2017). *THE EFFECT OF THE THERMODYNAMIC MODEL AND PARAMETERS IN PROCESS MODELLING*. Retrieved from LinkedIn: https://www.linkedin.com/pulse/effect-thermodynamic-model-parameters-process-alessandro-speranza/

Steel, L., Liu, Q., Mackay, E., & Maroto-Valer, M. (2016). CO2 solubility measurements in brine under reservoir conditions: A comparison of experimental and geochemical modeling methods. *Greenhouse Gases: Science and Technology, 6(2)*, 197-217.

Valderrama, J. (1990). A generalized Patel-Teja equation of state for polar and nonpolar fluids and their mixtures. *Journal of chemical engineering of Japan, 23(1)*, 87-91.